学位申請論文

野上大作

Spectroscopic and Photometric Observations of Dwarf Novae in the Optical Range

Daisaku NOGAMI

Department of Astronomy,

Faculty of Science,

Kyoto University

e-mail: nogami@kusastro.kyoto-u.ac.jp

14 January, 1999

Abstract

Accretion disk is in various kinds of astronomical objects and works as the central engine of variability in these objects. Cataclysmic variable stars (CVs) are quite useful for studying the basic accretion disk physics, as well as for studying the binary evolution. Based on their activity, non-magnetic CVs are roughly divided into four groups: NLs (including post novae) with constant brightness, SS Cyg-type dwarf novae showing (normal) outbursts, Z Cam-type dwarf novae exhibiting outbursts and occasional standstills, and SU UMa-type dwarf novae showing normal outbursts and superoutbursts with superhumps. This difference of activity is basically explained by the thermal-tidal instability model.

Many kinds of modulations in CVs are photometrically observed in the optical range: dwarf nova oscillations, quasi periodic oscillations, flickerings, orbital humps, eclipses, superhumps, normal outbursts, superoutburst, and nova explosions. Eclipse observations have given fruitful information on geometry, binary parameters, temperature distribution in the disk, and so on. The viscosity parameter α in the hot state was estimated, from the decline rate from outburst, to be ~ 0.3. Long term monitoring of outburst behavior and time-resolved photometry continuously have been yielding, from a few years ago, many surprising results having great influence on the disk instability scheme and the CV evolutionary scenario.

CVs have optical spectra with blue continuum and Balmer and herium lines, most of which come from the accretion disk. The accurate binary parameters (the orbital period, masses of the secondary and the primary, the inclination, and so on) have been measured by optical spectroscopy. Change of the line shape along the orbital phase have suggested location of the hot spot and existence of the mass flow. The two-armed spiral structure was recently indicated to exist in the accretion disk in IP Peg during outburst, using the Doppler mapping technique.

I introduce three major results among my recent works, two of which are examples that time resolved photometry and long term monitoring revealed interesting behavior of the accretion disk during a superoutburst in an enigmatic dwarf nova AL Com and proved that there is an active dwarf nova in the period gap (NY Ser). The other is the

spectroscopic observation of a Z Cam star AT Cnc during a standstill suggesting transient mass ejections and Na D to be formed near the Hα radiating region.

At the last, I mention that incredible CVs in the current view are possibly discovered by a deep CV survey, and that the time resolved spectroscopy of CVs may give constraints on the condition for jet formation and the structure of the accretion disk. A key for understanding the irradiation effect on the binary evolution may be obtained also by spectroscopy of dwarf novae with high mass transfer rates.

1 General Introduction

1.1 Significance of the Study of Cataclysmic Variable Stars

Cataclysmic variable stars are binary systems consisting of a primary white dwarf and a late-type main sequence secondary star transferring surface gas through the inner Lagrangian point (for a comprehensive review, Warner 1995). The orbital period ($P_{\rm orb}$) is scattered in the range from $\sim$ 1 hr to $\sim$ half a day.

Accretion disk is a common component of active galactic nuclei (AGNs), X-ray binaries, cataclysmic variables (CVs), protoplanetary systems, and so on, and is regarded as the central engine of the variability with a wide range of the time scale in these objects. Understanding physics of the accretion disk is important for explaining activities of various kinds of objects.

Astronomical jets have been discovered in all types of accretion-disk systems. The Hubble Space Telescope has been taking direct images of jets in AGNs and protoplanetary systems, and those in X-ray binaries and AGNs have been taken in the radio region. The most recent example in the X-ray transient CI Cam (= XTE J0421+560 = MWC 84) was reported by Hjellming and Mioduszewski (1998). The mechanism to produce the collimated mass flow, however, is one of the hot topics in the study of accretion disks.

CVs (for a comprehensive review, Warner 1995) are binary stars consisting of a primary white dwarf and a red dwarf secondary star which loses surface gas forming an accretion disk around the white dwarf. Dwarf novae, a subclass of CVs, show various modulations and are quite useful stars for studying the dynamical aspect of accretion disks, which can be applied to other objects, from the following reasons: 1) they are relatively bright among accretion-disk systems in the optical bands, 2) we can directly observe the accretion disk by optical light since the disk is the dominant source in that region, 3) CVs exhibit a rich variety of light modulations due to changes of the physical status in the accretion disk on time scales of seconds $\sim$ a few tens years, for which the observations can be carried out in our life time. Actually, researchers have been trying to apply the thermal disk instability theory developed to explain the outburst behavior of dwarf novae (for a review, Osaki 1996) to outbursts in X-ray transient (e.g. Shahbaz et al. 1998) and to those in FU Ori stars, a kind of active T Tau stars (e.g. Hartmann, Kenyon 1996). Most recently, Burderi

et al. (1998) published a work concerning accretion disks in AGNs by using an idea of the thermal disk instability.

Dwarf novae are useful objects in the view point of the study of the binary evolution, since they immediately reflect, in their outburst behavior, change of the mass transfer rate ($\dot{M}_{\rm tr}$) which is expected to be caused by change of the physical status of the secondary surface. The evolution of binary stars is more complicated than that of single stars, since the special effect owing to the binary system, for example, mass exchange, irradiation, and so on, must be taken into account. The mass transfer rate in CVs has is a strong function of $P_{\rm orb}$ in the standard theory of the CV evolution below the period gap of $\sim$ 2–3 hr where the number density of known CVs is reduced, because the gravitational-wave radiation controls $\dot{M}_{\rm tr}$ in CVs there (for a review of the theory of evolution, e.g. King 1988). However, dwarf novae and nova-like variables with mass transfer rates 10 times or more higher the rate expected using $P_{\rm orb}$ recently have been discovered below the period gap. If we can clarify how the mass transfer rate is kept high, the scheme of the binary evolution may be dramatically changed. This change would have an effect to the theoretical estimate of the metallicity and the spectral energy distribution of galaxies, which is one of the big problems in the cosmology and the galaxy evolution.

1.2 Classifications of CVs

In non-magnetic CVs, which mean that the white dwarf does not have a strong magnetic field, the gas from the secondary forms an accretion disk around the primary star. In the case of magnetic systems called as intermediate polars (or DQ Her stars) and polars (or AM Her stars), the mass flow is controlled by the magnetic field of the primary star. They are also interesting systems, but I here give only reviews which are Patterson (1994) for intermediate polars and Cropper (1990) for polars, since the magnetic field of the primary star is out of the scope of this thesis. Hereafter in this paper, CVs mean non-magnetic systems unless otherwise stated.

Depending on their activity, non-magnetic CVs are basically divided into four subclasses: 1) classical novae, 2) recurrent novae, 3) nova-like variables (NLs), and 4) dwarf novae.

Classical novae are CVs which have experienced nova explosion caused by the thermonuclear runaway reaction of transferred hydrogen on the surface of the white dwarf (for a review, e.g. Starrfield 1989) in the history of the observational astronomy[1] .

If the nova explosion has been observed two times or more, this object is called as recurrent nova. The recurrence time of the nova explosion is shorter in systems where the primary star has a mass close to the Chandrasekhar limit ($\sim 1.4\ M_{\odot}$) and the mass transfer rate is high (e.g. Livio, Truran 1992).

NLs are CVs where the nova explosion has never been observed but have spectra very similar to those of classical nova remnants. In the optical range, their spectra have very blue continuum[2] and shallow wide Balmer absorption lines with/without emission core. Those features are also seen in spectra of dwarf novae in outburst. NLs basically do not show drastic photometric variability like classical novae and dwarf novae. Then, NLs are considered to be in the thermally stable state in the disk instability theory (for a review, Osaki 1996), which will be briefly summarized in section 2.

The most definitive character of dwarf novae is that they show various kinds of photometric variability caused by change of physical properties in the accretion disk. Dwarf novae have three main subclasses showing different photometric behaviors: 1) SS Cyg type with normal outbursts, 2) Z Cam type with normal outbursts and standstills, and 3) SU UMa stars with normal outbursts and superoutbursts.

Normal outbursts typically have an amplitude of 2–5 mag and an duration of a few to several days, while some outbursts in SS Cyg stars last over ten days. The recurrence cycle of normal outburst ($T_{\rm n}$) is ten to several ten days. That cycle tends to be shorter in Z Cam stars and longer in SU UMa stars.

Z Cam stars aperiodically enter the standstill phase during which these stars stay for several days to a few years at the level of about 1 mag fainter than their maximum brightness of an outburst.

The superoutburst is the definitive character of SU UMa-type dwarf novae. SU UMa

[1] The nova explosion can occur also in magnetic systems. For example, DQ Her is the remnant of Nova Herculis 1934

[2] Actually, many CVs were discovered as a result of the Palomar-Green Survey (Green et al. 1986) for detecting quasars by selecting photometric blue-color objects.

stars occasionally undergo superoutbursts which reach a maximum of 0.5–1.0 mag brighter than the maximum of the normal outburst and show characteristic modulations, called superhumps. Superhumps have amplitudes of from 0.1 to 0.3 mag, and the superhump period ($P_{\rm SH}$) is longer by a few percent than $P_{\rm orb}$. The recurrence time of superoutburst (supercycle, T_s) is typically the a few hundred days, and the normal outburst occur several to ten times during 1 supercycle. The parameters of know SU UMa stars are listed in table 1 which is an updated version of table 1 in Nogami et al. (1997).

1.3 Disk Instability Theory

Here I briefly summarize the disk-instability theory as the current standard scheme for understanding various types of non-magnetic CV behavior in a unified way. I again recommend Osaki (1996) as the concise best review for readers interested in that theory.

The key of this scheme is the combination of two types of intrinsic instabilities in the accretion disk simply but well modeled by Shakura and Sunyaev (1973). They are the thermal instability and the tidal instability.

1.3.1 Thermal Instability

This instability concerns transition between the neutral and ionized states of hydrogen which is the dominant material in accretion disk of CVs. The idea of the thermal instability is best exhibited by the S-shaped thermal-equilibrium curve in a surface-density (Σ) versus mass-accretion rate ($\dot{M}$) diagram (figure 1). This curve is calculated to equate the local viscous-heating rate Q^+ and the local radiative-cooling rate Q^-.

You assume the mass transfer rate is represented by $\dot{M}_0$ in figure 1. If the mass accretion rate $\dot{M}$ is on the lower equilibrium branch ($\dot{M} < \dot{M}_{\rm tr}$), the surface density increase. During this phase, the temperature T is lower than the critical one for ionization of hydrogen, and the kinematic viscosity ν is low since ν is given by the equation,

$$\nu = \frac{2}{3}\alpha(\Re/\mu)T/\Omega, \tag{1}$$

where $\alpha, \Re, \mu, \Omega$ are the viscosity coefficient, the gas constant, the mean molecular weight, and the Keplerian angular velocity. When Σ reaches the critical value $\Sigma_{\rm max}$, sudden

increase of T and ionization of hydrogen cause jump of $\dot{M}$ to the high branch. After this transition, the mass accretion rate become larger than the mass transfer rate ($\dot{M} > \dot{M}_{\rm tr}$), Σ decreases. When Σ reaches the critical value $\Sigma_{\rm min}$, sudden decrease of T and recombination of hydrogen cause jump of $\dot{M}$ to the low branch.

This thermal relaxation oscillation occur at a given point in accretion disk. However, the transition front propagates inward and outward due to flow of mass (and flow of heat, possibly).

This scheme explains the (normal) outburst in dwarf novae as the following way: the outburst occurs when the heating front begin to propagate and the brightness decreases with the cooling front going inward. The cooling front starts at the outer edge of the accretion disk, since the mass is first depleted there. Smak (1984), however, found that the heating front may starts either at the outer edge or at the inner edge. Computer calculations (e.g. Cannizzo et al. 1986) predict: 1) the outburst sharply rises and slowly declines (the outburst shape is very asymmetric) in the case of "outside-in" outburst where the thermal transition first occur at the outer part of the accretion disk and the heating front propagates inward, and 2) the rise of outburst is rather slow and the outburst shape is more symmetric in the case of "inside-out" outburst. The former type of outburst is usually seen in all types of dwarf novae, while the "anomalous" outburst with a slow rise sometimes seen in SS Cyg stars is considered as the "inside-out" outburst.

1.3.2 Tidal Instability

In 2-D computational hydrodynamic simulations, Whitehurst (1988) discovered an instability phenomenon in the accretion disk, which is now called as tidal instability or tidally driven eccentric instability. This instability in his calculations made the accretion disk evolved to an eccentric form in a CV with a low mass ratio ($q = M_2/M_1 < 0.25$; M_2: secondary mass, and M_1: primary mass) and the eccentric disk slowly rotated in the prograde way in the inertial frame of reference. It is know that the tidal instability occurs due to the 3:1 resonance between the fluid flow and the binary (e.g. Lubow 1991). The upper limit of the mass ratio ($q < 0.25$) is determined by the constraint that the 3:1 resonance radius $r_{3:1} \sim 0.46A$(A: the binary separation) must be smaller than the tidal truncation radius.

1.3.3 Thermal-tidal Instability as the Unified Scheme of CV behavior

As mention in section2, non-magnetic CVs have four major subgroups, classical novae, recurrent novae, NLs, and dwarf novae. In addition, the dwarf novae have 3 major subtypes, SS Cyg type, Z Cam type, and SU UMa type. NLs are hereafter used as the general term for classical novae, recurrent novae, and NLs, since the classical novae and the recurrent novae long time after the nova explosion are generally same as NLs in observable features. Then, the thermal-tidal instability theory can essentially explain four types of behavior: 1) NLs with constant brightness, 2) SS Cyg-type dwarf novae showing (normal) outbursts, 3) Z Cam-type dwarf novae showing (normal) outbursts and standstills, and 4) SU UMa-type dwarf novae showing normal outbursts and superoutbursts, in an unified way.

First, difference of NLs and dwarf novae is explained by difference of the mass transfer rate. In the thermal instability scheme, the accretion disk is thermally stable and the outburst does not occur if the mass transfer rate is higher than the critical mass accretion rate $\dot{M}_{\rm crit}$ given as equation 2 in Smak (1983)

$$\dot{M}_{\rm crit} = \frac{8\pi}{3}\sigma T_{\rm e,crit}^4 \frac{R_{\rm d}^3}{GM_1}\left\{1-\left(\frac{R_1}{R_{\rm d}}\right)\right\}^{-1}, \tag{2}$$

where σ, G, $R_{\rm d}$, and R_1 are the Stefan-Boltzmann constant, the gravity constant, the disk radius, and the radius of the primary star, and $T_{\rm e,crit}$ is the critical effective temperature below which no hot state exist. This equation is simplified as equation 4 in Osaki (1996) under reasonable assumptions

$$\dot{M}_{\rm crit} \simeq 2.7\times10^{17}\left(\frac{P_{\rm orb}}{4\ {\rm hr}}\right)^{1.7}\ {\rm g\ s^{-1}}. \tag{3}$$

The mass transfer rate in NLs is considered to be over $\dot{M}_{\rm crit}$ and dwarf novae have a mass transfer rate below $\dot{M}_{\rm crit}$.

Among dwarf novae, Z Cam stars are supposed to have $\dot{M}_{\rm tr}$ close to $\dot{M}_{\rm crit}$ (Meyer, Meyer-Hofmeister 1983). Z Cam stars repeat outbursts in the ordinary state. However, when the mass transfer rate becomes slightly high for some reason and exceeds $\dot{M}_{\rm crit}$, the Z Cam star enter a standstill. The brightness during the standstill phase is fainter by $\sim$ 1 mag than the outburst maximum. This is explained by that the mass accretion rate is

equal to the mass transfer rate which is smaller than the mass accretion rate at the peak of outburst.

SU UMa stars show superoutbursts in addition to normal outbursts. In the thermal-tidal instability model, the normal outbursts are supposed to be caused by the thermal instability, as mentioned above, and the superoutburst occur due to mixture of the thermal instability and the tidal instability. During the phase when SU UMa stars repeat normal outbursts, the mass and the angular momentum is gradually accumulated in the accretion disk because of insufficient mass accretion and angular momentum removal. There is the critical total angular momentum ($J_{\rm crit}$) in the accretion disk (see equation 3 in Osaki 1989)

$$J_{\rm crit} = \frac{8}{7}\pi R_{\rm crit}^2 \Sigma_{\rm min} (G M_1 R_{\rm crit})^{0.5}, \tag{4}$$

where $R_{\rm crit}$ is the critical radius for the 3:1 resonance. When the outburst occur in the disk angular momentum over $J_{\rm crit}$, the disk radius reaches $R_{\rm crit}$ and the accretion disk evolves to a eccentric shape due to the tidal instability. For this critical angular momentum, a time scale $t_{\rm wait-S}$ is defined (see Osaki 1995)

$$t_{\rm wait-S} \sim \frac{J_{\rm crit}\ f_J}{\dot{M}_{\rm tr} j_0}, \tag{5}$$

where f_J and j_0 are the fraction of the total angular momentum of the disk removed during the superoutburst and the specific angular momentum of transferred mass, respectively. This equation is replaced as equation 4 in Osaki (1995) under reasonable assumptions

$$t_{\rm wait-S} \sim \left(\frac{128\ d}{\dot{M}_{tr,16}}\right) \alpha_{\rm H,0.3}^{-0.7} P_{\rm orb,110}^2 (m_1+m_2) m_1^{-0.33} \left\{\frac{(R_{\rm crit}/R_{\rm LS})}{2.4}\right\}^{0.5} \left(\frac{f_J}{0.65}\right), \tag{6}$$

where $\dot{M}_{tr,16}, \alpha_{\rm H,0.3}, P_{\rm orb,110}, m_1, m_2, R_{\rm LS}$ are the mass transfer rate in units of $10^{16} g\ s^{-1}$, the viscous coefficient in the hot state in units of 0.3, the orbital period in units of 110 min, the primary mass in units of $M_\odot$, the secondary mass in units of $M_\odot$, and the Lubow-Shu radius, respectively. When an outburst arises after it has passed longer time than $T_{\rm wait-S}$ since the last superoutburst, the disk radius reaches $R_{\rm crit}$. The tidal torque by the secondary star efficiently removes angular momentum from the eccentric disk and the disk is maintained in the hot state. This outburst, therefore, grows to a superoutburst which has a brighter maximum and lasts longer than the normal outburst. The superoutburst

makes most of mass in the disk accreted to the white dwarf (see e.g. figure 8 in Osaki 1996) and resets the disk for a new sequence of normal outbursts and a superoutburst.

The superhump phenomenon is explained to be produced by the periodic variation of angular momentum removal from the disk to the secondary due to the tidal torque. The superhump period is, then, calculated as beat between the prograde precession of the eccentric disk and the secondary star

$$\frac{1}{P_{\rm SH}} = \frac{1}{P_{\rm orb}} - \frac{1}{P_{\rm pr}}, \tag{7}$$

where $P_{\rm pr}$ is the precession period.

The content described so far is summarized as the following: 1) NLs have thermally stable accretion disks, 2) SS Cyg stars exhibit outbursts due to the thermal instability, 3) Z Cam stars do the same as SS Cyg stars, but they sometimes enter the standstill phase when $\dot{M}_{\rm tr}$ increases for some reason, and 4) SU UMa stars also show normal outbursts, however, a normal outburst grows to a superoutburst when the disk expands to the critical radius for the tidal instability at the maximum of the outburst. Note that it is only in CVs with low mass ratios that the critical radius is within the region where the stable orbit exists; $R_{\rm crit}$ is smaller than the tidal truncation radius. SU UMa stars are concentrated below the period gap, while only two exceptions are NY Ser at the midst of the gap (Nogami et al. 1998b, see section 3.1) and TU Men at the upper edge of the gap (Mennickent 1995). This fact is in good accordance with the constraint on the mass ratio.

In these years, extraordinary behavior of WZ Sge stars (Bailey 1979; Downes, Margon 1981; O'Donoghue et al. 1991) and ER UMa stars (Nogami et al. 1995a; for a review, see Kato et al. 1999a) has been revealed. The supercycles of WZ Sge stars and ER UMa Stars are far from those of usual SU UMa stars (see figure 2). In addition, WZ Sge stars seldom show normal outbursts, but show some kinds of rebrightening after the main superoutburst. Osaki (1995a, b, c) and Osaki et al. (1997) suggested that behavior of those stars and permanent superhumpers (a kind of NLs with permanent superhumps) can be explained in the standard disk instability theory by assuming a proper complex of a high/low mass transfer rate, low efficiency of the tidal torque, low α in quiescence, and temporal increase of α in a cold state (see figure 3 in Osaki 1996). For WZ Sge stars,

however, Lasota et al. (1995), Warner et al. (1996), Hameury et al. (1997), and Meyer-Hofmeister et al. (1998) proposed models with a hole around the white dwarf produced by evaporation to the coronal layer above the disk (Meyer, Meyer-Hofmeister 1994) or by magnetosphere of the white dwarf (Livio, Pringle 1992). It seems to take some more time to complete the unified theory of CVs.

2 What Can We Understand on CVs by Photometry and Spectroscopy?

There are four major methods in the astronomical observation: photometry, spectroscopy, imaging, and polarimetry. The latter two methods, however, have not yielded so much results that give great impacts in the CV study. In this section, I summarize what has been revealed and is currently expected to be found in CVs by photometry and spectroscopy in the optical range.

2.1 Photometry

The strong points of photometry compared to spectroscopy are that we can observe fainter objects with more ease, that the exposure time can be shorter, and that the observation can be carried out with more compact instruments (small telescopes, simple detectors, and so on). Making use of these points, many CVs have been photometrically observed for studying various types of modulation. Information of the modulation directly revealed by photometry is existence/non-existence, the time scale, the shape, reproducibility, and so on. These make constraints on the model for such modulations.

CVs show many kinds of periodic or quasi periodic photometric modulations. They are, generally in the order of short time scale, dwarf nova oscillations (DNOs), quasi periodic oscillations (QPOs), flickerings, orbital humps, orbital humps, superhumps, (normal) outbursts, superoutbursts, nova explosions.

DNOs (e.g. Warner et al. 1989) are observed only in outburst and have very small amplitudes of < 0.005 mag and quite short periods of $10 - 30$ s (see table 8.2 in Warner 1995). QPOs (e.g. Patterson et al. 1977) are also seen only in outburst and have small amplitudes of ~ 0.005 mag and short time scales of several 10 – several 100 seconds. The most apparent difference between these short period oscillations is the peak shape of the power spectrum: the very sharp peak for DNOs and the broad peak for QPOs. This is due to the short coherent length of QPOs. Since these oscillations in CVs are observed in soft X-ray (e.g. Cordova et al. 1980), they are supposed to be caused near the inner edge of the disk. However, the mechanism for those oscillations have not been established,

though several models have been proposed (see section 8.6.5 in Warner 1995). In some dwarf novae, QPOs with quite large amplitudes of ~ 0.2 mag, called super-QPOs (Kato et al. 1992; see also Nogami et al. 1998a), seem to be observed.

Flickerings are modulations with amplitudes of $0.01 - 0.2$ mag and time scales of several 10 s – 10 min, and they are seen in dwarf novae in quiescence as well as NLs. The site producing flickerings have been suggest to be the hot spot (e.g. Warner, Nather 1971) or to be the inner region (Horne, Stiening 1985) by using analyses of eclipses, but a consensus has not been reached (see also Welsh et al. 1996).

In quiescence, the hot spot is the dominant source of optical light in some dwarf novae. The anisotropic radiation from the hot spot is seen observed as photometric humps with the orbital period (orbital hump), especially in high-inclination systems in quiescence. The orbital period of dwarf novae is determined by measuring the period of the orbital hump other than measuring that of the radial velocity variation of spectral lines, especially in the case of faint dwarf novae. The orbital humps appear just before eclipse, which means that the hot spot is located closest to observers before eclipse.

Eclipse analyses as well as superhump observations have been playing an important role. These analyses have revealed the location of the hot spot, the temperature distribution of the accretion disk in quiescence (almost flat) and in outburst ($T \propto R^{-3/4}$), the mass accretion rate, and so on (for a review, e.g. Horne 1993). These results are obtained using comparatively simple models, but new techniques including e.g. non-LTE effects is being developed (see e.g. Vrielmann 1997).

Observational finding of two types of outburst: 1) "normal" outburst with a rapid rise and a slow decline, and 2) "anomalous" outburst with a slow rise and a slow decline led to theoretical discovery of two types of outburst: the outside-in type and the inside-out type (Smak 1984), as mentioned above. He also deduced the value of α in the high state to be ~ 0.3 by fitting the theoretical model to the empirical relation between the decline rate of outburst and the orbital period.

The thermal-tidal instability theory have been developed as the observations of superhumps and superoutbursts have been piled up. They are that some dwarf novae sometimes show long, bright outburst (superoutburst) instead of normal outburst, that some superoutbursts once decline soon after the onset of outburst and re-brighten a few – several

days after (see Richter 1992), periodic oscillations with amplitude 0.1 – 0.5 mag and period of a few percent longer than the orbital period (superhumps) certainly appear only during superoutbursts instead of orbital humps, the superhump period becomes shorter (or at least keep constant) during the superoutburst, there seems to exist an activity classification (see table 1 of Osaki 1996, originally proposed by Vogt 1993), and so on.

The observations of superhumps and long-term dense monitoring of CVs are still, or more productively now, proposing new problems. Among discoveries in these a few years, I select 1) large-amplitude superhumps in ER UMa stars during just after the superoutburst maxima (Kato et al. 1996c; see also Kato et al. 1999), 2) permanent "positive" and "negative" superhumps of some NLs (for a review, Patterson 1999), 3) increase of $P_{\rm SH}$ during superoutbursts in short-$P_{\rm orb}$ systems (AL Com: Nogami et al. 1997a; HV Vir: Kato, Sekine 1999, in preparation; V1028 Cyg: Baba et al. 1999; SW UMa: Nogami et al. 1998a; V485 Cen: Olech 1997; WX Cet: Kato et al. in preparation), 4) behavior after main superoutburst of WZ Sge stars from no outburst to the second superoutburst (e.g. Nogami et al. 1998c), 5) supercycle of $\sim$ 200 d in V844 Her with no normal outburst? (Kato 1997b, see table 1), 6) appearance of superhumps during the precursor outburst triggering the 1993 superoutburst in T Leo (Kato 1997a), 7) in-the-gap dwarf nova NY Ser with a usual mass transfer rate (Nogami et al. 1998b, and see section 3.1), 8) 59-min orbital period of the SU UMa star, V485 Cen, below the period minimum (Olech 1997), 9) permanent superhumps in V1974 Cyg after the nova outburst (Retter et al. 1997). The latter three are very important discoveries also in a view point of the CV evolution.

All the objects listed in the last paragraph are short orbital systems and most of them have $P_{\rm orb}$ near the period minimum theoretically predicted (e.g. Paczynski 1981). While the theoretical models of the CV evolution predict almost all ($\sim$ 99 %) CVs are currently located below the period gap, below-the-gap CVs found so far are smaller in number than CVs with $P_{\rm orb}$ longer than the period gap (see Ritter, Kolb 1998). This probably results from the intrinsic brightness of below-the-gap dwarf novae fainter than the other (see e.g. section 3.3.3.3 in Warner 1995) and the lower activity of below-the-gap dwarf novae due to the smaller $\dot{M}_{\rm tr}$. Actually, short-$P_{\rm orb}$ CVs were discovered by the Palomar-Green survey (Green et al. 1982, 1986) of ultraviolet excess objects. A similar color-selection survey for more fainter objects will surely lists objects urging us to change the view of CVs.

These recent surprising observations have been realized, (at least partly) because the relationship between professional and amateur astronomers has been developed (see web pages of VSNET, http://www.kusastro.kyoto-u.ac.jp/; the CBA group, http://cba.phys.columbia.edu/; AAVSO, http://www.aavso.org/) and rather inexpensive but efficient CCDs have spread among amateurs, which enabled the prompt observations just after transient objects entering scientifically interesting phases and the long term monitoring of fainter objects in collaboration with amateurs. I hope this good relationship be kept or be more and more developed.

2.2 Spectroscopy

What we can directly know about point sources of astronomical objects by spectroscopy is the intensity and shape of the continuum, the shape, equivalent width, and shift from the rest wave length of various atomic and molecular lines and bands. The information of the location is added to those in the case of extended sources. In the case of variable objects like CVs, time variations of such quantities include, of course, precious information. Physical parameters are deduced by analyzing such observational results under assumptions of the physical status of the source, the radiation process, the chemical abundance, and so on.

The main radiation region of each components in a typical CV is summarized as below: infrared by the late-type main-sequence secondary star, optical–UV by the accretion disk, the white dwarf, and the hot spot, EUV–soft X-ray by the boundary layer between the accretion disk and the white dwarf surface, and hard X-ray by the corona. Then, the optical spectroscopy of CVs basically gives knowledge concerning the accretion disk, the hop spot, the white dwarf.

The typical optical spectrum of CVs is characterized by the very blue continuum, Balmer lines, and lines of HeI (and HeII in some systems) (see the atlas of Zwitter, Munari 1994, 1995, 1996; Munari et al. 1997; Munari, Zwitter 1998). The Balmer lines are in emission produced by the accretion disk in dwarf novae in quiescence and in absorption (sometimes with an weak emission core) produced by the accretion disk and the white dwarf in dwarf novae in outburst and standstill and in NLs. This transition

between emission/absorption is explained by the change of optical thickness of the disk for continuum; optically thicker in outburst than in quiescence (see above description of the thermal instability theory). Balmer emission lines in dwarf novae with moderately high inclinations have double peaks, which is theoretically expected to be formed in the Keplerian disk (Horne, Marsh 1986). A moving emission component seen in Balmer lines and HeI (e.g. Honeycutt et al. 1987) is supposed to originate in the hot spot (e.g. Krzeminski, Kraft 1964).

Piché and Szkody (1989) and Marsh and Horne (1990) observed IP Peg in outburst by time-resolved spectroscopy and found that the blue wing of Hα was cut before the eclipse minimum and the red wing was cut after the eclipse minimum, suggesting that the Hα emission was formed in the disk. They also found two interesting facts which are that HeII λ4686 was not in the double-peaked shape but filled in the center of the line, suggesting a wind to contribute to the helium emission, and that the irradiated secondary formed a narrow Balmer emission component.

The Doppler tomography using an emission line in time-resolved spectra (Marsh, Horne 1988) has recently been a standard tool for reconstructing a intensity map in the velocity field, which supports interpreting the source distribution of the line. An recent epoch-making result by this technique is that Steeghs et al. (1997) discovered the two-armed spiral structure in IP Peg in outburst.

The most reliable and useful method to measure binary elements (the orbital period, masses of the white dwarf and the secondary, the inclination) is the analysis of the radial velocity variation of Balmer lines supposed to represent the orbital motion of the primary. The eclipse analysis is also an efficient method for the measurement (e.g. Wood et al. 1986), but this can be applied only to CVs showing deep eclipses by nature.

The radial velocity analysis has been carried out for Na D or other metal lines in optical and in IR regarded as being formed in the secondary surface, if they were detected. However, the suggestion that the Na D absorption may be produced in the accretion disk was recently proposed by Patterson et al. (1998c) and Nogami et al. (1999).

Nogami et al. (1999) discovered an absorption component in the blue wing at Hα, that is, the P Cyg profile, in AT Cnc during standstill. The P Cyg profile appeared during a limited period in its orbital phase. This profile variation is interpreted to be caused by

transient mass ejection episodes.

3 Three Major Results among My Recent Works

In this section, I describe three major results, referred to in section 2, among my recent works. The abstracts of them are below.

- Photometric observations of the 1995 superoutburst of AL Comae Berenices (Nogami et al. 1997a)

Time-resolved photometric observations of the first superoutburst confirmed since 1975 in a most enigmatic cataclysmic variable, AL Comae Berenices during 1995 April - June is reported. Double-peaked modulations in the early phase of the outburst (early superhumps), the period of which is slightly shorter than the superhump period were detected, following them in WZ Sge and HV Vir. Three possibilities for the mechanism causing these oscillations are discussed. As seen during the 1978 outburst of WZ Sge, a dip of over 2 mag in the light curve occurred in the 1995 outburst. After recovery from this dip, AL Com again declined 0.5 mag and re-brightened showing modulations with a same period as the superhump one, which indicates that a "second" superoutburst occurred. These modulations disappeared before the final decline. After decline, AL Com stayed about or over 1 mag brighter than its quiescence level for at least two weeks. It is likely that the accretion disk remained in its hot state near the inner edge during the dip and after the end of the outburst.

- Discovery of the first in-the-gap SU UMa-type dwarf nova, NY Serpentis (Nogami et al. 1998b)

Photometric monitoring and time-resolved observations of NY Ser were carried out between 1995 July 25 and 1997 March 11. During the 1996 April superoutburst, superhumps were clearly observed and the superhump period was 0.106 ($\pm$ 0.001) d, which suggests that the orbital period is located near to the middle of the period gap. NY Ser shows normal outbursts with a recurrence time of 6–9 days and superoutbursts with a recurrence time of 85–100 days in the range of 14.6–18.0 mag in the V band. These cycle lengths are rather short among SU UMa stars (see table 1), implying $\dot{M}_{\rm tr}$ in this star is larger than the average value of SU UMa stars, while CVs evolving in the period gap is considered to have $\dot{M}_{\rm tr} \sim$ zero in the standard theory of the CV evolution.

- Spectroscopic and photometric observations of a Z Cam-type dwarf nova, AT Cancri, in standstill (Nogami et al. 1999)

Quasi-simultaneous spectroscopic and photometric observations of a Z Cam star, AT Cnc, in standstill were performed. V-band time-resolved photometry marginally revealed small-amplitude ($\sim$ 0.01 mag) oscillations with period candidates of 0.132 d (and its two day aliases 0.124 d and 0.142 d) and 0.249 d, all of which do not match the orbital period derived in this study. Low resolution spectra show the singly peaked Hα emission line, Hβ emission superposed on an absorption component, Hγ absorption, and Na D absorption. The analysis of radial velocity variation of Hα in mid-resolution spectra provided system parameters: the orbital period = 0.2011 ($\pm$ 0.0006) d, the semi-amplitude = 80 ($\pm$ 4) km s^{-1}, the systemic velocity = 11 ($\pm$ 3) km s^{-1}. Using these parameters, the primary mass is estimated to to be 0.9 ($\pm$ 0.5) $M_{\odot}$. The phase of the velocity variation of Hα is very close to that of Na D, which suggests that the centers of the Hα emitting region and the Na D formation region were in the same direction from the gravity-center if their motions were limited in the orbital plane. There are two possibilities: the Hα emission line was radiated a) from the secondary star, or b) from the accretion disk. The inclination is estimated to be 17° ($\pm$ 5°) and 36° ($\pm$ 12°) based on the respective possibilities. The Doppler map drawn under the possibility a) revealed on a broadly extended component in the ($-V_x$, $-V_y$) region. Such peaks are also seen in Doppler maps of most of SW Sex stars. In the Doppler map drawn under the possibility b), the peak exists on the irradiated side of the Doppler position of the secondary and the ($+V_x$, $+V_y$) region. An absorption component in the blue wing at Hα, that is, the P Cyg profile was discovered. The P Cyg profile appeared during a limited period in its orbital phase. This profile variation is interpreted to be caused by transient mass ejection episodes.

3.1 Photometric Observations of The 1995 Superoutburst of AL Comae Berenices

3.1.1 Introduction

AL Com is a dwarf nova which has attracted many investigators' interest, but its nature has remained a mystery. The story of AL Com began with the report of Rosino (1961). He discovered a variable star near NGC 4501 (M 88) and suggested that it was a supernova or a U Gem star. He also mentioned that the spectrum at maximum had a blue featureless continuum. Bertola (1964) presented a finding chart and a light curve of the 1961 outburst, which showed a bright state lasting at least 30 days and an approximately 3-mag-deep dip in the course of the bright state. According to Zwicky (1965), AL Com varied in the range $19.0 < m_p < 22.0$ in 1962 January - 1965 January and was $m_p \simeq 13.4$ on 1965 March 26 and 27. Moorhead (1965), then, reported results of photoelectric observations on 1965 March 29.21 (UT): $V = 13.24$, $U - B = -0.42$, $B - V = +0.09$ and that the star was below the photovisual limit magnitude of $m_{pv} = 15.8$-16.0 on April 25.26, May 4.27, May 18.21, May 26.24 and June 2.27. Outbursts were further observed in 1974, 1975, and possibly 1976 (Scovil 1975, Howell & Szkody 1987). Based on these records, Kholopov & Efremov (1976) calculated the outburst cycle to be 325 days. No outburst, however, has been found since the 1976 outburst. Howell et al. (1996a) compiled these (1961, 1974, 1975 and 1976) light curves.

During quiescence, various observations and suggestions have been made, though the faintness have hindered the observations. Howell & Szkody (1988) found 0.4 mag periodic modulations with a best estimated period of 38 min and suggested AL Com to be a DQ Her-type star or (less likely) an AM CVn-type star, a double-degenerate system. Szkody et al. (1989) again found 42 ($\pm$ 1) min modulations and mentioned that AL Com is likely to be a DQ Her star. Spectroscopy by Mukai et al. (1990) revealed strong hydrogen emission lines and ruled out the idea that the variable belongs to the AM CVn type. They interpreted that AL Com is an intermediate polar with a 42 min spin period of the magnetic white dwarf. Further photometric observations by Howell and Szkody (1991), however, gave a power spectrum showing only a single strong period of 84 min and a very weak indication of a period near 40 min. They interpreted this as a change of the

active accretion area in AL Com, behavior often seen in AM Her stars. Abbott et al. (1992) discovered 87-90 min modulations, although these variations were unstable. They interpreted this period as the orbital period. Patterson et al. (1993b) noted that it seems natural to attribute the 84 min period to the orbital period and that the 90 min period found by Abbott et al. (1992) looks like a reasonable candidate for the superhump period.

As described above, the interpretation of AL Com has undergone many changes. The chance, however, to reveal the nature of AL Com has finally come: an outburst was caught in early April 1995 (Mattei 1995). Each of many astronomer groups has hastened to set up their observations.

By late April, Patterson (1995), DeYoung (1995) and Pych and Olech (1995a) found photometric modulations with a period of 81.8 (± 1.4), 81.2, and 81.5 (± 0.2) min, respectively, using their April 5-11 data. Nogami and Kato (1995) pointed out that the modulation period changed from 0.05666 (± 0.00002) day in April 7-12 to 0.0576 (± 0.0002) day on April 17. Spectroscopic observation by Augusteijn (1995) on April 9 revealed shallow wide absorption lines of Balmer series and HeI, which are similar to ones in early stage of a superoutburst in SU UMa-type dwarf novae. He also noted that the total widths of Balmer lines at the continuum level were ~10000 km s^{-1} for Hα to ~5500 km s^{-1} for Hδ and the equivalent widths were ~10 Å for Hα to ~4 Å for Hδ, the color $B-V$ being ~0.0.

Detailed discussion, then, has been published. Howell et al. (1996b) reported that AL Com could not be detected in the sub-mm region during the outburst. Pych and Olech (1995b) mentioned that the modulations observed during 1995 April 10-12 were unstable, but those during 1995 April 20-26 were stable with a period of 0.05729 (± 0.00001) day. They suggested AL Com belongs to WZ Sge-type (Baily 1979; Downes, Margon 1981; O'Donoghue et al. 1991). Kato et al. (1996b) interpreted two types of modulations reported by Nogami and Kato (1995) as "immature" superhumps and genuine superhumps. This adjunction "immature" comes from their idea that those modulations observed at the early phase of the current outburst might grow to usual superhumps seen a week after the onset, which behavior is predicted by the simulation by Whitehurst (1994) based on the tidal-instability model. However, in the following part, we call those humps as the early superhumps in order to make the nomenclature consistent (see Patterson et

al. 1996). Similarities and differences between AL Com and WZ Sge have been discussed also in Kato et al. (1996b). Howell et al. (1996a) found periodic modulations with 81 min period early in the outburst, those with 82.5 min (superhump) period ~10 days after from the maximum, and those with 41 min period throughout the outburst. They suggested that the last two modulations are of related origin and presented a hypothesis on variation of the physical parameters of the accretion disk during the outburst in AL Com. Szkody et al. (1996) obtained optical spectra from 3 to 20 days and UV spectra from the International Ultraviolet Explorer spacecraft (IUE) at 10 and 19 days after the maximum of the outburst. The optical spectra are typical of those observed in dwarf novae during the decline phase from the outburst. There is no evidence of P Cyg profiles in the IUE spectra. The latter IUE spectrum shows the broad Lyα absorption line. Szkody et al. (1996) measured the temperature of the white dwarf to be 25,000 K by model fitting of the line.

3.1.2 Observation

The observations were made using a 60-cm telescope at Ouda Station (Kyoto University) and by a 51-cm telescope at Osaka Kyoiku University. The observations at Ouda were carried out using a CCD camera (Thomson TH 7882, 576 × 384 pixels) attached to the Cassegrain focus of the 60 cm reflector (focal length=4.8 m) at Ouda Station, Kyoto University (Ohtani et al. 1992). To reduce the readout noise and dead time, an on-chip summation of 2×2 pixels to one pixel was adopted.

The observations at Osaka Kyoiku University were carried out using a CCD camera (EEV 88200, 1152 × 790 pixels) attached to the Cassegrain focus of the 51-cm reflector (focal length=6.0 m; for more detail, see section 2 in Yokoo et al. 1994).

An interference filter was used at both observatories, which had been designed to reproduce the Johnson V band. The exposure time at Ouda Station was between 40 and 420 s, depending on the brightness of the object; the dead time between exposures was 12 – 13 s. Bias frames were taken in every ten to twenty object frames. The exposure time at Osaka Kyoiku University was between 90 and 180 s; the dead time between exposures was 30 s. A total of 2227 and 315 useful object frames were obtained at Ouda Station and Osaka Kyoiku University, respectively. The journal of the observations is summarized in

table 2.

The Ouda frames were, after a correction for standard de-biasing and flat fielding, processed by a personal-computer-based automatic aperture photometry and PSF photometry packages developed by Taichi Kato. The differential magnitudes of the variable were determined using a local standard star, V=13.51 (Bertola 1964), whose constancy was checked against two anonymous 15-th mag stars in the same field. A similar procedure was performed for the Osaka Kyoiku University data using the IRAF package. A systematic difference between these two telescopes wes determined by comparing overlapping points. The magnitudes obtained at Osaka Kyoiku University were corrected by subtracting 0.146 mag so as to match the more abundant Ouda data. This correction was confirmed to introduce no detectable bias to the resultant light curve, at least to a level of 0.01 mag. A heliocentric correction to the observed times was applied before a following analysis.

Figure 3 shows the whole light curve we obtained.

3.1.2.1 The first stage of the outburst

As reported in Kato et al. (1996b), periodic modulations were discovered within two days of the outburst maximum. On the first night of our observation, a double-humped modulation (see figure 2 in Kato et al. 1996b) with an amplitude of about 0.1 mag clearly exists. This feature, with a period of 0.05666 $\pm$ 0.00002 day (Kato et al. 1996b), showed a continuous decay in amplitude until Apr. 12 (figure 3). The outburst decline rate in this phase is 0.13 mag d^{-1}, which is a typical value during the plateau phase of superoutbursts in SU UMa stars (Warner 1995b).

Thereafter, the decline rate suddenly decreased to 0.09 mag d^{-1} around HJD 2449820. Howell et al. (1996) mentioned that the variable once stayed at almost constant brightness for about five days, which they called a "standstill" or "glitch" (see also Kuulkers et al. 1996), and entered the gradual decline phase. Their opinion is, however, mostly based on the visual data. Judging from figure 1 in this paper and figure 2 in Howell et al. (1996a), clearly acceptable seems to be the view that AL Com entered the gradual decline phase

[2] IRAF is distributed by the National Optical Astronomy Observatories, U.S.A.

without a "standstill" just after the initial rapid decline. WZ Sge showed similar behavior in the 1978 outburst (see light curves given by Ortolani et al. 1980 and Patterson et al. 1981).

It is worth noting that another short-term modulations had grown up to 0.2 mag by April 17, the early day of gradual decline phase (figure 5). The light curve of the modulations is of a definitely single-peaked, fast rising and slowly declining triangular shape, typical one for superhumps in usual SU UMa stars. This feature was identified to be genuine superhumps with a period of 0.05722 $\pm$0.00010 day in AL Com in Kato et al. (1996b) (see also Pych & Olech 1995 and Howell et al. 1996). As the superoutburst was proceeding, the amplitude of the superhumps gradually became smaller, and finally reached 0.1 mag on April 28, a few days before the rapid decline.

Table 3 lists the times of superhump maxima measured in the light curve we obtained, those measured from figures by Pych and Olech (1995b) by eye and those given by Howell et al. (1996a). Cycle counts in the table were calculated for the period of the early superhumps (0.05666 day). The last points of a cycle count of 499 include an error of $\pm$1 in the count. Figure 6 shows these timings. By fitting the data with cycle counts between 200 and 400, we obtained a quadratic polynomial:

$$O - C = 1.18(\pm 0.19) \times 10^{-6} E^2 - 2(\pm 11) \times 10^{-5} E - 1.6(\pm 1.6) \times 10^{-2}, \qquad (8)$$

where E represents a cycle count calculated from the first hump-maximum we caught on April 7. Note that the equation indicates the superhump period became longer.

AL Com suddenly decayed 28 days after the onset of the current outburst (figure 3), which we regard as the end of the first stage. There seems to be no difference between the light curve around the termination of this outburst and those in usual SU UMa stars. The light curve of the 1978 superoutburst in WZ Sge also exhibits almost the same behavior (Ortolani et al. 1980; Patterson et al. 1981), and the both star entered the second stage after dawdling a few days at a level a few mag brighter than their quiescence.

3.1.2.1 The second stage

The enhanced light curve during HJD 2449836 - 2449858 is drawn in figure 7. After the temporary minimum around HJD 2449840, AL Com recovered up to about $V = 15.2$.

CCD images obtained by Pietz (1995) confirm the dip. After a subsequent decline to $V = 15.8$, the variable became bright again to $V = 15.2$ on HJD 2449844. Since then, the light curve of AL Com became flat again. The first maximum was caught only by visual observations and probably includes some error in magnitude. However, AL Com was declining with a rate of about 0.8 mag d^{-1} on March 5 (figure 8), which supports the secondary dip episode.

In addition, within a week from recovery, the object again started to show a low-amplitude modulation. An analysis gives a period of 0.05737 ($\pm$ 0.0004) day consistent with the superhump period observed earlier. The light curve during HJD 2449846 - 2449848 folded with the period is shown in figure 9. This finding is first to clearly demonstrate that "after-the-dip" behavior traces the usual course of a superoutburst.

After the plateau phase with superhumps, AL Com started to show rather irregular variability with a time-scale of hours to a day. The superhumps seemed to have completely disappeared (figure 10 and figure 11). Soon after this stage, the object showed a precipitous decline with a rate of about 1 mag d^{-1}. The quiescent magnitude was not yet reached during our observations. AL Com stayed at about $V = 18.6$ at least for some days after the rapid decline. Our additional observation on 1995 July 25 told that the variable had reached $V = 19.6 \pm 0.4$.

3.1.3 Discussion

3.1.3.1 The first stage

In Kato et al. (1996b), we proposed an interpretation that the modulations observed just after maximum with a period shorter than that of the genuine superhump are early superhumps, whose period is close to the orbital period rather than the superhump period. Our findings of the double-peaked shape and the declining of modulation amplitude (figure 4) before appearance of genuine superhumps might be the key to understand the nature of the modulation.

We propose two additional possible models causing the modulation; 1) a "jet" model (see figure 12), and 2) a "thickened-edge" model (see figure 13).

In the former model, imagine that bipolar "jets" spouted due to sudden increase of the mass accretion rate at the onset of the outburst. The jet consists of a component approaching us and a receding component. In this case, the eclipse of the latter component by the secondary star and the singly peaked early superhump can cause the double-peaked modulation, while the approaching component is never eclipsed. The model requires that the contribution of the jet to the total brightness was at least 5-10 % in the V band, since the amplitude of the modulation is 0.05-0.1 mag (figure 2).

The decline of the modulation amplitude would represent that the jet became weaker as the outburst was going. Szkody et al. (1996) shows that the IUE spectra obtained on April 16 and 25 have no evidence of P Cyg profiles, which suggests no jet until April 16 or had extinguished before their observation. Note that it may be because the P Cyg profile by the jet can be detected by IUE only when the binary is viewed nearly pole-on. Anyway, UV observations at the very early phase of the superoutburst in WZ Sge stars are interesting in this respect.

The shape of the modulation in the 1987 outburst of WZ Sge is singly peaked (Patterson 1978). This might be because only the approaching component of the jet spouted or the jet did not exist.

In the latter model, imagine that the thickness of the accretion disk is non-axisymmetrically enhanced when the outburst occurred, and the geometrical obscuration of the inner part of the disk yields the modulation. This idea is similar to the model proposed in order to reproduce the light curve of the supersoft source, CAL 87 by Schandl et al (1997), although the mass-transfer rate of WZ Sge stars are thought to be smaller by a few order of magnitude than that of the supersoft X-ray sources. The disappearance of the modulation may mean that the non-axisymmetry leveled off as the superoutburst progressed. Some constraints on this model would be obtained by observations of the color variation with a time scale of the orbital period, since large variation is expected as the inner portion of the accretion disk is hidden by the edge with low temperature in this model. Multi-wavelength simultaneous photometry (or time-resolved spectroscopy) of the next outburst is highly desirable.

In both models, the modulations are caused by the eclipse. Determination of the inclination of AL Com is crucial for these models. RE J1255+266, an EUV transient,

is suggested to have a very low inclination ($i < 5°$) and to be similar to WZ Sge stars (Watson et al. 1996). If an outburst in this variable is detected in optical range, it will give most important information on this subject.

While WZ Sge stars are a subgroup of SU UMa stars which exhibit quite rare outbursts, there is another subgroup, ER UMa stars (ER UMa, V1159 Ori and RZ LMi: Nogami et el. 1995a, and references therein, and most recently discovered one, DI UMa: Kato, Nogami, & Baba 1996a) which show quite frequent outbursts. Note that ER UMa stars, which have short orbital periods comparable to those of WZ Sge stars, show similar modulations near maximum of superoutbursts. These modulations also seem to disappear before entering the gradual decline phase in ER UMa (Kato, Nogami, & Masuda 1996c) and V1159 Ori, although the superoutbursts appear to end before the phase in RZ LMi and DI UMa. Since ER UMa stars and WZ Sge stars have the shortest orbital periods among the SU UMa-type dwarf novae, there may exist a mechanism causing appearance of the modulations at the initial phase of superoutburst in such dwarf novae with ultra-short orbital periods. Observers should therefore start observations as early as possible.

ER UMa is suggested to be a nearly pole-on dwarf nova based on the narrowness of its emission lines, non-detection of its orbital motion, and the presence of a P Cyg profile of C_{IV} (Ringwald 1993). Since it is hard to consider the eclipse of jets or the effect of the bulging of the disk in CVs with such low inclinations, the above models will not apply to the cause of the modulations in ER UMa. If the origins of the early modulations in WZ Sge stars and ER UMa stars are proved to be same, the models proposed here may be precluded.

While the modulation observed at the start of the superoutbust in ER UMa have a period the same as the superhump and an amplitude larger than the superhump (Kato et al. 1996c), the first modulation in AL Com have a period shorter than the superhump and an amplitude smaller than the superhump. These differences might be explained by the following; 1) fully grown superhumps may be observable in ER UMa stars since the normal outburst just before a superoutburst triggers the tidal instability, and 2) only immature ones may exist in WZ Sge stars since there is no outburst triggering the instability. If this

[2] Recently Meyer-Hofmeister et al. (1998) proposed a model where the accretion disk in WZ Sge extends to the 3:1 resonance radius a few years before the next superoutburst

explanation is true, the amplitude of the superhump repeat decay and growth a few times during an outburst in AL Com and ER UMa. These variations have not been reported so far, but the similar phenomenon was recently observed in V1028 Cyg (Baba et al. 1996, in preparation). More observational and theoretical study is needed to clarify the nature of the modulations.

Figure 6 shows the $O-C$ diagram for the timings of hump maxima based on the data listed in table 3. In the figure, we can see that the period of the modulations observed in the early stage of the outburst (early superhumps) is stable and the superhump period became longer. According to the equation (8), the rate ($\dot{P}$ / P) is 7.36×10^{-4} cycles. Although this type of variation has been found in SU UMa type dwarf novae with thorough coverage of superoutbursts, all rates have negative values (for a recent example, V1159 Ori; Patterson et al. 1995, see also, Patterson et al. 1993b). Our finding that AL Com has the positive value also implies that the physical conditions of the accretion disk in AL Com had varied in this superoutburst in a different way from those in usual SU UMa stars.

The fitted curve crosses the line of $O-C=0$ near the cycle count of 120. Since data were not obtained near that time, it is difficult to mention the physical status of the accretion disk at the transition between the two types of modulations. The points with cycle counts of 91 and 151, however, have values of $O-C$ near the half of the period, which means that the peaks of these cycle counts came amid other modulations. These points might represent "genuine" immature superhumps. In other words, superhumps began to grow about that time.

3.1.3.2 The dip

We do not have enough observational evidence about the origin of the dip. The decline rate, however, seems to be about 1 mag d^{-1}, calculated from the visual observations on HJD 2449838 and our data obtained on HJD 2449841, which is a typical value for the final decline of superoutbursts in SU UMa stars (Warner 1995b) and suggests that the dip may be produced by a thermal transition wave starting from the outer accretion disk

[2] After Nogami et al. (1997a) was published, several dwarf novae with $\dot{P}_{SH} > 0$ have been discovered. See section 2.1

(see figure 7).

The magnitudes during the dips were about or over 2 mag above quiescence in both AL Com and WZ Sge (see also figure 10 in Howell et al. 1996a). This implies that the inner part of the accretion disk remained hot even during the dip. The recovery rate is about 3 mag d^{-1} or less, which is smaller than that during the rising phases of superoutbursts in usual SU UMa stars, for recent example, Jensen (1996) reported that SW UMa had risen from $m_{vis} = 14.0$ to $m_{vis} = 11.4$ in about 0.15 day at the 1996 April superoutburst.

This implies that the recovery represents "inside-out" propagation of the thermal transition wave. This idea is supported by two reasons; 1) such an outburst is expected to rise slowly (e.g. Cannizzo, Wheeler, & Polidan 1986), and 2) the mass was accreted and insufficient for thermal transition at the outer edge of the accretion disk.

3.1.3.3 The second stage

After the dip, AL Com showed a short-lived maximum followed by a decline (figure 7). Nonexistence of orbital humps during this stage strongly supports that the recovery from the dip was not powered by a mass-transfer event, but by the thermal instability of the accretion disk.

After this "secondary dip", the star again entered the "plateau phase". The same features can be traced in the light curve of WZ Sge during 1978 outburst. However, the duration between the short-lived maximum and the plateau phase is about two days in the current outburst (figure 7) while it was at least 5 days in the 1978 outburst of WZ Sge (see figure 1 in Ortolani et al. 1980). The plateau phase lasted only about 9 days in the present outburst, while it did over 20 days in the 1978 outburst of WZ Sge. These differences might come from the difference of the superoutburst cycle length, when the mass is accreted, 20 years in AL Com and 33 years in WZ Sge.

As already described in Section 3.1.2.2., the superhumps grew during this phase (figure 7). We can therefore identify this stage as a start of a new superoutburst. A short-lived maximum after the main dip may represent a normal outburst which triggered this "second" superoutburst.

The final decline with a rate of 1 mag d^{-1} (figure 7) can be again considered to represent the propagation of a thermal transition wave through the accretion disk. The disappear-

ance of superhumps a few days before this decline (figures 10 and 11) implies that the cessation of the tidal instability is responsible for the decline.

After the decline, AL Com stayed about 1 mag brighter than the quiescence (figure 3). Although the observational materials are limited due to its faintness, it is likely that some inner part of the accretion disk remained hot even after the final decline. This mechanism may be responsible for the long fading tail of the 1978 outburst in WZ Sge, which still remains poorly understood. A similar phenomenon was also observed after the main (or super-) outburst of GRO J0422+32, a ultrasoft X-ray transient (USXT), which have been pointed out to have a number of similarities with WZ Sge-type dwarf novae (e.g. Kuulkers et al. 1996). Measurement of the contribution of the accretion disk and the hot spot to the observed light may be a clue in understanding this poorly understood unique feature of WZ Sge-type dwarf novae and USXTs. The persistent "superhump" periodicity observed in HV Vir, another object very similar to WZ Sge, during the same stage by Leibowitz et al. (1994) supports a significant contribution to the light from the accretion disk at this stage. [Although this modulation was originally ascribed to an orbital modulation (Leibowitz et al. 1994), a new analysis by Kato & Sekine (1999, in preparation) strongly favors the persistent superhumps.]

3.1.4 Summary

This study on AL Com is summarized as follows.

1. For the early superhump with a period shorter than the superhump period, we propose two new models, the "jet" model and the "thickened-edge" model in addition to the immature superhump model noted in Kato et al. (1996b).

2. The superhump period became longer as the superoutburst progressed.

3. A dip was observed in the course of the current outburst as seen in the 1978 superoutbust of WZ Sge. This dip may be caused by a thermal transition such as the termination of outbursts of usual dwarf novae. However, AL Com was brighter by about 3 mag than its quiescence.

4. AL Com recovered from the dip slowly, which might represent a "inside-out" type of the thermal transition in the accretion disk.

5. After the recovery, AL Com again declined and rose about 0.5 mag. Then, the superhumps with the same period as those seen in the first stage were observed. We identified the behavior after the dip as the second superoutburst.

6. The superhumps in the second superoutburst had extinguished before the final decline.

7. AL Com stayed about or over 1 mag brighter than its quiescence at least two weeks after the end of the outburst. The inner part of the accretion disk might remain at its hot state during the dip and after the outburst.

3.2 Discovery of the in-the-Gap Dwarf Nova, NY Serpentis

3.2.1 Introduction

The orbital period distribution of hydrogen-rich cataclysmic variables (CVs) has been suggested by many works (e.g. Robinson 1983) to have two major characteristics, which are 1) the period gap of about 2–3 hours where markedly reduced number density is seen, and 2) the sharp cut-off at the shorter edge about 80 min. The standard scenario of the CV evolution has been developed to explain these characteristics (for a review, see e.g. King 1988).

In the scenario, a CV evolves by decreasing its orbital period due to angular momentum loss by magnetic stellar wind braking (e.g. Verbunt, Zwaan 1981) above the period gap. The magnetic braking stops at the upper edge of the period gap when the secondary star becomes fully convective. Then, the mass transfer stops since the secondary shrinks into its Roche-lobe. The angular momentum loss, however, continues by gravitational wave radiation (e.g. Landau, Lifshits 1958). The mass transfer restarts at the lower edge of the period gap when the secondary fills its Roche-lobe again due to shrinkage of the binary system.

No dwarf novae has actually been confirmed in the range of the orbital period between 2.8 hr (TU Men) and 2.1 hr (IR Com = S 10932), although several nova-likes including post-novae and some fraction of magnetic systems has been discovered (see Ritter, Kolb 1998).

3.2.2 Observation

We made photometric observations on 86 nights between 1995 July 25 and 1997 March 11 at Ouda Station, Kyoto University (see the description in section 3.1.2). The observation procedure was same as that in the AL Com observation. The journal of observations are summarized in table 4.

3.2.3 Results and Discussion

The long-term light curve with an amplitude of V=14.6–18.0 is shown in figure 14. Besides the short normal outbursts with a recurrence time of 6–9 days, we can clearly find long-

lasting outbursts. Figure 15 shows results of time-resolved photometry of the first long outburst caught on HJD 2450195. On 1996 April 21, only small-amplitude ($\sim$ 0.05 mag) oscillations with a time scale of about a few 10 min may be seen. We, however, succeeded in revealing fully developed superhumps with an amplitude of 0.3 mag during April 23–25, revealing the SU UMa nature of NY Ser and that the long outburst is a real superoutburst.

After removing the linear trend of decline of those 3-day data, we performed a period analysis using the Phase Dispersion Minimization (PDM) method (Stellingwerf 1978), which indicates 0.106 ($\pm$ 0.001) d as the best estimated superhump period. Figure 16 shows the theta diagram and the light curve folded by the period. As the superhump period is known to have a close relation to the orbital period, we obtained a following equation using SU UMa stars with both periods measured listed in table 1:

$$P_{SH} = 1.037(\pm 0.003) \times P_{\rm orb}. \tag{9}$$

This equation suggests the orbital period of NY Ser to be 0.101 0.103 d. As the superhump excess ($(P_{\rm SH} - P_{\rm orb})/P_{\rm orb}$) is larger in an SU UMa star with a longer orbital period (table 1, see also Warner 1995), the largest superhump excess of 7.7% is measured in TU Men, which have a superhump period longer than NY Ser. Therefore, the orbital period is, at least, thought to be shorter than 0.098 d calculated using the superhump excess of TU Men. For these reasons, we can conclude that NY Ser has an orbital period near the meddle of the period gap.

Another long outburst lasting at least 15 days around HJD 2450300 is likely to be a super outburst. This suggests that the supercycle is 100 days or its half, as possibilities of its one-third or less are excluded by the data obtained during HJD 2450195–2450229. The variable, however, did not go into superoutburst during HJD 2450507–2450519, although a superoutburst might have ended just before the run. The outburst around HJD 2450465 may be a superoutburst also. It is because the recurrence cycle is meant to be as short as 4 days if the outburst consists of two subsequent normal outbursts. If this outburst was really the third superoutburst we caught, the period between the second one around HJD 2450295 and the third is about 170 days. This value is close to twice of the first recurrence time and we can not find a long outburst in 2450507–2450519 about 40–50 days after the third superoutburst. Thus, we can conclude that we succeeded in catching

three superoutburst and the supercycle seems to be 85–100 days.

Our observations are summarized as below: 1) NY Ser is an SU UMa type dwarf novae with a small amplitude of 3.4 mag, 2) its orbital period is thought to be near the middle of the period gap based on the superhump period of 0.106 (± 0.001) d, and 3) NY Ser seems to have a short supercycle of 85–100 days and a short recurrence time of the normal outburst of 6–9 days.

As mentioned above, NY Ser is the first dwarf nova whose estimated orbital period is located at the center of the period gap, though confirmation of the orbital period is still needed. On the contrary, the mass transfer rate of NY Ser is thought to be rather high for an SU UMa star because its supercycle is the fifth shortest among SU UMa star (table 1) and the supercycle is roughly proportional to $1/\dot{M}_{\rm tr}$ (equation 6). Since NY Ser may have peculiar properties, determination of the mass of each star and of the chemical abundance is desired. If the mass of the primary white dwarf is close to the Chandrasekhar limit, the secondary star may have mass enough to maintain the magnetic braking, even under the constraint that the tidal instability thought to cause the superoutburst works only in a dwarf nova with a mass ratio of the secondary mass to the primary mass less than 0.25 (for a review of the disk instability, see e.g. Osaki 1996). It has also been suggested by many works (e.g. Stehle et al. 1997) that the location and the width of the period gap depends on the chemical abundance.

If NY Ser is proven to have ordinal physical parameters and chemical abundance, we have to reconsider the evolution scenario of dwarf novae, taking NY Ser into account.

Nogami et al. (1995a) suggested two possibilities on the evolution of ER UMa stars: 1) ER UMa stars evolve on a entirely different evolutionary path from that of usual SU UMa stars, and 2) (some of) usual SU UMa-stars spend some fraction of its lifetime as high mass-transfer systems. In the sense of 1), NY Ser may be evolving on the ER UMa path in the period gap of usual SU UMa stars, though NY Ser is thought to have a mass transfer rate smaller than ER UMa stars based on the longer supercycle by a factor of 2 or more than those of ER UMa stars. In the sense of 2), NY Ser may be on the way from nova-likes to 'quiet' dwarf novae or vice-versa. If a nova shell is detected by the imaging in the infrared or radio region or the old behavior is revealed by searching old plate-archives, it will be a crucial evidence of the second possibility.

The other possibility is that NY Ser became semi-detached in the period gap. Politano (1996) suggested that about 20% of CVs come to be semi-detached in the period gap. In this case, the existence of NY Ser in the period gap is explainable. The high mass-transfer rate, however, is still left unexplained, since the mass transfer should be controlled by the gravitational wave radiation in the period gap as well as below the period gap.

For testing the above possibilities, NY Ser must be a key object in investigating the CV evolution.

3.3 Spectroscopic and Photometric observations of a Z Cam star, AT Cancri during standstill

3.3.1 Introduction

AT Cnc was discovered by Romano and Perissinotto (1968), and designated as GR 151. Bond and Tifft (1974) found broad, shallow hydrogen absorption lines and possible presence of Na D absorption. They suggested AT Cnc to be an eclipsing binary system composed of the DA white dwarf and a faint red dwarf companion. Greenstein et al. (1977b) noted a spectrum of AT Cnc, which had shallow hydrogen absorption lines with superposed rapidly variable emission lines. The almost same result was published by Greenstein et al. (1977a), but they added some notes that Hα was an emission and the other hydrogen absorption lines were too shallow and weak for a 9500-K DA white dwarf which matches the continuum of AT Cnc. We judge the spectra in Greenstein et al. (1977a, b) to have been obtained during a standstill because of the V magnitude of 13.6 at that time and similarity with our spectra which will be described in subsection 4.2.

Intensive observations with plate emulsion were then carried out by Meinunger (1981), Götz (1983, 1985, 1986, 1988a, 1988b, 1990, 1991), and Huruhata (1984). Götz (1986) detected photometric variations with a period of 0.2386913 d from the data obtained during both the faint ($14.5 \leq m_B \leq 16.5$) and bright states ($12.4 \leq m_B \leq 14.0$), and attributed these modulations to its orbital motion. Götz (1988a, 1988b, 1990, 1991) confirmed the oscillations, but suggested that the shape had varied, accompanying phase shifts of the faintest point.

Zwitter and Munari (1994) measured the equivalent width (EW) of the Hα emission to be 3Å on 1993 December 12, but Hβ was in absorption at that time. They could not detect helium lines and the cool component in the red region ($\lambda > 8000$Å). In 1991 April 28-30, Smith et al. (1997) obtained two spectra, in both of which Hα was an emission line having a P Cygni profile, while the other Balmer lines were in absorption. From the presence of the Na absorption line and the absence of TiO band in their spectra, they suggested that the secondary star is of late-K to early M type, most possibly K7–M0. AT Cnc was in standstill at the times of the observations by Zwitter and Munari (1994) and Smith et al. (1997), judging from observations by members of Variable Star Observers

League in Japan (VSOLJ). These data are available at the URL: ftp://ftp.kusastro.kyoto-u.ac.jp/pub/vsnet/VSOLJ/database/stars/CNCAT.ut.

3.3.2 Observation

In order to examine the physical status of the accretion disk in standstill, we observed AT Cnc on 1997 February 1, 3, and 5 photometrically, and on 1997 February 4, 5, and 6 spectroscopically. Table 5 lists the journal of our observations.

The photometric observations were carried out at the Ouda Station (details are same as those in the case of AL Com).

Figure 17 is a finding chart of AT Cnc. The magnitude of AT Cnc was measured by differential photometry relative to the star C_I of $V = 12.15$ in the VSNET chart calibrated by using Misselt (1996) (URL: ftp://ftp.kusastro.kyoto-u.ac.jp/vsnet/charts/AT_Cnc.ps). Differential magnitudes of the check stars, C_{II} and C_{III}, relative to C_I assured that the nominal 1-σ error did not exceed 0.03 mag for all the photometric frames and the magnitude of C_I was constant within the error throughout the runs.

For the spectroscopic observations, we used a 1.88 m telescope with the New Cassegrain Spectrograph which equipped a 150 grooves mm^{-1} gratings (hereafter, abbreviated to 150G) and a 600 one (hereafter, 600G) at the Okayama Astrophysical Observatory (a branch of the National Astronomical Observatory, an inter-university research institute operated by the Ministry of Education, Science, Sports and Culture of Japan). The detector was an SI502AB CCD (512 × 512 pixels). The spectral coverages were 4210–7200 Å for 150G and 6090–6863 Å for 600G, respectively. The wavelength resolution is 6.1 Å pix^{-1} in the case of 150G and 1.5 Å pix^{-1} in the case of 600G.

We reduced the spectroscopic data, using the Spectronebulagraph reduction system (SNGRED) developed mainly by M. Yoshida of the National Astronomical Observatory Japan, on IRAF package. The averaged signal to noise ratios (S/N) at the continuum level were 36 for 150G data and 20-32 for 600G data.

3.3.3 Results

3.3.3.1 Photometry

The long-term light curve of AT Cnc between 1995 January and 1998 June is generated from visual observations posted to VSNET (figure 18a). Our photometric observations were carried out during the 1996-1997 long standstill. Figure 18b shows the results making it clear that AT Cnc stayed within 0.1 mag around $V = 13.56$ throughout the runs. Enlarged light curves of each night are drawn in figure 19.

After subtracting nightly averages from all data shown in figure 19, we have applied a program LANCELOT (period analysis using artificial neural networks, Gaspani 1995a, b). Figure 20a shows the resultant G(f) function in the period range from 7 m to 8 h. The maximum point gives the best estimate of the period as 0.249 d, and the light curve folded by the period is drawn in figure 20b. This curve has a doubly peaked shape.

We processed χ-square tests assuming a profile of the sinusoidal curve for 189 data points obtained by averaging a sequence of 5 data points in order to reduce the scatter. The tests yielded three possible periods, 0.132 d, and its two-day aliases, 0.142 d and 0.124 d (figure 21a), for which the significance levels of the one-sided test are given to be 5%, 7%, and 7%, respectively. F-tests for these periods in the model of the Phase Dispersion Minimization method (Stellingwerf 1978) bore the significance level of 21%, 21%, and 22%, respectively. These periods correspond to the small peaks around log(frequency) = 0.88 in figure 20a. The period of 0.124 d is a half of the period indicated in figure 20a. Figure 21b exhibits the singly peaked light curve folded by the period $P = 0.132$ d.

In order to reject a suspicion of spurious period detections caused by uneven data spacings, we applied the same period analyses for five data sets which consist of two columns of the times of observation same as the original one and of the magnitudes randomly shuffled within each day. These procedures yielded peaks different from all above periods with much lower G(f) values for the artificial neural-network period analysis and with much higher significance levels, which supporting the reality of those modulations.

3.3.3.2 Spectroscopy

A low-resolution 150G averaged spectrum obtained from two spectra observed on 1997 February 4 and 5 is shown in figure 22a. We could detect were apparent lines of Hα in emission, Hβ in emission superposed on absorption, Hγ in absorption, and Na D line in absorption. Concerning other lines including HeI and HeII often seen in dwarf novae,

we can mention merely that they were not so strong. The other apparent features are superficial: the strong absorption around 6880 Å and the broad dip around 4600 Å result from oversubtraction of H_2O and O_2 lines, and the broad emission feature around 4420 Å, from the poor normalization.

Figure 22b shows a 600G spectrum of a high S/N (~120) at the continuum level, obtained by combining all 36 spectra. The Hα emission line has a mean equivalent width of 4.4Å and the full width at half maximum is 12.6 Å. The emission line is accompanied by a weak absorption in the blue side in some spectra. This P Cyg-type profile is clearly seen also in spectra published by Smith et al. (1997). Appearance of P Cyg profile is variable in our spectra. Figure 23 demonstrates two typical Hα spectra with no absorption feature and with a strong absorption feature. We will discuss this topic later.

We measured heliocentric radial velocities (V_{Hel}) of Hα in 600G spectra by calculating intensity-weighted-mean wavelengths between zero-intensity ends. We summarize EW, visibility of the P Cyg profile, and the V_{Hel} of Hα in table 6.

We performed parameter search for the velocity curve assuming the sinusoidal shape,

$$V_{\rm Hel} = \gamma + K \times \sin\left(2\pi \times \frac{HJD - T_0}{P}\right). \tag{10}$$

The results are listed in table 7. The epoch for phase 0.0 was determined to be HDJ 2450484.128 for the blue-to-red crossing point in the Hα velocity curve. Figure 24 shows the measured radial velocities against heliocentric Julian Days, where we superimpose the fitting curve expressed by equation 10 with parameter values given in table 7.

16 Z Cam-type dwarf novae are registered in the 6th catalogue of CVs, low-mass X-ray binaries, and related objects (Ritter, Kolb 1998). Among stars in which we confirmed the standstill phase by VSNET/VSOLJ database (available via http://www.kusastro.kyoto-u.ac.jp/vsnet/LCs/index/ and http://www.kusastro.kyoto-u.ac.jp/vsnet/VSOLJ/) in these 16 Z Cam stars, the star having the longest orbital period is UY Pup (P = 0.423 d) and the star having the shortest orbital period is SV CMi (P = 0.127 d). The orbital period of 0.2011 d of AT Cnc is a typical, or slightly shorter one as a Z Cam star.

We also measured variations of the mean wavelength at the half maximum and the quarter maximum and the center wavelength obtained by Gaussian fitting for the data above the half maximum. The results of sine curve fitting to these variations are consistent

with those in table 7.

3.3.4 Binary Elements

Figure 25 shows the observed radial velocities folded by the period of 0.2011 d and the sinusoidal curve with parameters in table 7. The radial velocities of Na D absorption lines and Hα from 150G spectra are also plotted by open triangles and squares, respectively. These radial velocities of Na D are calculated for the simple mean of the doublet as the rest wavelength. If we calculate the rest wavelength weighted by their intensities in the Sun, the radial velocities of Na D should be added by 23 km s^{-1}. In both cases, the phase of the radial velocity variation of Hα is very close to, or a little later than that of Na D. If we calculate the sinusoidal curve having the systemic velocity of 11 km s^{-1} and passing on the two points of Na D in figure 24, the resulting velocity curve of Na D has a semi-amplitude of 80 km s^{-1}, same as that of Hα, and a phase earlier by ~ 0.23 than that of Hα listed in table 7. However, the phase difference measured by using the Na D and Hα only in 150G spectra become much smaller. We conclude that the sources of the Hα emission line and the Na D absorption line are, roughly speaking, in the same direction from the system-gravity center if their motions were limited in the orbital plane.

This scheme might be confirmed by checking phase differences of the radial velocity between Hα emission and absorption components of Hβ and Hγ which are thought to trace the orbital motion of the accretion disk and the white dwarf. However, these latter lines in our 150G spectra, unfortunately, did not give any help, because of large error of radial velocity determination caused by low S/N, contamination of the emission component in Hβ, and poor normalization around Hγ.

The Na D absorption has usually been considered to originate in the secondary star, but the radial velocity variation of the Hα emission line is usually interpreted to trace the orbital motion of the white dwarf. In the below context, we make a discussion keeping in mind two possibilities that both lines of Na D and Hα are originated a) in the secondary and b) in the accretion disk.

We here estimate the primary mass M_1. Under the assumption that the secondary is a

main sequence star filling its Roche lobe, we can use two equations:

$$\frac{R_2}{a} = 0.38 + 0.20 \log q \qquad (0.3 < q < 20, \text{accurate to } 2\%) \tag{11}$$

given by Paczynski (1971) where R_2 is the secondary radius, a is the binary separation, and q is the mass ratio (M_2/M_1), and

$$\frac{R_2}{R_\odot} = \left(\frac{M_2}{M_\odot}\right)^{0.88\pm0.02} \qquad (0.1 < \frac{M_2}{M_\odot} \leq 0.8) \tag{12}$$

deduced by Patterson (1984) as an empirical ZAMS mass-radius relation. In addition to these two equations, the Kepler's third law naturally holds:

$$P^2 = \frac{4\pi^2 a^3}{G(M_1 + M_2)}, \tag{13}$$

where P is the orbital period. The secondary mass can be estimated to be 0.47 $M_\odot$ from the empirical mass-radius relation given by Warner (1995) as equation 2.100:

$$\frac{M_2}{M_\odot} = 3.5 P^{5/4} \quad (0.054 \leq P \leq 0.38). \tag{14}$$

The error is thought to be about 0.05 $M_\odot$. This value is in good accordance with $M_2 =$ 0.46 ($\pm$ 0.02) $M_\odot$ corresponding to K7–M0 main-sequence star suggested by Smith et al. (1997) which can be adopted under the assumption that the possibility a) is true. The coincidence of the secondary mass leads us to derive the primary mass independently on the possibilities a) and b). By calculation using $M_2 = 0.47(\pm0.05) M_\odot$ and $P = 0.2011$ ($\pm$ 0.0006) d, we obtain the primary mass to be 0.9 ($\pm$ 0.5) $M_\odot$ from equations (11) – (13). These masses for the primary and the secondary are very normal for a CV having an orbital period about 0.2 d (see Ritter, Kolb 1998).

In the case of the possibility a), The inclination i of AT Cnc can be also estimated to be 17° ($\pm$5°) by substituting above binary parameters and $K_2 = 80$ ($\pm$ 4) km s^{-1} to the secondary's semi-amplitude in the mass function:

$$f(M_1) = \frac{M_1 \sin^3 i}{(1+q)^2} = \frac{P K_2^3}{2\pi G} = 1.05(\pm0.15) \times 10^{-2} M_\odot. \tag{15}$$

If the radial velocity variation of Hα reflects the orbital motion of the white dwarf (possibility b), the inclination is calculated to be 36° ($\pm$ 12°) by substituting $K_1 = 80$ km s^{-1} in the mass function:

$$f(M_2) = \frac{M_2 q^2 \sin^3 i}{(1+q)^2} = \frac{P K_1^3}{2\pi G}. \tag{16}$$

In both cases, the estimated inclination of AT Cnc is low and is consistent with a fact of no dependence of Hα emission intensity against the phase. Because of such a low inclination, it is hard to suppose that AT Cnc shows orbital humps with an amplitude reaching 0.6 mag in quiescence, as suggested by Götz (1986) under the current view of the orbital hump due to anisotropic radiation from the hot spot. The time-resolved photometry of AT Cnc in quiescence is important to clarify whether the large-amplitude modulations exist in quiescence or not.

3.3.5 Doppler Tomography

We produced two Doppler maps (see Marsh, Horne 1988) in figures 26 and 27 from all the 600G spectra using a software developed by Spruit (1998), which was downloaded from his web page (http://www.mpa-garching.mpg.de/~henk/). Figure 26 is drawn under the assumption that the Hα (and Na D) is originated in the secondary (possibility a). We adopted $M_1 = 0.9\ M_\odot$, $q = 0.511$, $P_{\rm orb} = 0.2011$ d, $i = 17°$, and $\gamma = 11$ km s^{-1} and measured the phase from the blue-to-red crossing point in the Hα velocity curve ($T_0 =$ HJD 2450484.128). If we assume the Hα comes from the accretion disk (possibility b), the Doppler map is given by figure 27 by inputting 36° as the inclination and shifting T_0 by the orbital phase 0.5, keeping the same values for other quantities. The intensity map in figure 27 remains basically the same as figure 26 but rotated by 180°. The distances among marks, the Doppler shade of the secondary and the trajectory in figure 11 are expanded in size, reflecting the increase of the inclination.

In figure 26, we confirmed that the center of the intensity locates in the Doppler shade of the secondary, which is naturally in accordance with the assumption of the possibility a). The 'bright' region, however, is extended around the center by about 500 km s^{-1} and the intensity peaks are tied from the position of (V_x, V_y) $\sim$ (0 km s^{-1}, -130 km s^{-1}) to that about (-220 km s^{-1}, 0 km s^{-1}). Such a region is seen in most of SW Sex stars, a small subgroup of nova-likes (see Thorstensen et al. 1991), for example, BH Lyn (Hoard, Szkody 1997), although the contribution of that region to the total Hα intensity is much lower in AT Cnc in this study than in such SW Sex stars and our spectra do not show an apparent moving dip component in the Hα emission line. This may suggest a mechanism commonly working in Z Cam stars in standstill and in SW Sex stars.

The Doppler map in figure 27 (possibility b) implies that Hα is radiated mainly from the vicinity of the white dwarf and/or the outer region of the accretion disk and partly from the irradiated region of the secondary star. Irradiation to the secondary from the accretion disk and the white dwarf may make the surface of the secondary hotter and extend over the Roche lobe, which emits the Hα. This process may support to maintain the state of mass transfer higher than the critical rate. In this model, the Na D absorption line must be originated in the accretion disk. Patterson et al. (1998c) found this absorption line in EG Cnc, one of WZ Sge-type dwarf novae, during the re-brightening phase after the main superoutburst and concluded that the Na D absorption line was formed in the accretion disk because of broadness of the line at the continuum level and disappearance during the long fading tail. The Na D absorption line may be produced in an accretion disk in a certain different state from that in quiescence.

In the case of Z Cam, intensive spectroscopic studies using Hα were carried out by Robinson (1973) in quiescence and Szkody and Wade (1981) in standstill. Although equivalent widths of Hα in Z Cam measured by Szkody and Wade (1981) were 3 – 6 Å, much smaller than 32.66 Å in quiescence measured by Smith et al. (1997), system parameters (the period of the radial-velocity variation, γ, K, and T_0) obtained by Szkody and Wade (1981) were almost completely consistent with those by Robinson (1973). This suggests that Hα of Z Cam in standstill is emitted from the same region as in quiescence. In order to judge which possibility a) or b) is true, the radial velocity measurement of Hβ, Hγ absorption component is crucial. The comparison of the Doppler map in quiescence and in outburst with the present map will proceed understandings concerning the effect of the secondary-surface state on the mass transfer and the structure of the accretion disk in standstill.

3.3.6 Discussion

As for photometric variations, we made a possible detection of periods of 0.249 d and 0.132 d (or the latter's alias, 0.124 d, or 0.142 d). We can not reject any candidate and we can not strongly assert the presence of that modulation, since the amplitudes of these variations seem quite small, and comparable to or even less than observational errors. The period $P = 0.249$ d is longer than the orbital period by about 24%, and the other period

is shorter than the orbital period by about 34%. These suggest that the oscillations did not originate purely only in the orbital motion. As seen in intermediate polars (IPs, for a review, e.g. Patterson 1994), these photometric waves might be caused by the irradiation effect of the secondary by X-ray or UV photon emitted by the polar cap of magnetized white dwarf with the oblique rotation axis, although the HeII in AT Cnc did not appear as strong as IPs and we can not detect modulations with the expected rotation period of 0.11 d.

Those periods are also different from the period which Götz (1986, 1988a, 1988b, 1990, 1991) claimed to find in the low state and also in the high state. Some doubt concerning reality of Götz's photometric oscillations is still left. The modern time-resolved photometry in quiescence and in outburst would yield interesting results.

The most remarkable feature of the present 600G spectra is the P Cyg profile. From the blue end of the absorption feature, the line-of-sight flow velocity is about 1000 km s^{-1} at maximum. The blue-shifted absorption feature is observed during the only limited phase 0.16 – 0.53 (see table 6), which implies the local formation region, at least not larger than the size of this binary system. The secondary star is moving on the orbital path of around 1/3 phase before the superior conjunction during this phase under the view that the radial velocity variation of Hα accurately traces the orbital motion of the secondary. This may give some hints in considering geometrical structure which makes the absorption feature. There is a fact that the absorption component which clearly appears in a spectrum disappears in the next spectrum obtained only 15 min after. Thus, this absorption feature is transient in its nature and one may introduce mass ejection episodes, for instance, which last for 10 to 30 min, or clumpy flows.

There are many CVs in which the P Cyg profile of the lines in UV (e.g. CIV λ1549) was observed. Except for SW Sex stars and classical novae, however, only two are known to be non-magnetic CVs where the P Cyg profile was observed in the optical range: AT Cnc (Smith et al. 1997; this work) and BZ Cam (Ringwald, Naylor 1998). Although AT Cnc and BZ Cam may be extraordinary systems, the mechanism making outflow from a binary system is a quite interesting subject, which might lead to the jet. It is important to check whether the P Cyg profile is observed during quiescence and during outburst.

3.3.7 Summary

We made time-resolved photometry and spectroscopy of AT Cnc during its standstill phase.

Photometric modulations with an amplitude of ~0.01 mag, which is a little smaller than the observational errors, might be detected at the period of 0.249 d or 0.132 d (or its two-day alias, 0.124 d or 0.142 d). These periods are different from the orbital period and the period found in a series of Götz's works in AT Cnc. It is important to make time-resolved photometry with smaller errors in all states.

Low resolution spectra showed Hα in emission, Hβ in emission superposed on an absorption component, Hγ in absorption, and Na D absorption. We derived orbital elements of AT Cnc from the radial velocity study of Hα: the orbital period $P = 0.2011$ ($\pm$ 0.0006) d, the systemic velocity $\gamma = 11$ ($\pm$ 3) km s^{-1}, the semi amplitude $K = 80$ ($\pm$ 4) km s^{-1}, and the zero point of the phase T_0 = HJD 2450484.128 which is defined so that the blue-to-red crossing point of Hα is at the phase = 0. By using these parameters and under the assumption that the secondary star is a late-type main sequence star filling its Roche lobe, we deduced the primary mass $M_1 = 0.9$ ($\pm$ 0.4) $M_\odot$.

From the closeness of the phases of the Hα and Na D radial velocity variations, we consider two possibilities that the Hα emitting region is 1) on the secondary star and 2) in the accretion disk. In the possibility a), the system inclination was estimated to be 17° ($\pm$ 3°). The Doppler map drawn by using these parameters have peaks tied from the position of (V_x, V_y) ~ (0 km s^{-1}, -130 km s^{-1}) to that about (-220 km s^{-1}, 0 km s^{-1}) on a broadly extended component. These peaks are also seen in most of SW Sex stars. The possibility b) gives the inclination as 36° ($\pm$ 12°). The Doppler map was rotated by 180° from the former one, so the intensity peak locates on the secondary star. Time-resolved spectroscopy with high S/N enough for Balmer lines and the Na D line with full coverage of the phase will promisingly be helpful for solving this problem.

The P Cyg profile of Hα was observed with three characteristics: 1) the profile appears during only the limited phase (0.16 – 0.53), 2) the velocity of the blue edge of the absorption component reached 1000 km s^{-1}, and 3) there is a sequence of spectra obtained at the 15 min interval where the P Cyg profile disappears – appears – disappears, These

characteristics strongly suggest the localized outflow with a short time scale, for example, the transient mass ejection episode or the clumpy flow. Comparison of these results with further time-resolved spectroscopy of Balmer and Na D lines during quiescence and outburst will bring new insight concerning the cause of the P Cyg profile.

4 Summary and Future Works

In this thesis, I reviewed what had been understood by optical photometric and spectroscopic observations of CVs, mainly dwarf novae.

In the field of photometry, super long-term dense monitoring and high speed photometry are presently revealing surprising features of CVs, especially dwarf novae with short orbital periods, unpredictable from the classical view. The collaboration with amateur observer is clearly supplying power to these discoveries. While CVs with shorter $P_{\rm orb}$ are intrinsically fainter and such CVs are dominant in number, the current knowledge is mostly based on observations of relatively bright CVs. A deep CV survey, most possibly by color selection, may find many *incredible* stars, renewing our *standard*.

Spectroscopic observations helped to modeling the accretion disk and determining the binary parameters of CVs. The variable P Cyg profile of Hα in AT Cnc gave a prospect for the problem of the jet formation. The condition for causing transient mass ejection may be understood by comparison of time-resolved spectroscopic observations of AT Cnc (and other dwarf novae) among in quiescence, standstill, and outburst. The same observations should be carried out in X-ray transients. Radio jets have been discovered in X-ray transients after outbursts, for example, GRO J1655–40 (see Tingay et al. 1995), and the trigger of the transient mass ejection may be rooted in the disk instability. If the mass ejection episode in the dwarf nova is found to be related with outburst and/or standstill, the same mechanism may be applied to jets in X-ray transients.

The AT Cnc observation revealed that the Hα emission line and the Na D absorption line originate in the close position. The temperature and the density for making such lines, however, are different. It is significant to specify the source of these lines, since it may lead to clarify the three-dimensional structure of the temperature on the accretion disk or on the surface of the secondary star. The optical time-resolved spectroscopy covering Balmer lines and Na D is crucial also from this point of view.

Recurrence cycles of the normal outburst and the superoutburst in ER UMa stars are supposed to be about one-tenth of the typical values of SU UMa stars. ER UMa stars are located near the shorter edge of the orbital period distribution as well as WZ Sge stars, and those cycle lengths in ER UMa stars are about 1/100 of WZ Sge stars. This suggests

that the mass transfer rate in ER UMa stars are at least by one order of magnitude higher than $\dot{M}_{\rm tr}$ expected from the orbital periods. In these stars, the secondary star is supposed to be in a physical condition different from the secondary in the other dwarf novae. The difference will be made clear by comparison of results of time-resolved spectroscopy between in ER UMa stars and the other SU UMa stars in optical (and in the infrared region where the secondary star is expected to be the dominant source). The irradiation effect on the binary evolution may be also understood by such a study.

Acknowledgment

First of all, I would express my sincere thanks to Ryuko Hirata for useful discussions, comments, continuous encouragement, and all of invisible supports. If I did not meet him, I would give up the astronomical study. In this sense, he changed my life. This change does not head for a worse direction, I hope :-). Thanks are also to Taichi Kato and Shin Minesige for invaluable comments and discussions. They have drugged me into the bog of CV research, but I have enjoyed swimming in the bog. I appreciate Yoji Osaki for having taken care of me in many scenes. The colleagues at this department, especially members of the *KUIDAORE* tour, Motohiko Tsugawa at Univ. of Tokyo, and Kohji Kawabata (the President of the universe!) at Tohoku Univ. and Dodaira observatory have given me pleasant time as well as scientific knowledge. I'm grateful to Hiroshi Ohtani and Yoshio Tomita for the maintenance of the Ouda Station and almost free assignment of the machine time. I highly acknowledge Super Users for maintenance of computers at the sacrifice of their own time for all users. I am indebted to all staffs, postdocs, students of this department for scientific discussions and making good atmosphere I like.

References

Abbott T. M., Robinson E. L., Hill G. J., Haswell, C. A. 1992, ApJ 399, 680

Antipin S. V. 1996, IBVS 4360

Arenas J., Mennickent R. E. 1998, A&A 337, 472

Augusteijn T. 1994, A&A 292, 481

Augusteijn T. 1995, IAUC No. 6160

Augusteijn T., van der Hooft F., de Jong J. A., van Paradijs J., 1996, A&A 311, 889

Baba H., Kato T., Nogami D., Hirata R. 1999, PASJ submitted

Bailey J. 1979, MNRAS 188, 681

Baptista R., Catalán M. S., Horne K., Zilli D. 1998, MNRAS 300, 233

Bateson F. M. 1988, Vistas in Astronomy 31, 301

Beasley A. J., Bastian T. S., Ball L., Wu, K. 1994, AJ 108, 2207

Berriman G. 1984, MNRAS 210, 223

Bertola F. 1964, Ann. d'Ap., 27, 298

Bond H. E., Kemper E. 1982, ApJ 260, L79

Bond H. E., Tifft W. G. 1974, PASP 86, 981

Bruch A. 1983a, IBVS No. 2286

Bruch A. 1983b, IBVS No. 2287

Bruch A., Engel A. 1994, A&AS 104, 79

Burderi L., King A. R. 1998, ApJ 509, 85

Cannizzo J. K., Wheeler J. C., Polidan R. S. 1986, ApJ 301, 634

Chen J. -S., Liu X, -W., Wei M. -Z. 1991, A&A 242, 397

Cordova F. A., Chester T. J., Tuohy I., Garmire G. P. 1980, ApJ 235, 163

Cook M. C. 1985, MNRAS 215, 211

Cropper M. 1990, Space Science Review 54, 195

de Martino D., Gonzalez-Riestra R., Rodriguez P., Buckley D., Dickson J., Remillard R. A. 1992, IAUC No. 5481

DeYoung J. E. 1995, IAUC No. 6157

Downes R. A., Margon B. 1981, MNRAS 197, 35p

Duerbeck H. W., Mennickent R. E. 1998, IBVS 4637

Dyck G. 1990, IAUC No. 5089

Echevarría J. 1983, PhD Thesis, University of Sussex

Echevarría J., Tovmassian G., Shara M., Tapia M., Bohigas J., Jones D. H. P., Gilmozzi R., Costero R., Lepez J. A., Roth M., Alvarez M., Rodriguez L. F., Delara E., Stover R. J., Martinez-Roger C., Garzon F., Asatrian N., Vogt N., Szkody P., Zsoldos E., Mattei J., Bateson F. M. 1996, ApJ 467, 851

Feiswog L., Szkody P., Garnavich P. 1988, AJ 96, 1702

Gaposhkin S. I. 1976, IBVS No. 1204

Gaspani A. 1995a, GEOS Fiche Technique, No. 78

Gaspani A. 1995b, in "Proceedings of the 27th Conference on Variable Star research" (Brno), p37

Gilliland R. L. 1982, ApJ 254, 653

Götz W. 1983, IBVS No. 2363

Götz W. 1985, IBVS No. 2734

Götz W. 1986, IBVS No. 2918

Götz W. 1988a, IBVS No. 3066

Götz W. 1988b, IBVS No. 3208

Götz W. 1990, Mitteilungen über Veränderliche Sterne 12, 60

Götz W. 1991, Mitteilungen über Veränderliche Sterne 12, 111

Green R. F., Schmidt M., Liebert J. 1986, ApJS 61, 305

Greenstein J. L., Arp H. C., Shectman S. 1977a, PASP 89, 741

Greenstein J. L., Oke J. B., Richstone D. 1977b, ApJ 218, L21

Haefner R., Schoembs R., Vogt, N. 1979, A&A 77, 7

Hamuery J. -M., Lasota J. -P., Huré J. -M. 1997, MNRAS 287, 937

Harlafits E. T., Hassall B. J. M., Naylor T., Charles, P. A., Sonneborn G. 1992, MNRAS 257, 607

Hartmann L., Kenyon S. J. 1996, ARAA 34, 207

Harvey D., Patterson J. 1995, PASP 107, 1055

Harvey D., Skillman D. R., Patterson J., Ringwald F. A. 1995, PASP 107, 551

Hassall B. J. M. 1985, MNRAS 216, 335

Henden A. A., Honeycutt R. K. 1995, PASP 107, 324

Hessman F. V., Mantel K. -H., Barwig H., Schoembs R. 1992, A&A 263, 147

Hjellming, R.M., Mioduszewski, A.J. 1998, IAUC No. 6872

Hoard D. W., Szkody P. 1997, ApJ 481, 433

Hoffmeister C. 1966, Astron, Nachr. 289, 139

Honeycutt R. K., Schlegel E. M., Kaitchuck R. H. 1987, ApJS 65, 451

Honeycutt R. K., Turner, G. W. 1992, in Robotic Telescopes in the 1990's, ed. A. V. Filippenko (Astronomical Society of the Pacific, San Francisco), p77

Honeycutt R. K., Vesper D. N., White J. C., Turner G. W., Adams B. R. 1990, in CCD's in Astronomy II, ed. A. G. D. Philip, D. S. Hayes, and S. J. Adelman (Schenectady, L. Davis Press), p177

Horne K. 1993, in Accretion Disks in Compact Stellar Systems, ed. J. C. Wheeler (World Science Publications Co., Singapore), p117

Horne K., Marsh T. M. 1986, MNRAS 218, 761

Horne K. Stiening R. F. 1985, MNRAS 216, 933

Howell S. B., DeYoung J. A., Mattei J. A., Foster G., Szkody P., Cannizzo J. K., Walker G., Fierce E. 1996a, AJ 111, 2367

Howell S. B., Herzog A., Robson I. 1996b, AJ 111, 899

Howell S. B., Hurst G. M. 1994, IBVS No. 4043

Howell S. B., Liebert J. 1994, IBVS No. 4073

Howell S. B., Mitchell K. J., Warnock A. 1987, PASP 99, 126

Howell S. B., Mason K. O., Reichert G. A., Warnock A., Keidl T. J. 1988, MNRAS 233, 79

Howell S. B., Reyes A. L., Ashley R., Harrop-Allin M. K., Warner B. 1996c, MNRAS 282, 623

Howell S. B., Schmidt R., DeYoung J. A., Fried R., Schmeer P., Gritz L. 1993, PASP 105, 579

Howell S. B., Szkody P. 1988, PASP 100, 224

Howell S. B., Szkody P. 1990, ApJ 356, 623

Howell S. B., Szkody P., Kreidl T., Dobrzycka D. 1991, PASP 103, 300

Howell S. B., Wagner R. M., Bertram R., Szkody P. 1992, IAUC No. 5503

Huruhata M. 1984, IBVS No. 2556

Iida M., Nogami D., Kato T. 1995, IBVS No. 4208

Iriarte B., Chavira E. 1957, Boletin de Los Observatorios Tonantzintla y Tacubay 16, 3

Jensen T. 1996, vsnet-obs 2562

Kato T. 1991, IBVS No. 3671

Kato T. 1993, PASJ 45, L67

Kato T. 1995a, IBVS No. 4243

Kato T. 1995b, IBVS No. 4152

Kato T. 1995c, IBVS No. 4242

Kato T. 1996a, PASJ 48, 777

Kato T. 1996b, IBVS No. 4369

Kato T. 1997a, PASJ 49, 583

Kato T. 1997b, vsnet-alert 940

Kato T., Fujino S., Iida, M. 1989, Var, Star Bull. Japan 9, 33

Kato T., Hirata R., Mineshige S. 1992, PASJ 44, L216

Kato T., Kunjaya C. 1995, PASJ 47, 163

Kato T., Kunjaya C., Okyudo M., Takahashi A. 1994, PASJ 47, L199

Kato T., Nogami D. 1997a, PASJ 49, 341

Kato T., Nogami D. 1997b, PASJ 49, 481

Kato T., Nogami D., Baba H. 1996a, PASJ 48, L93

Kato T., Nogami D., Baba H., Masuda S., Matsumoto K., Kunjaya C. 1999a, in Disk Instabilities in Close Binary Systems, ed S. Mineshige and C. Wheeler (United Academy Press, Tokyo), in press

Kato T., Nogami D., Baba H., Matsumoto K., Arimoto J., Tanabe K., Ishikawa K. 1996b, PASJ 48, L21

Kato T., Nogami D., Masuda S. 1996c, PASJ 48, L5

Kato T., Nogami D., Masuda S., Baba H. 1998a, PASP 110, 1400

Kato T., Nogami D., Masuda S., Hirata R. 1995, IBVS No. 4193

Kato T., Nogami D., Masuda S., Hirata, R. 1996d, PASJ 48, 45

Kato T., Nogami D., Matsumoto K., Baba H. 1999b, ApJ, submitted

Kemp J., Patterson J. 1996, vsnet-obs 3461

Kholopov P. N., Efremov Y. N. 1976, Perem. Zvezdy 20, 277

Kholopov P. N., Samus N. N., Kazarovets B. V., Frolov M. S., Kireeva N. N. 1989, IBVS No. 3323

King A. R. 1988, QJRAS 29, 1

Kiyota S., Kato T. 1998, IBVS 4644

Krzeminski W., Kraft R. P. 1964, ApJ 140, 921

Kunjaya C., Kato T., Hirata R. 1994, IBVS No. 4023

Kurochkin N. E. 1970, Perem. Zvezdy 17, 186

Kuulkers E., Howell S. B., van Paradijis, J. 1996, ApJ 462, L87

Landau L, Lifshitz E. 1958, The Classical Thoery of Field (Pergamon Press, Oxford)

Lasota J. -P., Hameury J. -M., Huré J. -M. 1995, A&A 302, L29

Leibowicz E. M., Mendelson H., Bruch A., Duerbeck H. W., Seitter W. C., Richter G. A. 1994, ApJ 421, 771

Lemm K., Patterson J., Thomas G., Skillman D. R. 1993, PASP 105, 1120

Levy D. H., Howell S. B., Kreidl T. J., Skiff B. A., Tombaugh C. W. 1990, PASP 102, 1321

Liller W. 1996, IBVS No. 4299

Livio M., Pringle J. E. 1992, MNRAS 259, 23p

Livio M., Truran J. W. 1992, ApJ 389, 695

Lubow S. H. 1991, ApJ 381, 259

Marsh T. M., Horne K. 1988, MNRAS 235, 269

Marsh T. M., Horne K. 1990, ApJ 349, 593

Mason K. O., Reichert G. A., Bowyers S. 1982, PASP 94, 521

Matsumoto K., Nogami D., Kato T., Baba, H. 1998, PASJ 50, 405 submitted

Mattei, J. A. 1995, IAUC No. 6155

Maza J., Gonzalez L., Wischnjewsky M., Barrientos F. 1992, PASP 104, 1060

Meinunger L. 1981, Mitteilungen über Veränderliche Sterne 9, 59

Meinunger I. 1984, MVS 10, 56

Mennickent R. E. 1994, A&A 285, 979

Mennickent R. E. 1995, A&A 294, 126

Mennickent R. E., Arenas J. 1998, PASJ 50, 333

Mennickent R. E., Diaz M. 1996, A&A 309, 147

Mennickent R. E., Nogami D., Kato T., Worraker W. 1996, A&A 315, 493

Mennickent R. E., Sterken C. 1998, PASP 110, 1032

Meyer F., Meyer-Hofmeister E. 1983, A&A 121, 29

Meyer F., Meyer-Hofmeister E. 1994, A&A 288, 175

Meyer-Hofmeister E., Meyer F., Liu B. F. 1998, A&A 339, 507

Misselt K. A. 1996, PASP 108, 146

Moorhead, J. M. 1965, PASP 77, 468

Moriyama M., Schmeer P. 1991, IAUC No. 5377

Mukai K., Mason K. O., Howell S. B., Allington-Smith J., Callanan P. J., Charles P. A., Hassall B. J. M., Machin G., Naylor T., Smale A. P., van Paradijis, J. 1990 MNRAS 245, 385

Munari U., Zwitter T. 1998, A&AS 128, 277

Munari U., Zwitter T., Bragaglia A. 1997, A&AS 122, 495

Naylor T., Bath G. T., Charles P. A., Hassall B. J. M., Sonneborn G., van der Woerd, H., van Paradijs J. 1988, MNRAS 231, 237

Nogami D., Baba H., Kato T., Novák R. 1998a, PASJ 50, 297

Nogami D., Kato T. 1995, IAUC No. 6164

Nogami D., Kato T. 1995b, IBVS No. 4227

Nogami D., Kato, T. 1997, PASJ 49, 109

Nogami D., Kato T., Hirata R. 1994, IBVS No. 4059

Nogami D., Kato T., Hirata R. 1996, PASJ 48, 607

Nogami D., Kato T., Baba H., Masuda S. 1998b, PASJ 50, L1

Nogami D., Kato T., Baba H., Matsumoto K. 1998c, in Proceedings of the 29th Conference on Variable Star Research, ed Jiří Dušek and Miloslav Zejda (Nicholas Copernicus Observatory and Planetarium Brno, Brno), p145

Nogami D., Kato T., Baba H., Matsumoto K., Arimoto J., Tanabe T., Ishikawa K. 1997a, ApJ 490, 840

Nogami D., Kato T., Masuda S. 1998d, PASJ 50, 411

Nogami D., Kato T., Masuda S., Hirata R., Matsumoto K., Tanabe K., Yokoo T. 1995a, PASJ 47, 897

Nogami D., Kato T., Masuda S., Hirata R. 1995b, IBVS No. 4163

Nogami D., Masuda S. 1997, IBVS No. 4532

Nogami D., Masuda S., Kato T. 1997b, PASP 109, 1114

Novák R. 1997, IBVS 4489

O'Donoghue D. 1987, ApSS 136, 247

O'Donoghue D., Chen A., Marang F., Mittaz J. P. D., Winkler H. 1991, MNRAS 250, 363

Ohtani H., Uesugi A., Tomita Y., Yoshida M., Kosugi G., Noumaru J., Araya S., Ohta K. 1992, Memoirs of the Faculty of Science, Kyoto University, Series A of Physics, Astrophysics, Geophysics and Chemistry 38, 167

Oke J. B., Wade R. A. 1982, AJ 87, 670

Olech A. 1997, Acta Astron. 47, 281

Ortolani S., Rafanell P., Rosino L., Vittone A. 1980, A&A 87, 31

Osaki Y. 1989, PASJ 41, 1005

Osaki Y. 1995a, PASJ 47, 47

Osaki Y. 1995b, PASJ 47, L11

Osaki Y. 1995c, PASJ 47, L25

Osaki Y. 1996, PASP 108, 39

Osaki Y., Shimizu S., Tsugawa M. 1997, PASJ 49, L19

Pietz J. 1995, vsnet-obs 394

Paczynski B. 1971, Annual Review of Astronomy and Astrophysics 9, 183

Paczynski B. 1981, Acta Astron. 31, 1

Patterson J. 1978, IAUC No. 3311

Patterson J. 1979, AJ 84, 804

Patterson J. 1984, ApJS 54, 443

Patterson J. 1994, PASP 106, 209

Patterson, J. 1995, IAUC No. 6157

Patterson J. 1999, in Disk Instabilities in Close Binary Systems, ed S. Mineshige and C. Wheeler (United Academy Press, Tokyo), in press

Patterson J., Augusteijn T., Harvey D. A., Skillman D. R., Abbott M. C., Thorstensen J. 1996, PASJ, 108, 748

Patterson J., Bolt G., Harvey D. A., O'Donoghue D., 1998a, Cataclysmic Variable Circular 165 (vsnet-alert 1622)

Patterson J., Bond H. E., Grauer A. D., Shafter A. W., Mattei J. 1993a, PASP 105, 69

Patterson J., Jablonski F., Koen C., O'Donoghue D., Skillman D. R. 1995, PASP 107, 1183

Patterson J., Kemp J., Gabriel R., Harvey D. A., Stull J., Jensen L., Bolt G. 1998b, vsnet-alert 1859

Patterson J., Kemp J., Skillman D. R., Harvey D. A., Shafter A. W., Vanmunster T., Jensen L., Fried R., Kiyota S., Thorstensen J. R, Taylor C. J. 1998c, PASP 110, 1290

Patterson J., McGraw J. T., Coleman L., Africano J. L. 1981, ApJ 248, 1067

Patterson J., Robinson E. L., Nather R. E. 1977, ApJ 214, 144

Patterson, J., Thomas, G., Skillman, D. R., and Diaz, M. 1993b, ApJS 86, 235

Patterson J., Vanmunster T., Jensen L. 1997a, Cataclysmic Variable Circular 155 (vsnet-alert 1234)

Patterson J., Vanmunster T., Jensen L., Skillman D. R., Harvey D. A., Fried B. 1997b, vsnet-alert 953

Persson S. E. 1988, PASP 100, 710

Piché F, Szkody P. 1989, AJ98, 2225

Pietz, S. 1995, The Astronomer, 32, 41 and CCD images on the cover

Politano M. 1996, ApJ 465, 338

Pych W., Olech A. 1995a, IAUC No. 6162

Pych W., Olech A. 1995b, Acta Astron. 45, 385

Raykov A. A., Yushchenko A. V. 1988, Perem. Zvezdy 22, 853

Remillard R. A., Bradt H. V., Brissenden R. J. V., Buckley D. A. H., Schwarz D. A., Silber A., Stroozas B. A., Touhy I. R. 1994, ApJ 428, 785

Retter A., Leibowitz E. M., Ofek E. O. 1997, MNRAS 286, 745

Richter G. A. 1992, ASP Conf. Ser. 29, 12

Ringwald F. A. 1993, Ph. D. thesis, Dartmouth College

Ringwald F. A., Naylor T. 1998, AJ 115, 286

Ritter H., Kolb U. 1998, A&AS 129, 83

Robertson J. W. 1994a, vsnet-alert 4

Robertson J. W. 1994b, vsnet-alert 6

Robertson J. W., Honeycutt R. K., Turner G. W. 1995, PASP 107, 443

Robinson E. L. 1973, ApJ 186, 347

Robinson E. L. 1983, in Cataclysmic Variables and Related Objects, ed M. Livio, G. Shaviv (D. Reidel Publishing Company, Dordrecht) p1

Robinson E. L., Shafter A. W., Hill J. A., Wood M. A., Mattei J. A. 1987, ApJ 313, 772

Romano G., Minello S. 1976, IBVS No. 1140

Romano G., Perissinotto M. 1968, Pubblicazioni Obsservatorio Astronomico di Padova 151, 9

Rosino L. 1961, IAUC No. 1782

Sanduleak N., Pesch P. 1984, ApJS 55, 517

Schandl S., Meyer-Hofmeister E., Meyer F. 1997, A&A 318, 73

Schoembs R., Vogt N. 1981, A&A 97, 185

Scovil C. 1996, vsnet-obs 4061

Semeniuk I. 1980, A&AS 39, 29

Semeniuk I., Należyty M., Gembara P., Kwast T. 1997, Acta Astron. 47, 299

Shafter A. W., Hessman F. V. 1988, AJ 95, 178

Shafter A. W., Szkody P. 1984, ApJ 276, 305

Shafter A. W., Szkody P., Thorstensen J. R. 1986, ApJ 308, 765

Shahbaz T., Bandyopadhyay R. M., Charles P. A., Wagner R. M., Muhli P., Hakala P., Casares J., Greenhill J. 1998, MNRAS 300, 1035

Shakura N. I., Sunyaef R. A. 1973, A&A 24, 337

Sherrington M. R., Jameson R. F. 1983, MNRAS 205, 265

Smak J. 1983, ApJ 272, 234

Smak J. 1984, Acta Aston. 34, 161

Smith R. C., Sarna M. J., Catalán M. S., Jones D. H. P. 1997, MNRAS 287, 271

Sproats L. N., Howell S. B., Mason K. O. 1996, MNRAS 282, 1211

Spruit H. C. 1998, astro-ph/9806141

Starrfield S. 1989, in Classical Novae, ed. M. F. Bond, A. Evans (John Wiley & Sons, New York) p39

Steeghs D., Harlaftis E. T., Horne K. 1997, MNRAS 290, L28

Stehle R., Kolb U., Ritter H. 1997, A&A 320, 136

Stellingwerf R. F. 1978, ApJ 224, 953

Stolz B., Schoembs R. 1984, A&A 132, 187

Szkody P. 1985, AJ 90, 1837

Szkody P. 1987, ApJS 63, 685

Szkody P. 1989, PASP 101, 899

Szkody P. 1994, AJ 108, 639

Szkody P., Howell S. B. 1992, ApJS 78, 537

Szkody P., Howell S. B. 1993, ApJ 403, 743

Szkody P., Howell S. B., Mateo M., Kreidl T. 1989, PASP 101, 899

Szkody P., Mattei J. A. 1984, PASP 96, 988

Szkody P., Shafter A. W., Cowley A. P. 1984, ApJ 282, 236

Szkody P., Silber A., Sion E., Downes R. A., Howell S. B., Costa E., Moreno H. 1996, AJ 111, 2379

Szkody P., Wade R. A. 1981, ApJ 251, 201

Thorstensen J. R. 1997, PASP 109, 1241

Thorstensen J. R., Patterson J., Shambrook A., Thomas G. 1996, PASP 108, 73

Thorstensen J. R., Ringwald F. A., Wade R. A., Schmidt G. D., Nosworthy J. E. 1991, AJ 102, 272

Thorstensen J. R., Taylor C. J. 1997, PASP 109, 1359

Thorstensen J. R., Taylor C. J., Becker C. M., Remillard R. A. 1997, PASP 109, 477

Thorstensen J. R., Wade R. A., Oke J. B. 1986, ApJ 309, 721

Udalski A. 1988, IBVS No. 3239

Udalski A. 1990a, AJ 100, 226

Udalski A. 1990b, IBVS No. 3425

Udalski A., Szymański M. 1988, Acta Astron. 38, 215

van Amestrongen S., Bovenschen H., van Paradijs J. 1987, MNRAS 229, 245

Vanmunster T. 1996a, Cataclysmic Variable Circular No. 88[‡]

Vanmunster T. 1996b, Cataclysmic Variable Circular No. 97*

Vanmunster T. 1997, Cataclysmic Variable Circular 141 (vsnet-alert 935)

Vanmunster T. 1998, Cataclysmic Variable Circular 164 (vsnet-alert 1583)

van Paradijs J., van der Klis M., Pedersen H. 1989, A&A 225, L5

Verbunt F., Hassall B. J. M., Pringle J. E., Warner, B., Marang F. 1987, MNRAS 225, 113

Vogt N. 1981, Habilitation Thesis, Bochum University

Vogt N. 1983a, A&AS 53, 21

Vogt N. 1983b, A&A 128, 37

Vogt N. 1993, in 2nd Technion-Haifa Conference on Cataclysmic Variables and Related Physics, ed O. Regev and G. Shaviv (Israel Physical Society, Jerusalem), p367

Vogt N., Semeniuk I. 1980, A&A 89, 223

Voikhanskaya N. F. 1996, Astronomy Reports 40, 674

Vrielmann S. 1997, Ph.D. thesis, Göttingen

Wagner R. M., Kaitchuck R. H. 1988, BAAS 20, 461

Wagner R. M., Sion E. M., Liebert J., Starrfield S. G. 1988, ApJ 328, 213

Wagner R. M., Thorstensen J. R., Honeycutt R. K., Howell S. B., Kaitchuck R. H., Kreidl T. J., Robertson J. W., Sion E. M., Starrfield S. G. 1998, AJ 115, 787

Warner B, 1995a, Cataclysmic Variable Stars (Cambridge University Press, Cambridge)

Warner B. 1995b, ApSS 226, 187

Warner B., Livio M., Tout C. A. 1996, MNRAS 282, 735

Warner B., Nather R. E. 1971, MNRAS 152, 219

Warner B., Nather R. E. 1972, MNRAS 156, 297

Warner B., O'Donoghue D. 1988, MNRAS 233, 705

Warner B., O'Donoghue D., Wargau W. 1989, MNRAS 238, 73

Watanabe M., Hirosawa K., Kato T., Narumi H. 1989, Var. Star Bull. Japan 10, 40

Watson M. G., Marsh T. R., Fender R. P., Barstow M. A., Still M., Page M., Dhillon V. S., Beardmore A. P. 1996, MNRAS 281, 1016

Welsh W. F., Wood J. H., Horne K. 1996, in Cataclysmic Variables and Related Objects, ed A. Evans, J. H. Wood (Kluwer Academic Publishers, Dordrecht), p29

Wenzel W. 1987, Astron. Nachr. 308, 75

Wheatley P. J., Verbunt F., Belloni T., Watson M. G., Naylor T., Ishida M., Duck S., Pfeffermann E. 1996, A&A 307, 137

Whitehurst R. 1988, MNRAS 232, 35

Whitehurst R. 1994, MNRAS 266, 35

Wood J. H., Horne K., Berriman G., Wade, R. A. 1989, ApJ 341, 974

Wood J. H., Horne K, Berriman G., Wade R. A., O'Donoghue D., Warner B. 1986, MNRAS 219, 629

Zhang E. -H., Robinson E. L., Nather R. E. 1986, ApJ 305, 740

Zwicky, F. 1965, IAUC No. 1902

Zwitter T., Munari U. 1994, A&AS 107, 503

Zwitter T., Munari U. 1995, A&AS 114, 575

Zwitter T., Munari U. 1996, A&AS 117, 449

Table 1. Parameters of known SU UM stars.

Name	P_{SH} (d)	P_{orb} (d)	m_q^*	m_o^*	T_n (d)	T_s (d)
TU Men	0.1262[1]	0.1172[2]	18.5[3]	11.6[1]	37[4]	194[4]
PG 1510+234	0.106[5]		18.0[5]	14.6[5]	6-9[5]	85-100[5]
GX Cas	0.09297[6]			13.3vis[‡]	50-70[6]	386[6]
YZ Cnc	0.09204[7]	0.0868[8]	15.0[9,10,11,12]	11.0[7]	11[7]	134[7]
V344 Lyr	0.09145[13]		[20[14]	13.8[13]	16[13]	240[13]
DV UMa	0.090[15]	0.085853[15]	19.3[16,17]	14.9[15]	770[15]	
TY PsA	0.08765[18]	0.08400[18]	15.9[18]	12.4[18]	30 - 50[18]	
EF Peg	0.0871[19]		17.7[20]	10.7[19]		
HV Aur	0.0855[21]			14.9[21]		
TU Crt	0.0847[22,23]		17.5B[24]			
BF Ara	>0.083[25]					
BR Lup	0.0821[26,27]	0.0796[27]		13.7B[26]		
V503 Cyg	0.08101[28]	0.07768[28]	17.5[9,28,29,30,31]	13.95[28]	30[28]	89[28]
HS Vir	0.08059[32]		16.4[32]	13.6[32]	8[33]	
DH Aql	0.0805[34]		18.25[35]	12.4vis[34]	66*	300*
PV Per	0.0804[36]			15.3[37]	36[37]	
V419 Lyr	>0.08[6]			14.4pg[38]	8-14[38]	
RX Cha	0.08?[39]					
CU Vel	0.07999[40]	0.07850[41]	16.8[3,41]	10.7[42]	390*	700-900*
AW Gem	0.07943[43]		19.1[9]	13.2[43]		
V1113 Cyg	0.0792[44]		19.4[44]	13.6[44]	28*	170-230*
V630 Cyg	0.079[45]		18.8ccd[‡]	14.0vis[‡]	30-50*	290*
SU UMa	0.0788[46]	0.07635[47]	15.0[9,10,11,12,48,49]	11.3[50]	13[7]	160[7]
TT Boo	0.07811[51]	0.077:[52]	19.6[52]	12.7[51]	40*	245*
Z Cha	0.07740[53]	0.07450[54]	15.6[55]	12.7[56]	82[57]	287[57]
WX Hyi	0.07737[58]	0.07481[59]	14.9[58]	11.4[58]	14[57]	195[57]
VW Hyi	0.07714[60]	0.07421[60]	14.0[10,61,62,63]	8.5[64]	27[57]	179[57]
BE Oct	0.07711[65]		19.4[66]	15.86[65]		

Table 1. (continues)

Name	P_{SH} (d)	P_{orb} (d)	m_q^*	m_o^*	T_n (d)	T_s (d)
CC Cnc	0.0771[67]	0.07352[68]	18.5[48,69]	14.1[67]		370*
HT Cas	0.076077[70]	0.07367[71]	16.4[70,†]	11.3[72]	450[72]	
V1251 Cyg	0.07604[73]		[18.5[74]	12.4vis[75]		1160[73]
VZ Pyx	0.07576[76]	0.07332[68]	16.8[78]	11:[77]		270[78]
AY Lyr	0.0756[7,79,80]		18.5[48,81]	11.0[7]	8-43[79]	205[79]
KV And	0.07434[82]			13.6vis[‡]		
VW CrB	0.0743[83]					
FO And	0.07411[84]	0.07161[85]		14.2[84]	15-23[86]	380*
CY UMa	0.0724[87]	0.06957[85]	17.9[48,69]	12.3[87]	60-100[88]	300[87]
IR Gem	0.071[89]	0.0684[90]	16.7[89]	12.1[89]	26[57]	174[57]
RZ Sge	0.0704[91,92]		17.4[9,48]	12.2[93]	77[57]	266[93]
TY Psc	0.0701[85]	0.06833[85]	17.4[48,85]	11.7[94]	39[57]	333[57]
SS UMi	0.0701[95]	0.06778[85]	16.7[48,96,97]	12.6[97]		
V1504 Cyg	~0.07[98]	0.06951[99]	18.0pg[100]	13.4[98]		
V701 Tau	0.0689[101]			14.4[101]		
SX LMi	0.0687[102,103]	0.06717[103]	16.8[69,102]	13.3[102]	35[102]	250[102]
AK Cnc	0.06749[104]	0.0651[105]	18.9[69,106]	12.8vis[104]	47[104]	
UV Per	0.06641[107]	0.06489[99]	17.5[9,31,107,108]	11.7[107]	390*	960*
AQ CMi	0.06625[109]			14.5[109]		420[109]
DM Lyr	0.066[110]			13.6vis[‡]		230[110]
ER UMa	0.06573[111]	0.06366[112]	15.8[113]	12.9[113]	4.4[113]	43[113]
CT Hya	0.06505[114]		19.9[114]	14.3[114]		
TV Crv	0.0650[115]		19.0[116]	12.2[115]		
EK TrA	0.0649[117]	0.06288 [118]		11.9[117,119]	231[57]	487[57]
OY Car	0.06443[120]	0.06312[121]	15.6[122,123,124]	11.5[57]	25-50[125]	346[57]
VY Aqr	0.0644[126]	0.0631[99,127]	17.3[126,128]	10.3[57]	350*	800*
V1159 Ori	0.0641[129]	0.0622[112,129]	15.4[130]	12.8[130]	4.0[129]	48[129]
V2051 Oph	0.0641[131,132]	0.06243[133]	16.2B[133]			

Table 1. (continues)

Name	$P_{\rm SH}$ (d)	$P_{\rm orb}$ (d)	$m_{\rm q}^{*}$	$m_{\rm o}^{*}$	$T_{\rm n}$ (d)	$T_{\rm s}$ (d)
V436 Cen	0.06383[134]	0.0625[135]	15.5[134]	11.3[134]	32[4]	335[4]
CI UMa	0.0625[136]	0.060[106]	19.1[106]	14.5[136]		140[136]
AQ Eri	0.06225[137]	0.06093[85]	17.6[9,35,48]	12.5vis[138]		300:[57]
BC UMa	0.0619[139]	0.063:[106]	18.4[48,106]	10.9[140]		
V1028 Cyg	0.06154[141]			13.18[141]		1000[141]
HO Del	0.0607[142]			13.5[142]		730[142]
EG Cnc	0.06036[143,144]	0.05997[144]	19.25[143]	12.20[144]		7000[145]
V592 Her	0.06007[146]					
T Leo	0.0602[147]	0.05882[148]	15.8[11,12,148,149]	10.0[150]		420[57]
RZ LMi	0.05946[151]		17.0[151]	14.2[151]	3.8[113]	19[113]
WX Cet	0.05936[87]	0.0582[87]	17.76[66,152,153,154]	9.45pg[155]		1000:[57]
HV Vir	0.05865[156]	0.05799[156]	19.1[156,157,158]	11.5[159]		3500[57]
SW UMa	0.0582[160,161]	0.05681[162]	17.0[11,48,162]	10.4[162]		954[57]
AL Com	0.0572[163]	0.05666[163]	20.5[52]	11.8[163]		7000*
WZ Sge	0.05714[164]	0.05669[164]	15.3[12,48,165,166]	7.8[167]		12000[57]
LL And	0.05700[168]		20[152]	13.8[169]		5000[57]
USNO[△]	0.05672[170]					
V844 Her	0.05602[171]		17.5pg[172]	12.2[173]		220-230[174]
DI UMa	0.0555[175]		18.0[175]	15.1[175]	4[175]	25[175]
V485 Cen	0.04216[176]	0.04060[177]	18.3[177]			

*V magnitudes unless the notations of 'B' 'vis' 'pg' and 'ccd' are added to numbers. These 'B' 'vis' 'pg' and 'ccd' represent a B magnitude, a visual estimation, a photographic magnitude, and an observation with a CCD and no filter, respectively.

*Measured with the VSNET data archive.

†It is known that HT Cas sometimes enter the "low" state (see Wood et al. 1995, Patterson 1981).

‡From the VSNET archive.

△ USNO A-1.0 1425.09823278

Table 1. (continues)

References: [1]Stoltz & Schoembs 1984; [2]Mennickent 1995; [3]Zwitter & Munari 1995; [4]Bateson 1988; [5]Nogami et al. 1998b; [6]Nogami et al. 1998d; [7]Patterson 1979; [8]Shafter & Hessman 1988; [9]Szkody 1987; [10]Echevarría 1983; [11]Sherrington & Jones 1983; [12]Oke & Wade 1982; [13]Kato 1993; [14]Hoffmeister 1966; [15]Nogami et al. 1999, in preparation; [16]Howell et al. 1987; [17]Howell et al. 1988; [18]Warner et al. 1989; [19]Howell et al. 1993; [20]Howell & Liebert 1994; [21]Nogami et al. 1995b; [22]Vanmunster 1998; [23]Patterson et al. 1998a; [24]Maza et al. 1992; [25]Bruch 1983a; [26]O'Donoghue 1987; [27]Mennickent & Sterken 1998; [28]Harvey et al. 1995; [29]Szkody & Howell 1993; [30]Szkody 1989; [31]Szkody 1985; [32]Kato et al. 1998a; [33]Kato et al. 1995; [34]Nogami & Kato 1995b; [35]Vogt 1983a; [36]Kato & Nogami, 1999, in preparation; [37]Romano & Minello 1976; [38]Kurochkin 1970; [39]Kato & Garradd 1998; [40]Vogt 1981; [41]Mennickent & Diaz 1996; [42]Ritter & Kolb 1998; [43]Kato 1996a; [44]Kato et al. 1996d; [45]Nogami et al. 1999, in preparation; [46]Udalski 1990a; [47]Thorstensen et al. 1986; [48]Misselt 1996; [49]Echevarría et al. 1996; [50]Udalski 1988; [51]Kato 1995a; [52]Howell & Szkody 1988; [53]Warner & O'Donoghue 1988; [54]Wood et al. 1986; [55]Bruch & Engel 1994; [56]Harlaftis et al. 1992; [57]Warner 1995b; [58]Bailey 1979; [59]Schoembs & Vogt 1981; [60]van Amerongen et al. 1987; [61]Wheatley et al. 1996; [62]Verbunt et al. 1987; [63]Haefner et al. 1979; [64]Liller 1996; [65]Kemp & Patterson 1996; [66]Howell et al. 1991; [67]Kato & Nogami 1997a; [68]Thorstensen 1997; [69]Szkody & Howell 1992; [70]Zhang et al. 1986; [71]Baba et al. 1999, in preparation; [72]Wenzel 1987; [73]Kato 1995b; [74]Kato, unpublished; [75]Moriyama & Shmeer 1991; [76]Kato & Nogami 1997b; [77]Remillard et al. 1994;p [78]de Martino et al. 1992; [79]Udalski & Szymanski 1988; [80]Nogami et al. 1994; [81]Voikhanskaya 1996; [82]Kato et al. 1994; [83]Novák 1997; [84]Kato 1995c; [85]Thorstensen et al. 1996; [86]Meinunger 1984; [87]Harvey & Patterson 1995; [88]Watanabe et al. 1989; [89]Szkody et al. 1984; [90]Feinswog et al. 1988; [91]Kato 1996b; [92]Semeniuk et al. 1997; [93]Bond & Kemper 1982; [94]Szkody & Mattei 1984; [95]Chen et al. 1991; [96]Udalski 1990b; [97]Mason et al. 1982; [98]Nogami & Masuda 1997; [99]Thorstensen & Taylor 1997; [100]Raykov & Yushchenko 1988; [101]Kato & Nogami 1999, in preparation; [102]Nogami et al. 1997b; [103]Wagner et al. 1998; [104]Mennickent et al. 1996; [105]Arenas & Mennickent 1998; [106]Howell et al. 1990; [107]Udalski & Pych 1991; [108]Kato 1990; [109]Nogami & Kato 1999, in preparation; [110]Nogami et al. 1999, in preparation;

[111]Kato & Kunjaya 1995; [112]Thorstensen et al. 1997; [113]Robertson et al. 1995; [114]Nogami et al. 1996; [115]Howell et al. 1996c; [116]Levy et al. 1990; [117]Vogt & Semeniuk 1980; [118]Mennickent & Arenas 1998; [119]Hassall 1985; [120]Hessman et al. 1992; [121]Wood et al. 1989; [122]Cook 1985; [123]Berriman 1984; [124]Vogt 1983b; [125]Naylor et al. 1987; [126]Patterson et al. 1993a; [127]Augusteijn 1994; [128]Bruch 1983b; [129]Patterson et al. 1995; [130]Nogami et al. 1999, in preparation; [131]Kiyota & Kato 1998; [132]Patterson et al. 1998; [133]Baptista et al. 1998; [134]Semeniuk 1980; [135]Gilliland 1982; [136]Nogami & Kato 1997; [137]Kato 1991; [138]Kato et al. 1989; [139]Kunjaya & Kato 1999, in preparation; [140]Dyck 1990; [141]Baba et al. 1999; [142]Kato et al. 1999, in preparation; [143]Matsumoto et al. 1998; [144]Patterson et al. 1998c; [145]Kato et al. 1999; [146]Duerbeck & Mennickent 1998; [147]Lemm et al. 1993; [148]Shafter & Szkody 1984; [149]Persson 1988; [150]Kunjaya et al. 1994; [151]Nogami et al. 1995a; [152]Mennickent 1994; [153]van Paradijis et al. 1989; [154]Downes & Margon 1981; [155]Gaposhkin 1976; [156]Leibowitz et al. 1994; [157]Szkody 1994; [158]Howell et al. 1992; [159]Kilmartin 1992; [160]Robinson et al. 1987; [161]Nogami et al. 1998a; [162]Shafter et al. 1986; [163]Kato et al. 1996b; [164]Patterson et al. 1981; [165]Ortolani et al. 1980; [166]Warner & Nather 1972; [167]Patterson 1978; [168]Kato & Sekine 1999, in preparation; [169]Howell & Hurst 1994; [170]Patterson et al. 1997a; [171]Patterson et al. 1997b; [172]Antipin 1996; [173]Scovil 1996; [174]Kato 1997b; [175]Kato et al. 1996a [176]Olech 1997; [177]Augusteijn et al. 1996;

Table 2. Journal of observations of AL Com

	Date		Start (UT)		end (UT)		Exp*	N	Site
1995	April	7	11^h	41^m	19^h	14^m	40^s	490	Ouda
	April	8	10	25	18	12	60–120	290	Ouda
	April	9	13	48	14	26	120	18	Ouda
	April	10	13	09	16	59	90	129	Ouda
	April	12	11	36	18	59	80	291	Ouda
	April	13	11	06	11	12	80	5	Ouda
	April	17	10	33	16	41	120	163	Ouda
	April	20	13	32	17	20	90	100	Osaka
	April	20	15	56	18	18	90	85	Ouda
	April	22	10	26	10	46	240	5	Ouda
	April	23	14	35	18	13	90	120	Ouda
	April	28	13	39	17	13	120	60	Ouda
	May	3	11	48	14	54	300	15	Ouda
	May	5	10	43	17	19	360	54	Ouda
	May	6	11	06	17	24	180	95	Ouda
	May	8	10	36	17	07	120	73	Ouda
	May	8	11	53	14	55	120	54	Osaka
	May	9	12	57	16	48	180	57	Osaka
	May	10	11	12	16	12	120	75	Osaka
	May	13	11	01	12	04	120	17	Ouda
	May	17	13	57	16	12	180	29	Osaka
	May	17	14	10	16	36	120	66	Ouda
	May	18	10	32	16	31	120	160	Ouda
	May	19	11	05	16	01	240	53	Ouda
	May	22	12	57	14	18	420	11	Ouda
	May	26	11	41	11	56	420	3	Ouda
	May	27	10	53	14	59	420	32	Ouda
	June	2	11	27	13	39	420	14	Ouda

* Exposure time.

† Number of useful object frames.

‡ Abbreviations: Ouda (Ouda Station), Osaka (Osaka Kyoiku University).

Table 3. Timings of Superhump Maxima in AL Com.

Cycle	Time[a]	Source[b]	Cycle	Time[a]	Source[b]
000	15.031	1	253	29.4200	4
001	15.095	1	254	29.4778	4
017	16.001	1	256	29.5961	3
018	16.060	1	257	29.6562	3
054	18.088	1	271	30.4536	4
076	19.345	2	272	30.5084	4
077	19.399	2	273	30.5677	4
089	20.078	1	283	31.139	1
090	20.135	1	284	31.201	1
091	20.167	1	288	31.4293	4
092	20.238	1	289	31.4850	4
151	23.5693	3	290	31.5422	4
175	24.960	1	305	32.3995	4
176	25.017	1	306	32.4580	4
177	25.073	1	323	33.4360	4
178	25.132	1	324	33.4915	4
221	27.5925	3	325	33.5489	4
222	27.6525	3	326	33.6065	3
232	28.218	1	343	34.5843	3
234	28.3345	4	370	36.132	1
235	28.3931	4	378	36.5970	3
252	29.3636	4	499[c]	43.5732	3

[a] HJD-2449800

[b] 1) Our data, 2) Pych & Olech (1995b) (measured by eye), 3) Howell et al. (1996a), 4) Pych & Olech (1995b)

[c]This cycle counts includes an error of ± 1 since more than 100 maxima were not observed since the last cycle.

Table 4. Journal of the observations of NY Ser

Date (UT)			JD	Exposure time (s)	Number of exposure
1995	July	25	2449923.998 - 24.098	180	42
		26	2449924.949 - 25.103	180	70
		27	2449925.971 26.099	60	31
		28	2449926.985 - 27.095	240	36
		29	2449927.952 - 28.078	180	44
		30	2449928.949 - 29.077	240	39
		31	2449929.951 - 30.069	180	43
	August	1	2449930.951 - 31.085	120	81
		3	2449932.992 - 33.080	120	50
		4	2449933.987 34.032	240	12
		5	2449934.980 - 35.061	240	26
		6	2449935.977 - 36.060	240	28
		7	2449936.972 37.054	240	28
		8	2449937.974 - 38.065	240	34
		9	2449938.958 - 39.062	240	35
		12	2449941.947 - 41.974	240	9
		13	2449942.960 - 42.976	240	6
		14	2449943.954 - 43.967	240	5
		16	2449945.943 - 46.043	180	45
	December	23	2450075.350 - 75.378	90	18
		27	2450079.357 - 79.383	90	17
1996	January	13	2450096.363 - 96.388	90	2
	February	24	2450138.282 - 38.288	90	4
	March	3	2450146.321 - 46.327	90	5
		5	2450148.347 - 48.351	90	2
		6	2450149.184 - 49.188	120	2
		20	2450163.334 - 63.338	90	3
		23	2450166.193 - 66.328	90	117

Table 4. (cont.)

Date (UT)			JD	Exposure time (s)	Number of exposure
1996	March	25	2450168.323 - 68.327	90	3
		30	2450173.279 - 73.285	90	5
	April	1	2450175.223 - 75.227	90	3
		2	2450176.230 - 76.236	90	5
		4	2450178.215 - 78.218	90	2
		5	2450179.200 - 79.203	120	2
		9	2450183.264 - 83.268	90	2
		16	2450190.226 - 90.311	90	54
		21	2450195.162 - 95.295	90	110
		22	2450196.173 - 96.176	90	5
		23	2450197.153 - 97.292	90	114
		24	2450198.050 - 98.285	90	203
		25	2450199.153 99.304	120	56
	May	1	2450205.105 - 05.219	90	29
		5	2450209.243 - 09.261	90	12
		6	2450210.111 10.175	120	5
		9	2450213.242 13.247	90	4
		10	2450214.188 - 14.196	180	4
		13	2450217.189 17.284	90	78
		14	2450218.207 18.266	90	50
		15	2450219.090 - 19.093	90	3
		19	2450223.037 - 23.040	120	4
		21	2450224.998 - 25.002	120	3
		22	2450226.028 26.030	120	1
		23	2450226.974 - 26.978	120	3
		24	2450227.987 - 27.993	180	3
		25	2450229.000 - 29.005	180	3

Table 4a. (cont.)

Date (UT)			JD	Exposure time (s)	Number of exposure
1996	July	16	2450280.971 80.977	90	5
		17	2450282.037 - 82.042	90	5
		24	2450288.954 - 88.959	90	4
		28	2450292.972 - 93.093	90	98
		29	2450293.951 - 94.084	90	34
		30	2450295.001 - 95.002	90	1
1996	August	2	2450297.954 98.006	90	5
		4	2450299.957 - 99.976	90	11
		5	2450300.946 - 01.018	90	60
		8	2450303.945 - 03.955	90	9
		9	2450304.941 - 05.025	90	32
		11	2450306.943 - 07.038	90	51
		12	2450307.954 - 07.956	90	2
		17	2450312.940 - 12.942	90	2
		18	2450313.941 - 13.943	90	1
		19	2450314.940 13.944	90	3
	September	8	2450334.921 34.924	90	3
		14	2450340.955 40.957	90	1
1997	January	12	2450461.382 - 61.387	90	3
		15	2450464.341 - 64.344	90	4
		19	2450468.360 - 68.365	90	5
		20	2450469.367 69.373	90	5
	February	1	2450481.352 - 81.373	90	12
		27	2450507.212 - 07.216	90	5
	March	1	2450509.244 - 09.250	90	5
		4	2450512.273 - 12.285	90	10

Table 4a. (cont.)

Date (UT)			JD	Exposure time (s)	Number of exposure
1997	March	5	2450513.192 - 13.343	90	126
		6	2450514.332 - 14.354	90	8
		7	2450515.303 - 15.343	120	26
		8	2450516.195 - 16.346	60	177
		11	2450519.137 - 19.260	90	62

Table 5a. Journal of the photometric observations of AT Cnc at Ouda.

Date (UT)			HJD	Exposure time (s)	Number of exposure
1997	February	1	2450481.177 – 2450481.302	30	236
		3	2450482.954 – 2450483.122	30	313
		5	2450484.966 – 2450485.223	30	410

Table 5b. Journal of the spectroscopic observations at Okayama.

Date (UT)			HJD	Exposure time (s)	Number of exposure	Grating
1997	February	4	2450484.064 – 2450484.072	600	1	150
		4	2450484.082 – 2450484.292	600	19	600
		5	2450484.942 – 2450484.950	600	1	150
		5	2450484.960 – 2450485.048	600	9	600
		6	2450486.039 – 2450486.115	600	8	600

Table 6. Phase, equivalent width, and radial velocity of Hα, and visibility of the P Cyg profile.

Mid-exposure Time*	Phase	P Cyg Visibility	Equivalent Width	Radial Velocity	Mid-exposure Time*	Phase	P Cyg Visibility	Equivalent Width	Radial Velocity
4.13239	0.024		-5.0	6.8	6.04299	0.526		-4.4	21.3
4.14215	0.073		-5.0	33.9	4.23416	0.530	Y	-3.9	-5.5
(4.94918	0.086			101)†	5.04367	0.556		-3.9	-14.1
(4.94918	0.086			94)*	6.05271	0.574		-3.6	-15.2
4.15190	0.121		-4.6	83.0	4.24596	0.589		-3.9	-19.8
4.96412	0.160	Y?	-4.0	89.8	6.06244	0.622		-3.6	-31.9
4.16165	0.170		-5.2	88.8	4.25693	0.643		-4.4	-36.5
4.97406	0.210	Y?	-4.2	80.4	6.07214	0.670		-4.5	-71.9
4.17153	0.219	Y?	-5.4	109.6	4.26714	0.694		-4.8	-46.9
4.98372	0.258		-4.0	75.0	6.08188	0.719		-4.6	-28.9
4.18182	0.270	Y?	-4.9	92.1	(4.07115	0.720			-46)†
4.99357	0.307		-4.2	38.2	(4.07115	0.720			-23)*
4.19187	0.320		-5.1	96.8	4.27759	0.746		-4.6	-89.7
5.00333	0.355	Y	-4.7	54.6	6.09164	0.767		-4.2	-49.4
4.20226	0.372	Y	-4.3	103.2	4.08559	0.791		-4.9	-107.2
5.01307	0.404		-3.8	68.4	4.28802	0.798		-5.8	-62.7
4.21359	0.428	Y	-4.2	70.2	6.10159	0.817		-4.3	-65.5
5.02294	0.453		-3.9	23.8	4.09775	0.852		-5.2	-43.3
4.22380	0.479	Y	-5.0	73.7	6.11142	0.866		-4.4	-42.8
5.03295	0.503	Y	-4.2	37.8	4.10966	0.911		-5.1	-31.3

* HJD - 2450480

† Hα in a 150G spectrum

* Na D in a 150G spectrum

Table 7. Orbital elements.

Factor		Value
systemic velocity	γ	11 ($\pm$ 3) km s^{-1}
semi amplitude	K	80 ($\pm$ 4) km s^{-1}
zero point	T_0	HJD 2450484.128 ($\pm$ 0.002)
period	P	0.2011 ($\pm$ 0.0006) d

Figure Captions

Fig. 1. Schematic local thermal-equilibrium curve in a surface-density (Σ) versus mass-accretion rate ($\dot{M}acc$) diagram (figure 1 in Osaki (1989)). If the steady mass-transfer rate from the secondary is around $\dot{M}_0$, cyclic variation as shown by arrows occur.

Fig. 2. Superhump period versus supercycle diagram. WZ Sge stars ($\times$) and ER UMa stars ($\bigcirc$) are located away from usual SU UMa stars.

Fig. 3 The general light curve of the 1995 superoutburst in AL Com. Filled squares represent our data and open circles represent visual observations.

Fig. 4 Periodic modulations during the early stage of the superoutburst. The double-peaked features have declined as the superoutburst progressed. Nominal errors for individual points are shown by tic marks near each date.

Fig. 5 Genuine superhumps observed on April 17 at the midst of the "standstill" phase. The fluctuations have singly-peaked shape, different from the modulations observed in the early stage shown in Figure 3.

Fig. 6 The O – C diagram of the hump-maxima timings listed in table 3. Open circles represent the timings measured in our data. Open triangles are the points measured from figures in Pych and Olech (1995b) by eye. Filled triangles point as listed in Pych and Olech (1995b). The timing measured by Howell et al. (1996b) is shown by filled circles. The error of the points with no error bar does not exceed the value shown by the tic mark in the right bottom of this figure. The dashed line represents the quadratically polynomial curve obtained by fitting the points in the range from 200 to 400 in the cycle count. Note that the line represents a trend of the period becoming longer.

Fig. 7 The enhanced light curve of the dip and the second stage of the outburst. Once reaching the minimum around HJD 2449841, AL Com brightened up to about 15.2 mag in a day. After the variable declining about 0.6 mag around HJD 2449843, re-brightening occurred. This course of outburst is seen in the case of superoutbursts in usual SU UMa-type stars. A dotted line represents a possible light curve.

Fig. 8 The light curve at the secondary dip. The decline trend with a rate of about 0.8 mag d^{-1} clearly exists. The bar at the left bottom of the figure represents the typical estimated error for individual points.

Fig. 9 Folded light curve obtained during the "plateau" phase of the secondary outburst. Note that the best period agree with the superhump period obtained during the primary outburst within the error of the estimate, although the shape is different from that of the superhump (Figure 5). From the fact that the superhumps grew after the dip, we interpret the "plateau" phase as a new superoutburst.

Fig. 10 Time-resolved light curve just before the final decline. The superhumps have completely disappeared.

Fig. 11 Theta diagrams. The top one is for the periodic modulations observed in the early stage of the outburst. The second represents the superhump frequency slightly less than one pointed in the top. The third is for the modulation seen after the recovery of the dip. The frequency in the third is almost same as one in the third. The bottom shows that periodic oscillation with a frequency near the above ones had been extinguished before the end of the outburst.

Fig. 12 Schematic illustration for the "jet" model explaining the double-peaked shape of the modulations observed in the early stage of the 1995 superoutburst in AL Com. The upper panel shows AL Com viewed from the direction perpendicular to the line from the observer to the variable. The lower panel shows AL Com from the view point of the observer. In this model, singly peaked "immature" superhumps can be made doubly by the eclipse of the jet by the secondary located at the point drawn in the figure.

Fig. 13 Schematic illustration for the "thickened-edge" model. In this model, the complex shape of photometric data is explained by the eclipse of the inner part of the disk by the non-axisymmetrically thickened edge having lower temperature than the inner part.

Fig. 14 The long-term light curve of NY Ser. We can see normal outbursts with a recurrence time of 6–9 days and long-lasting outbursts around HJD 2450195, 2450300, and 2450365.

Fig. 15 Short-term light curves of the first long outburst around HJD 2450195. Fully developed superhumps are found on 1996 April 23-25, though superhumps had not yet grown on April 21.

Fig. 16 The upper panel shows the result of a period analysis of the PDM method on

the data obtained between 1996 April 23 and 25 after subtracting the linear trend of decline. The lower panel shows the light curve those data folded by the period of 0.106 d.

Fig. 17. Finding chart of AT Cnc. North is top, and the field of view is about $10' \times 7'$. The star C_I was used as the comparison star for differential photometry of AT Cnc. The stars, C_{II} and C_{III} were the check stars. The V magnitudes of these stars are given as 12.15, 13.52, and 14.02, respectively, in the VSNET chart (URL:ftp://www.kusastro.kyoto-u.ac.jp/vsnet/charts/AT_Cnc.ps), while Misselt (1995) measured V magnitudes of C_{II} and C_{III} as 13.50 and 14.05, respectively.

Fig. 18ab. (a, the upper panel) General light curve of AT Cnc drawn from visual observations posted to VSNET between 1995 January and 1998 June. Our photometric and spectroscopic observations were carried out during the the 1996-1997 long standstill. (b, the lower panel) Photometric results obtained on 1997 February 1, 3, and 5. During this period, AT Cnc stayed within 0.1 mag around $V = 13.56$.

Fig. 19. Enlarged light curve shifted properly. No apparent periodic feature is seen, although aperiodic signals with very small amplitudes may exist.

Fig. 20ab. (a, the upper panel) G(f) - frequency diagram calculated using LANCELOT with whole the data shown in figure 3 after subtracting the nightly averages. The maximum point corresponds to the best estimated period. (b, the lower panel) The processed data folded by the best estimated period.

Fig. 21ab. (a, the upper panel) χ^2 - frequency diagram. This figure show three possible periods, 0.132 d ($f = 7.58$ d^{-1}), 0.142 d ($f = 7.04$ d^{-1}), and 0.124 d ($f = 8.06$ d^{-1}). (b, the lower panel) The processed data folded by $P = 0.132$ d. This curve has a single peak.

Fig. 22ab. (a, the upper panel) Low-resolution 150G spectrum. Hα is in singly peaked emission and Hβ in emission superposed on absorption. Other lines, usually visible in dwarf novae, e.g. HeI, are not clear, because of difficulty of accurate subtraction of night lines and H_2O and O_2 lines. (b, the lower panel) High S/N 600G spectrum obtained by combining 36 spectra. The Hα emission line has a weak P Cyg profile (for detail, see text). We can see HeII 6678 in weak emission. The broad absorption feature between 6270 Å and 6320 Å is a blend of H_2O and O_2 lines.

Fig. 23. Typical spectra with Hα emission of the non-P Cyg profile and the P Cyg profile.

Fig. 24. Radial velocity of Hα. The curve is the sine curve best fit the radial-velocity variation (see text).

Fig. 25. Radial Velocity folded by the period of 0.2004 d and the best fit sine curve. The squares, triangles, and circles represent data shown in figure 8 obtained on 1997 February 4, 5, and 6, respectively. The open triangles and open squares are plotted for Na D lines and Hα in 150G spectra, respectively.

Fig. 26. Doppler map drawn from all the 600G spectra under the assumption that Hα emission originates near the secondary. The center of the intensity is located in the Doppler shade of the secondary star. The abscissa V_x and the ordinate V_y are in units of cm s^{-1}. The system center of mass (+), centers of the primary and the secondary ($\times$), the path of the mass stream (lower curve), and the Kepler velocity at the location of the stream (upper curve) are overplotted.

Fig. 27. Same as figure 10, but the inclination is assumed to be 36° and the center of the intensity is located near the white dwarf. Details are described in section 3.3.5.

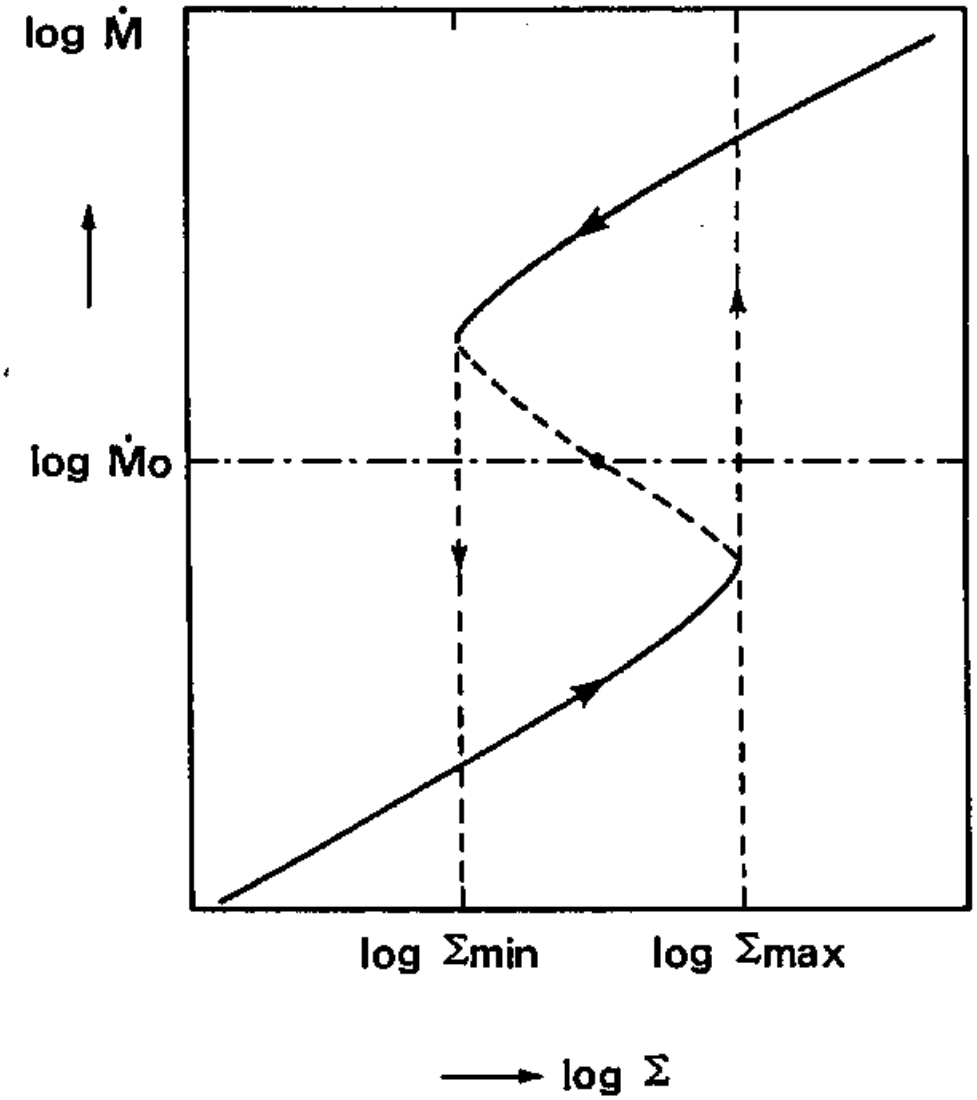

Fig. 1

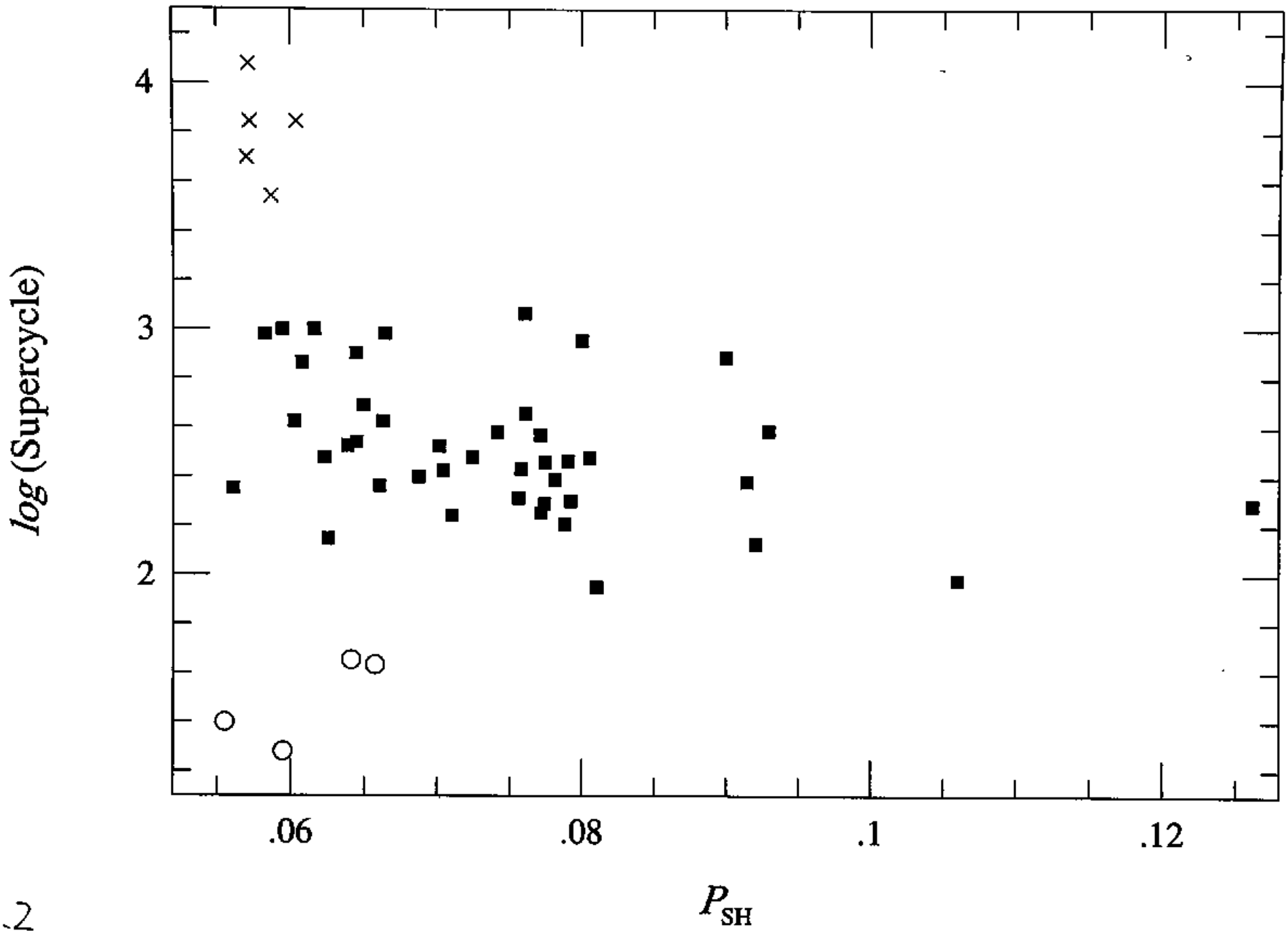

Fig.2

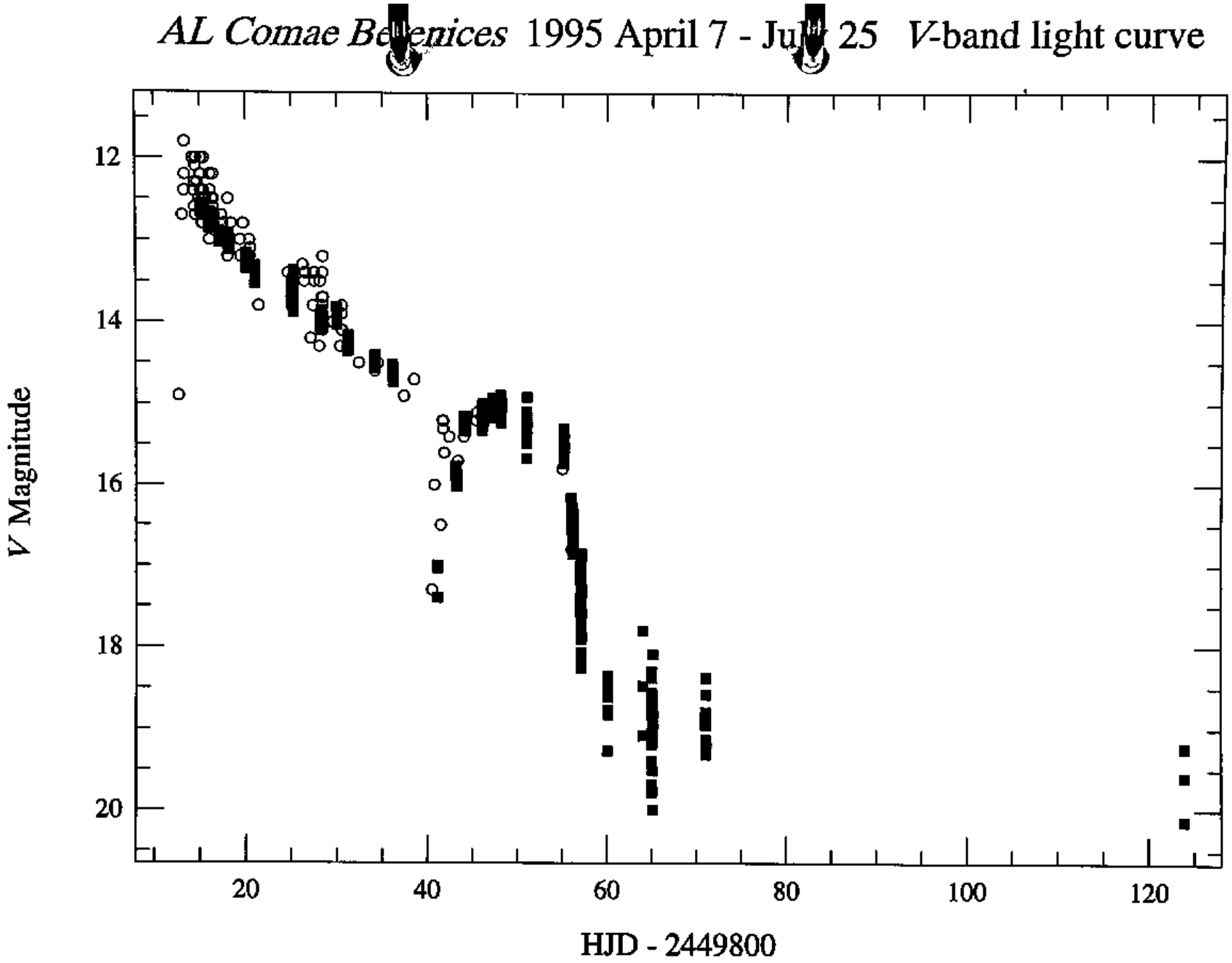
AL Comae Berenices 1995 April 7 - July 25 V-band light curve
V Magnitude
12
14
16
18
20
20
40
60
80
100
120
HJD - 2449800

Fig. 3

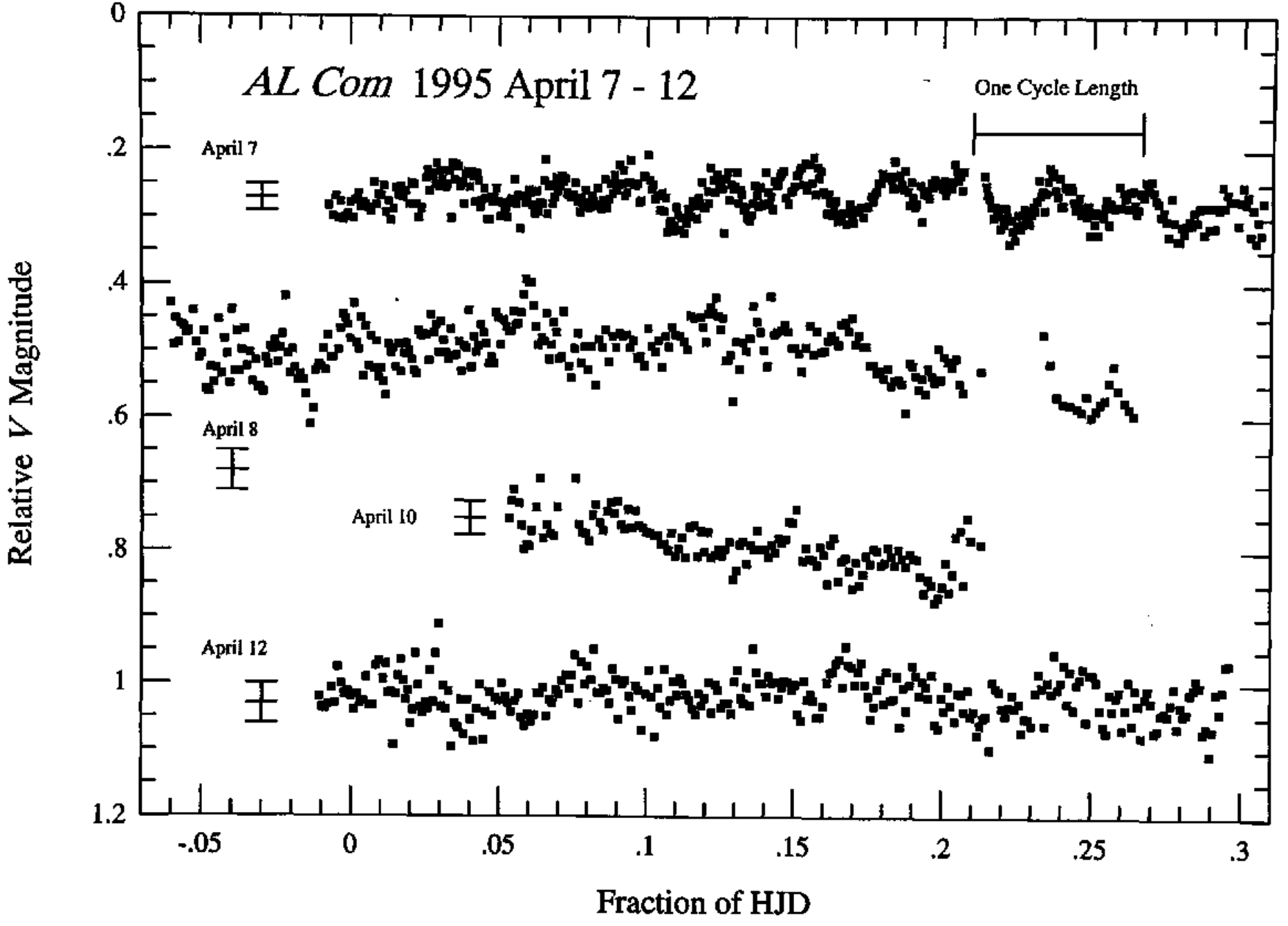
AL Com 1995 April 7 - 12
One Cycle Length
April 7
April 8
April 10
April 12
Relative V Magnitude
Fraction of HJD
0
.2
.4
.6
.8
1
1.2
-.05
0
.05
.1
.15
.2
.25
.3

Fig. 4

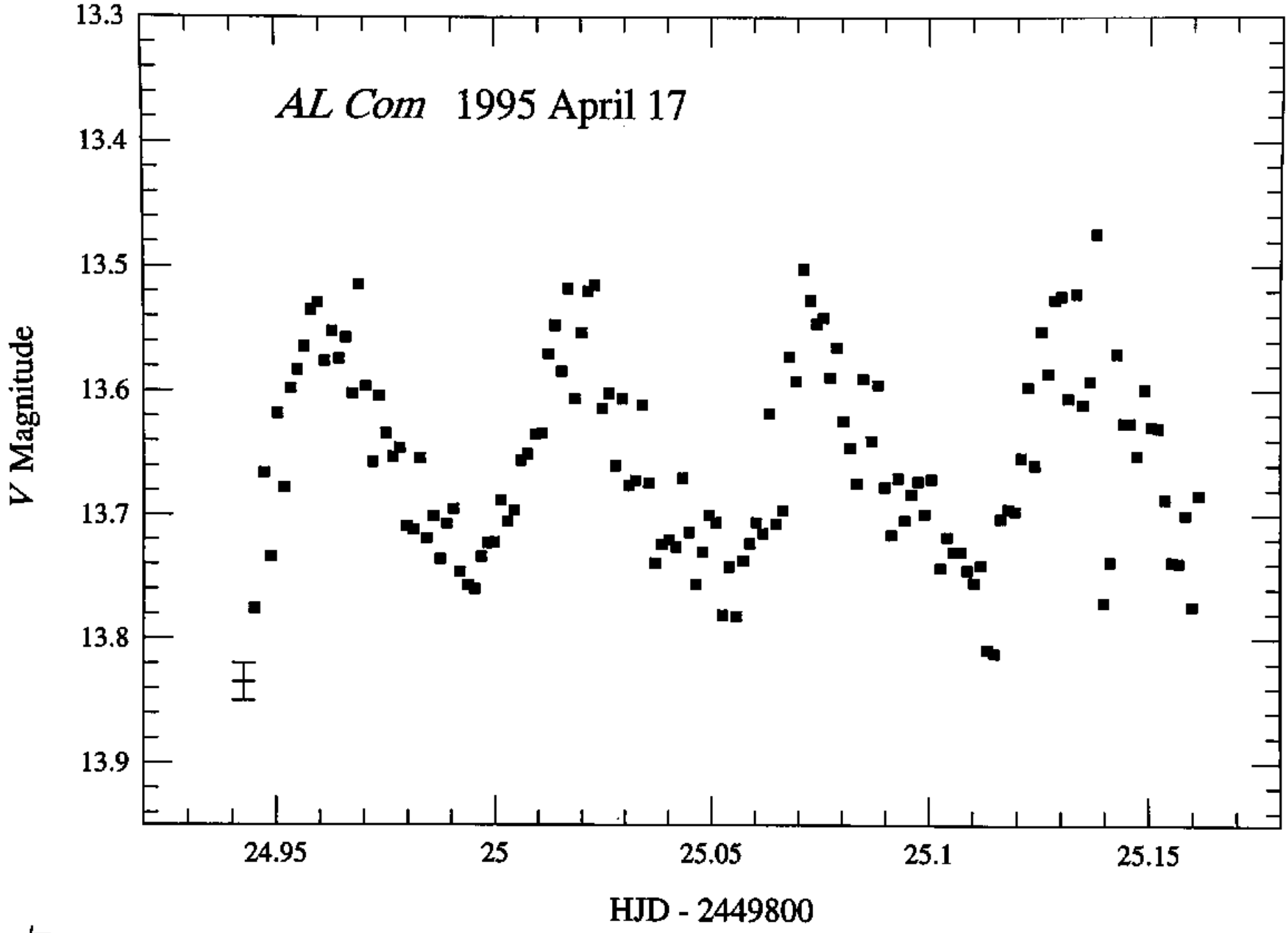
AL Com 1995 April 17
13.3
13.4
13.5
13.6
13.7
13.8
13.9
V Magnitude
24.95
25
25.05
25.1
25.15
HJD - 2449800

Fig. 5

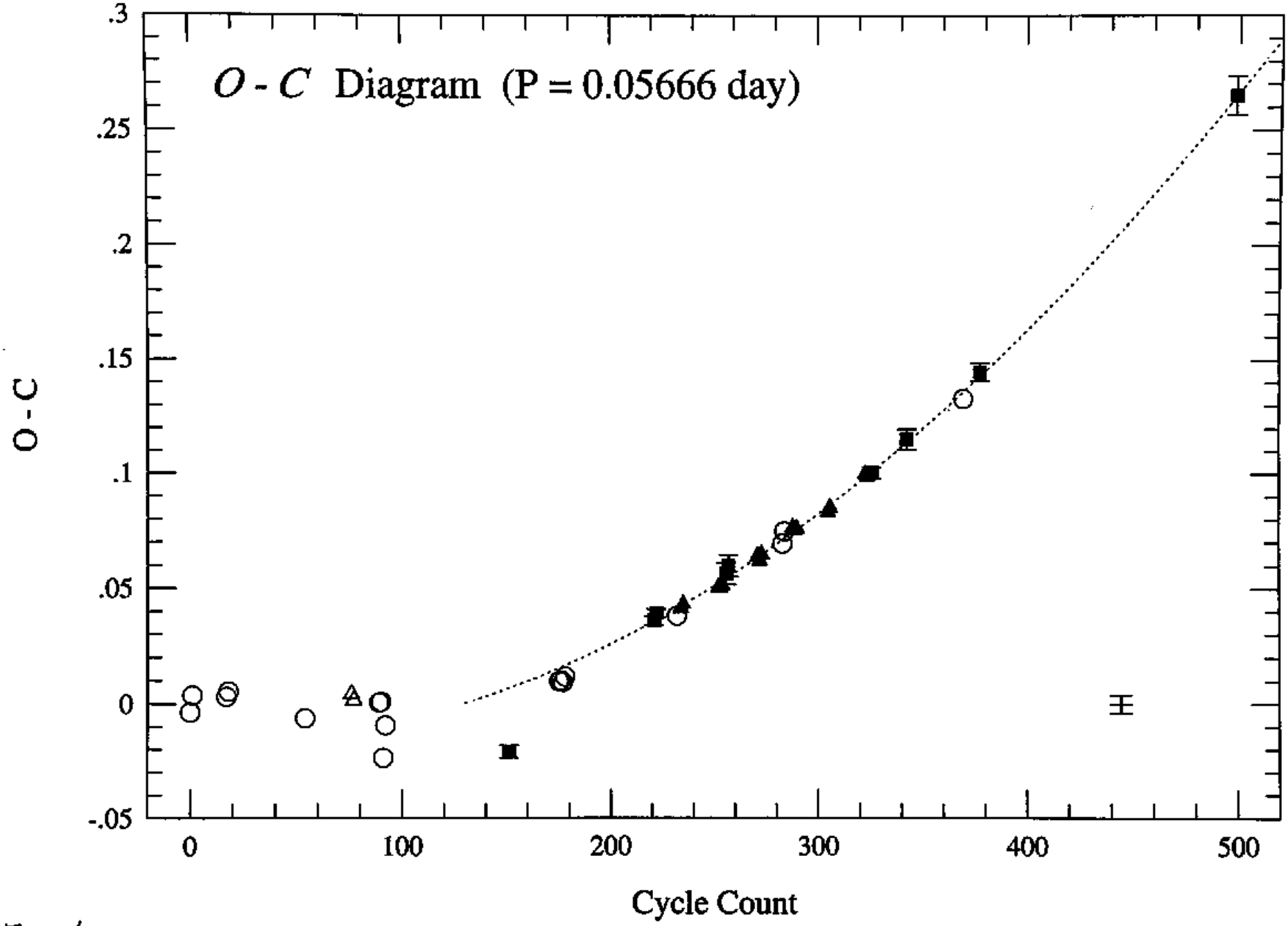
O - C Diagram (P = 0.05666 day)
O - C
Cycle Count
.3
.25
.2
.15
.1
.05
0
-.05
0
100
200
300
400
500

Fig. 6

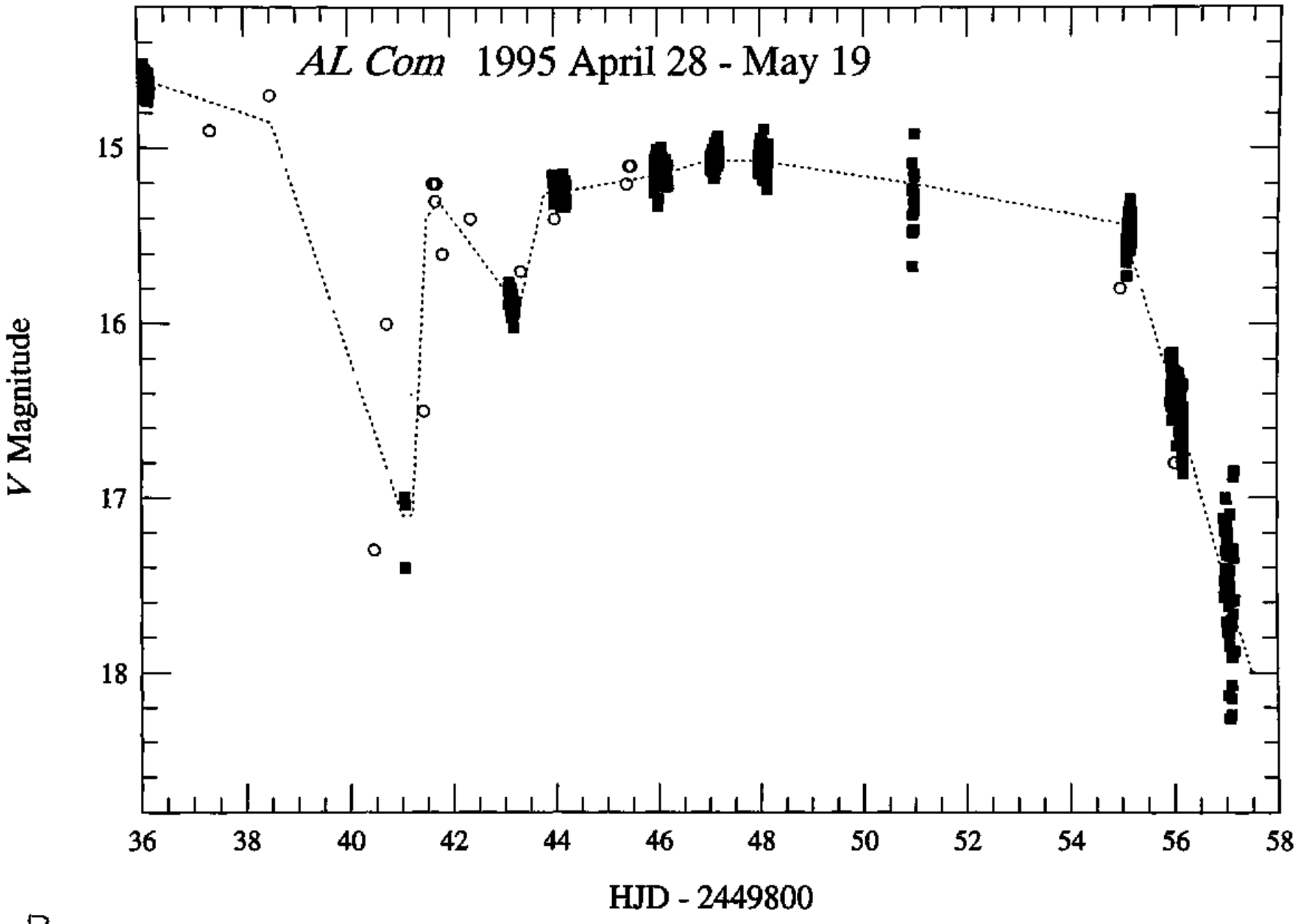
AL Com 1995 April 28 - May 19
V Magnitude
15
16
17
18
36
38
40
42
44
46
48
50
52
54
56
58
HJD - 2449800

Fig. 7

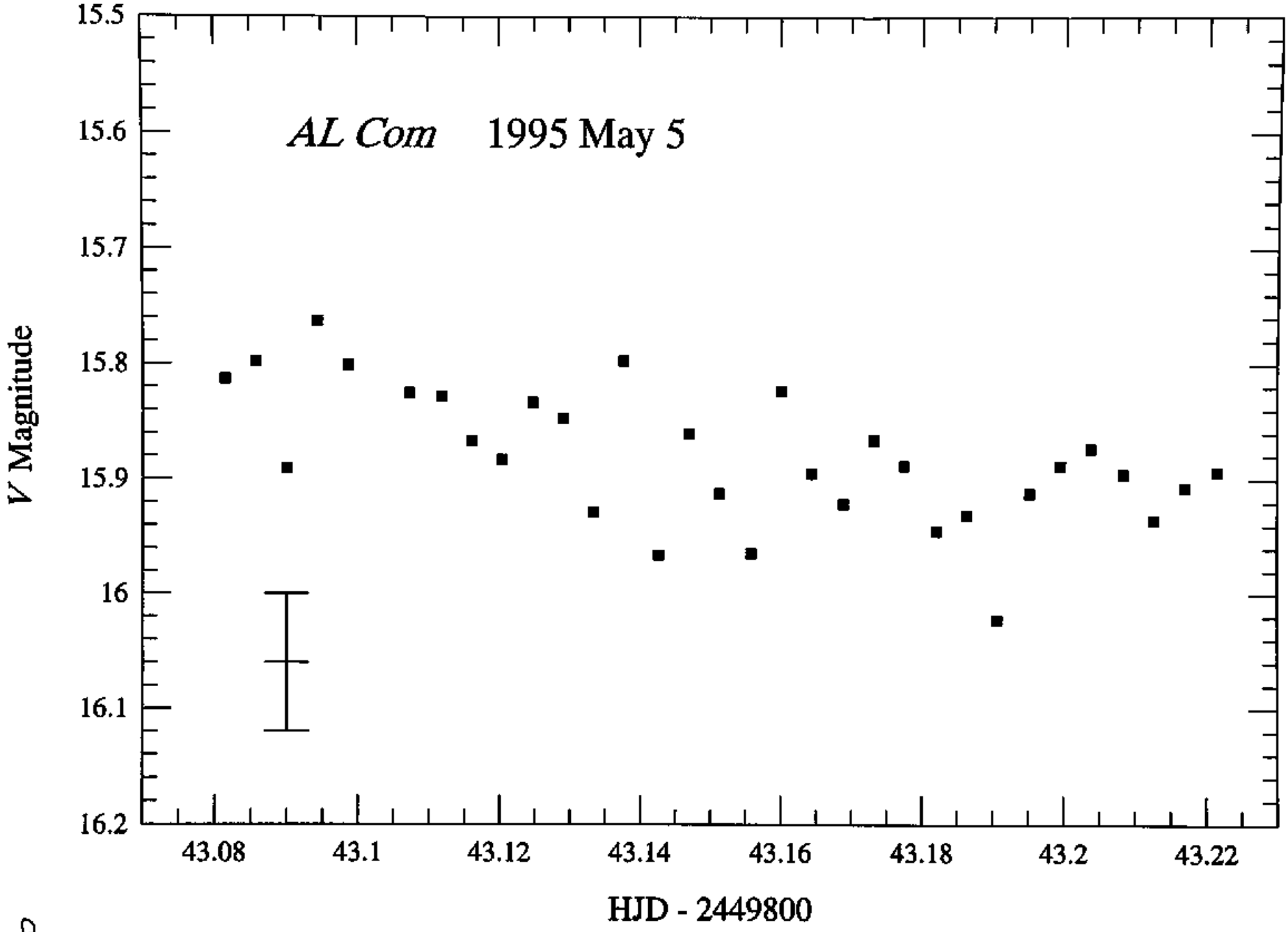
AL Com 1995 May 5
15.5
15.6
15.7
15.8
15.9
16
16.1
16.2
V Magnitude
43.08
43.1
43.12
43.14
43.16
43.18
43.2
43.22
HJD - 2449800

Fig. 8

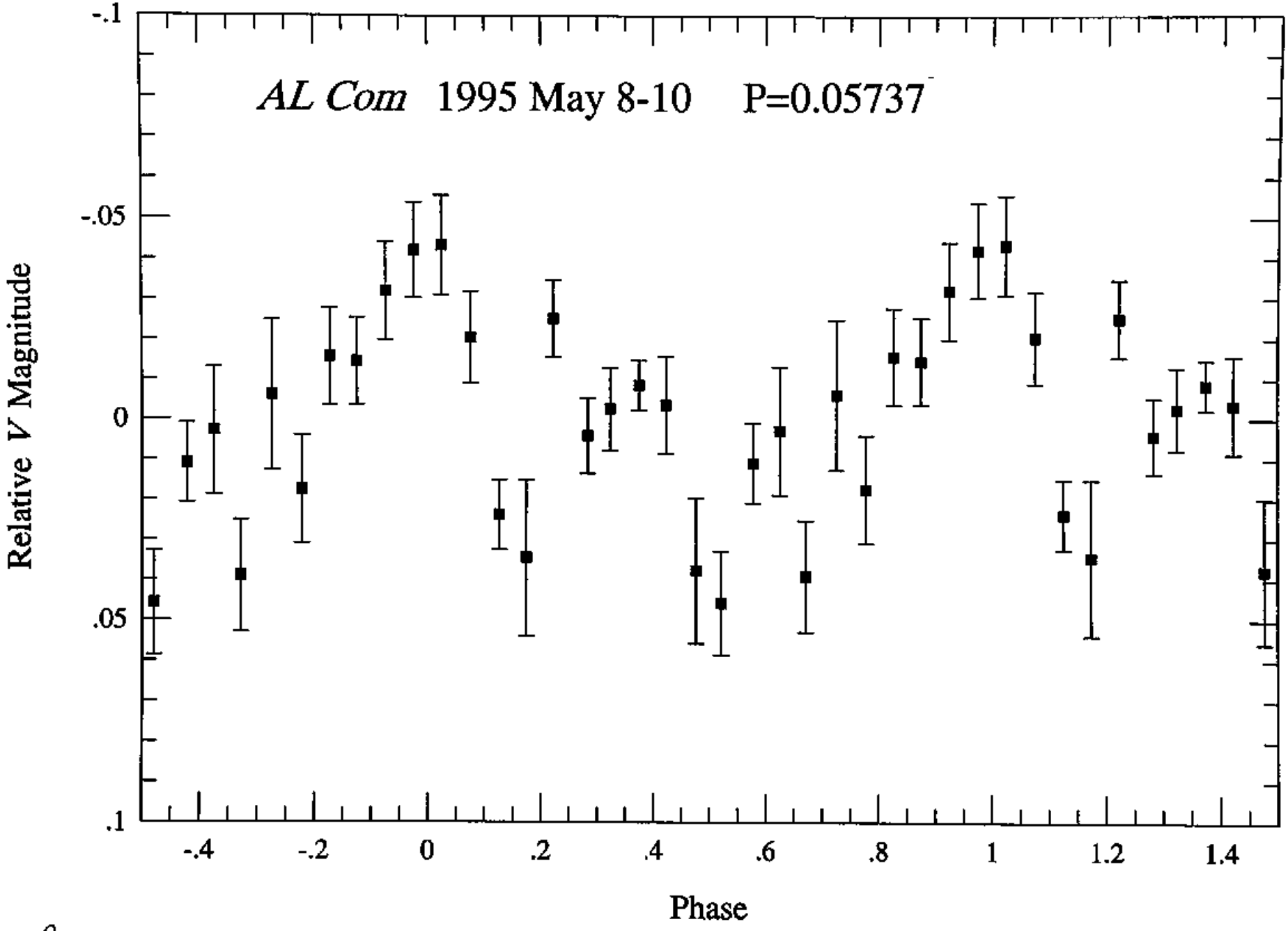
AL Com 1995 May 8-10 P=0.05737
Relative V Magnitude
-.1
-.05
0
.05
.1
-.4
-.2
0
.2
.4
.6
.8
1
1.2
1.4
Phase

Fig. 9

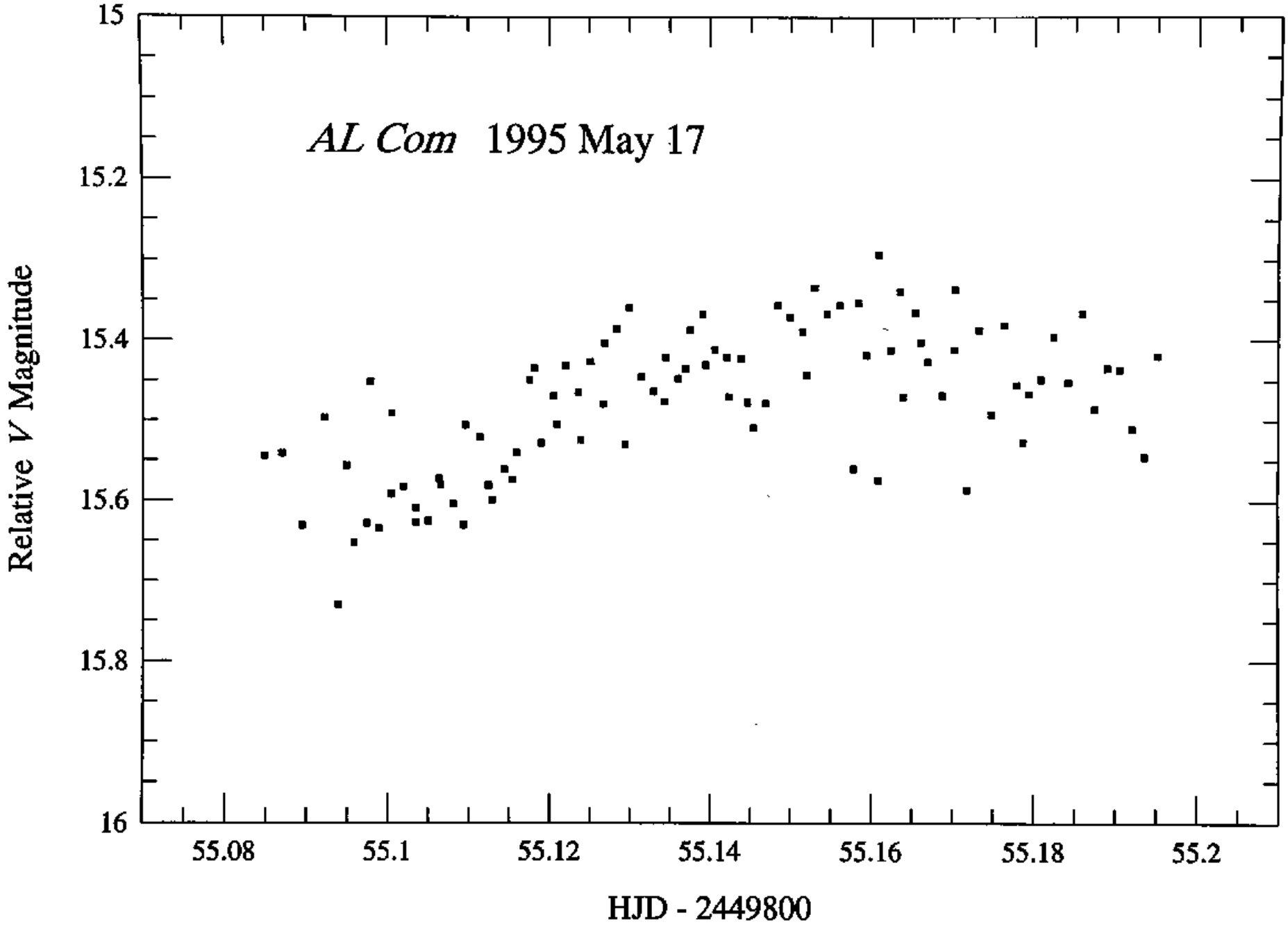
AL Com 1995 May 17
Relative V Magnitude
15
15.2
15.4
15.6
15.8
16
55.08
55.1
55.12
55.14
55.16
55.18
55.2
HJD - 2449800

Fig. 10

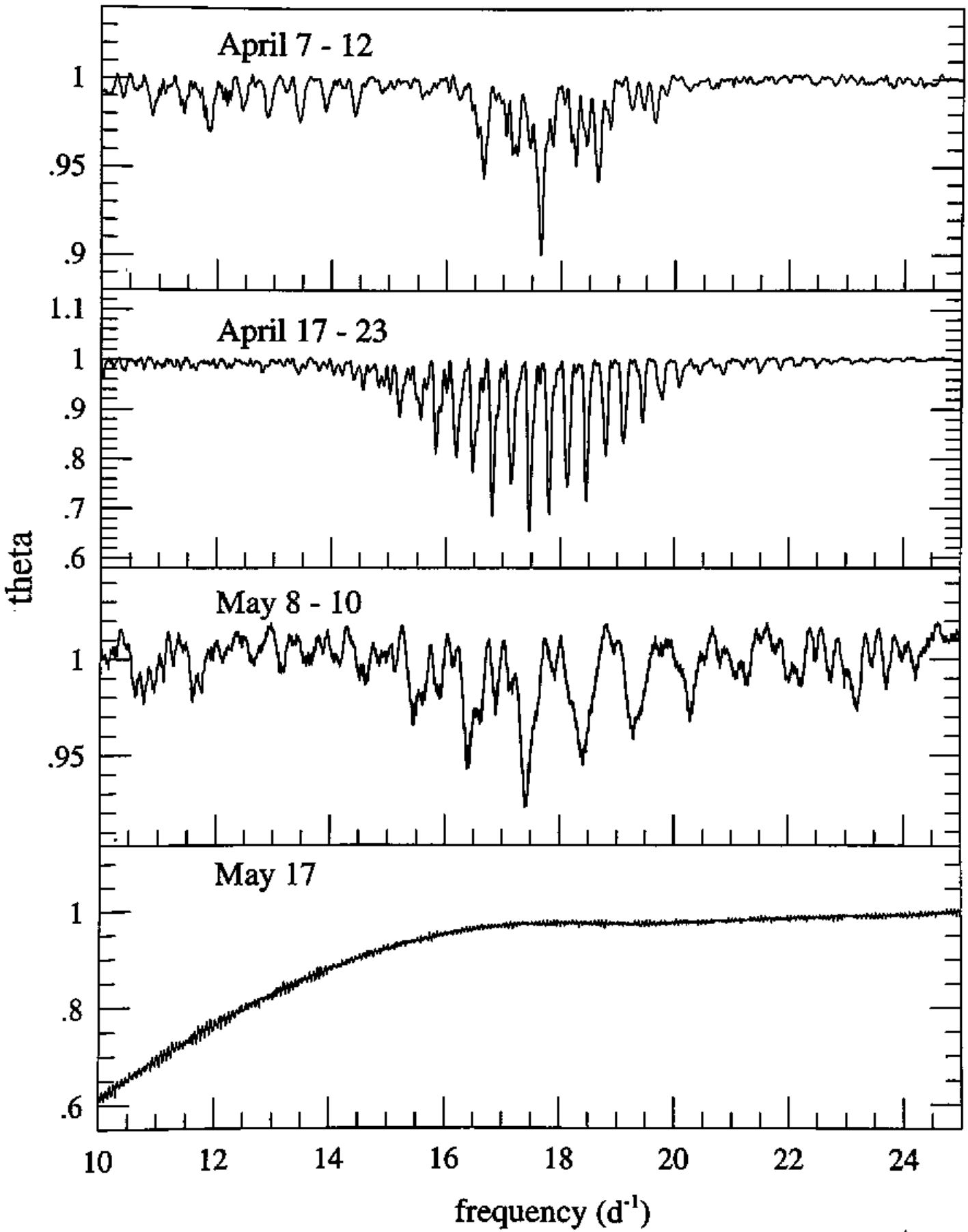
April 7 - 12
April 17 - 23
May 8 - 10
May 17
theta
frequency (d-1)
1
.95
.9
1.1
.8
.7
.6
10
12
14
16
18
20
22
24

Fig-11

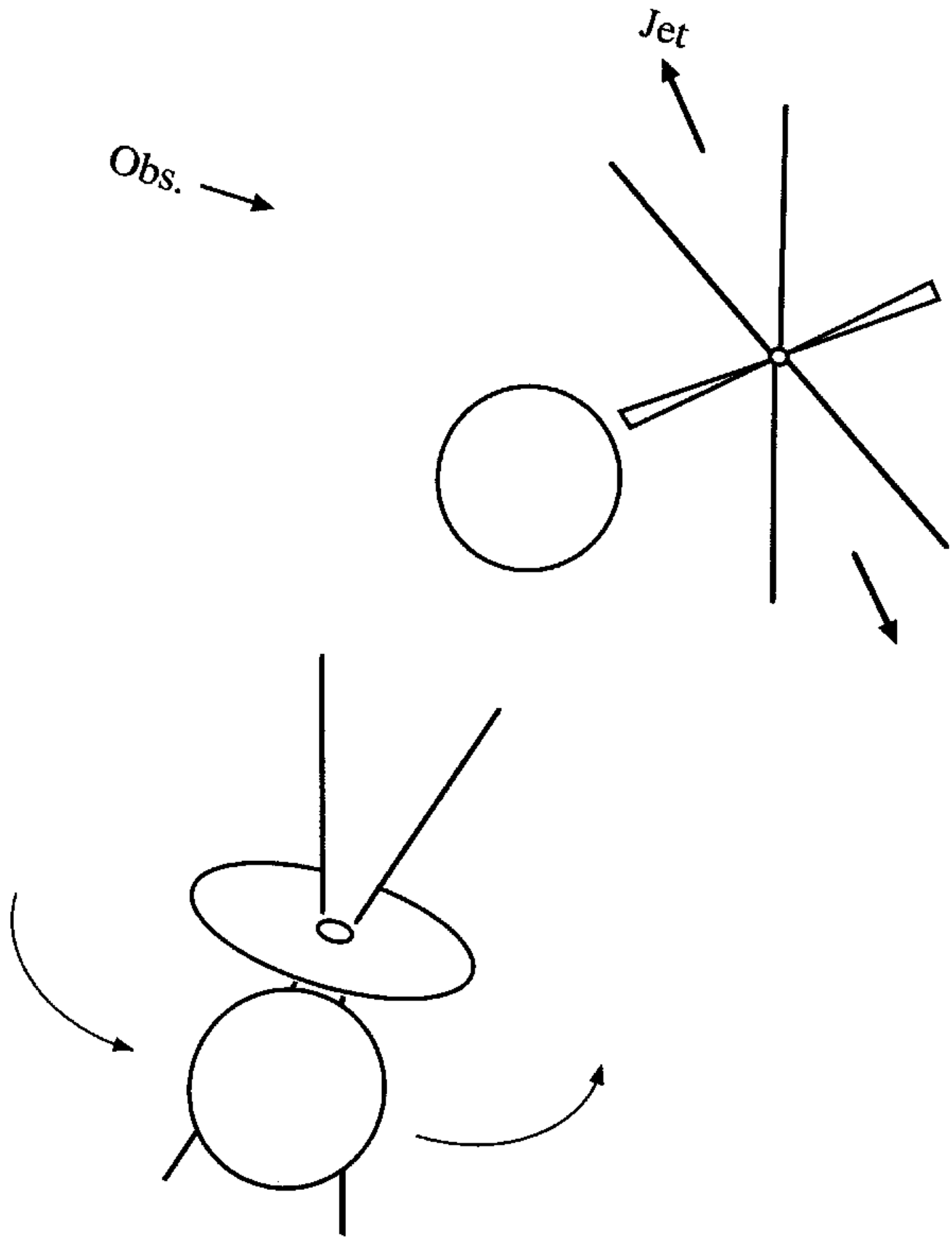

Fig. 12

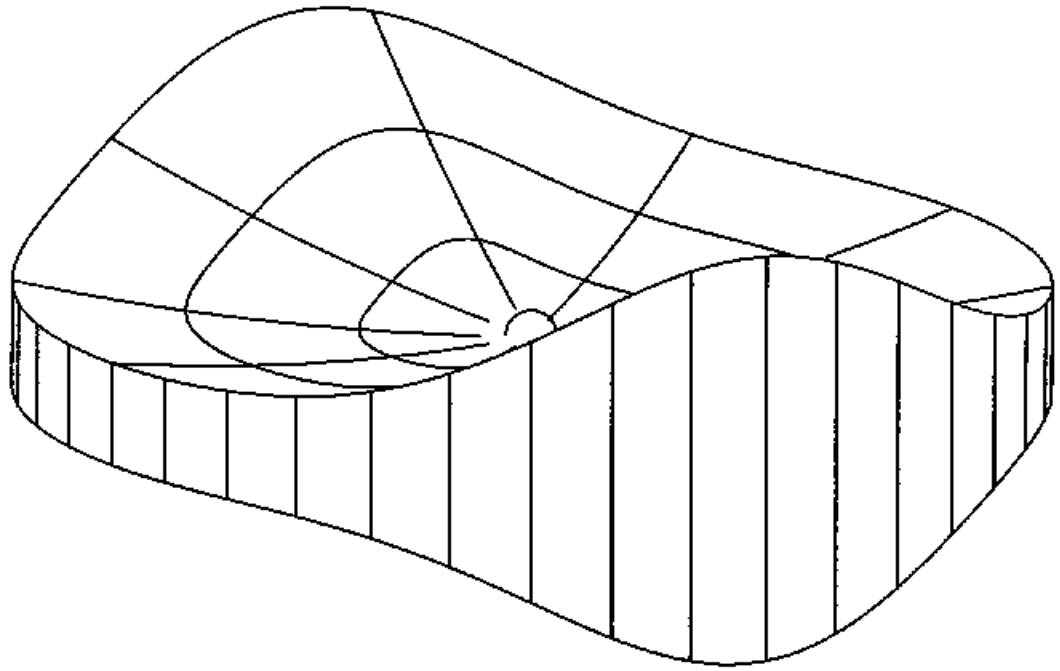

Fig. 13

NY Ser 1995 July 25 - 1997 March 11

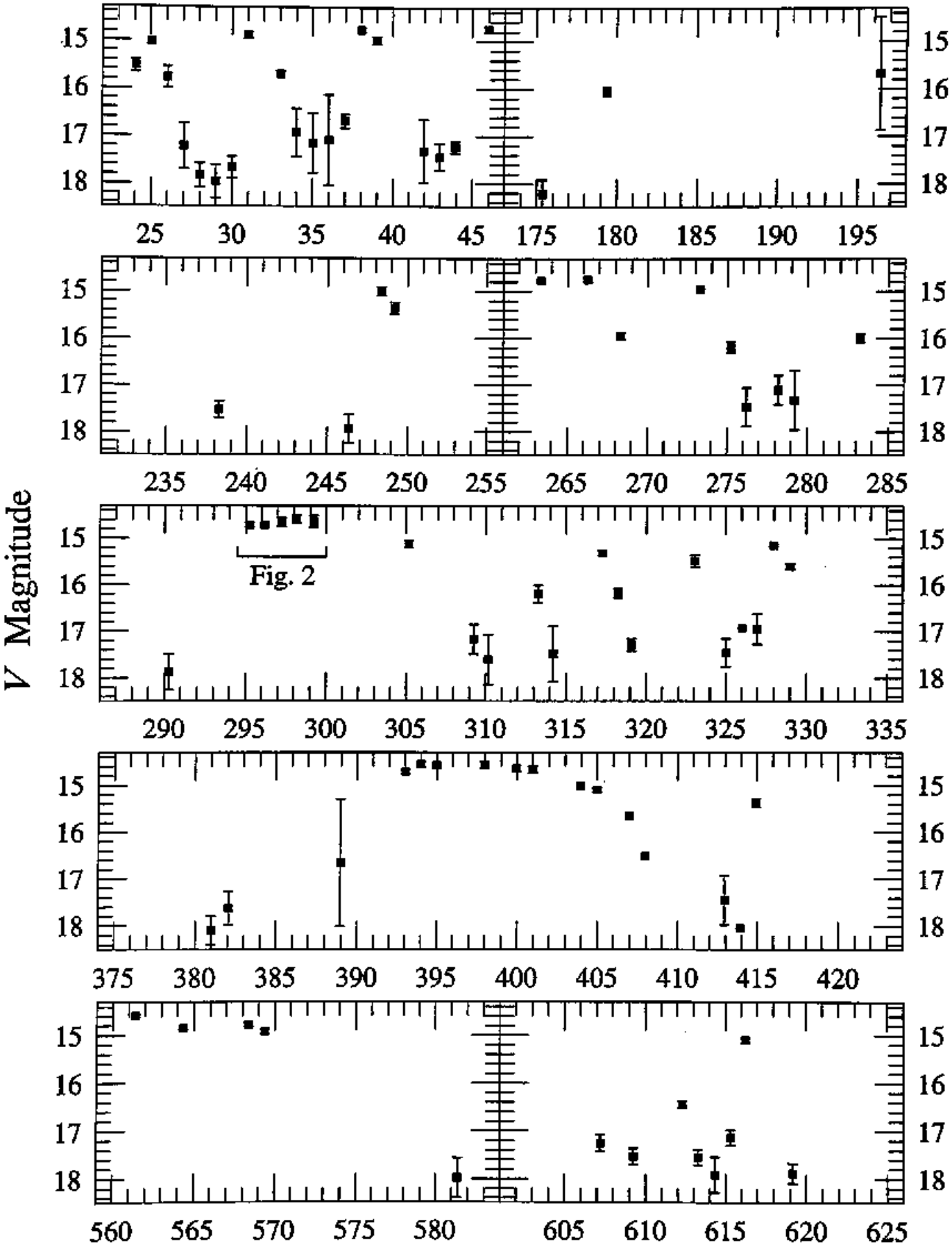

Fig. 14

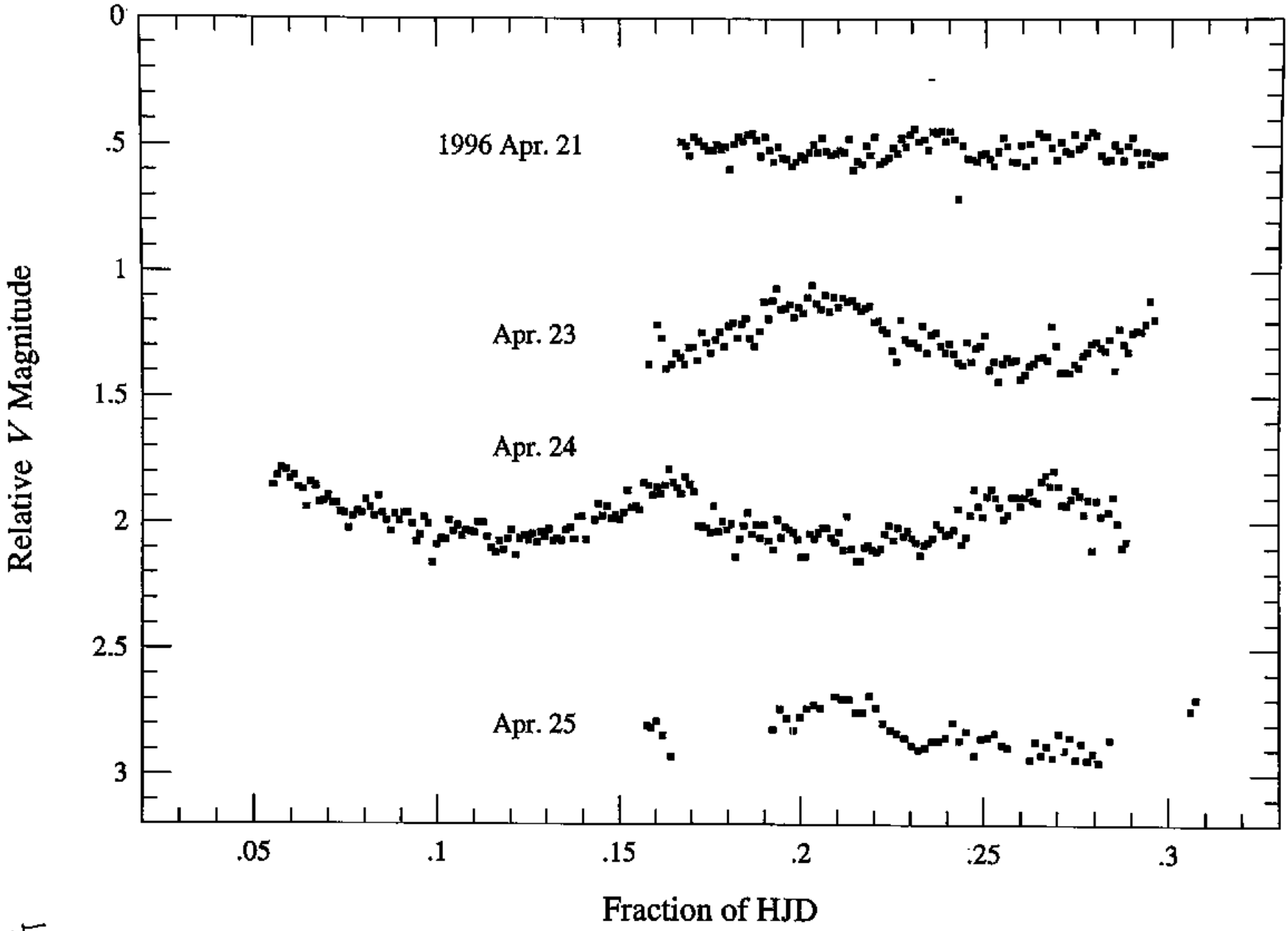
0
.5
1
1.5
2
2.5
3
Relative V Magnitude
1996 Apr. 21
Apr. 23
Apr. 24
Apr. 25
.05
.1
.15
.2
.25
.3
Fraction of HJD

Fig. 15

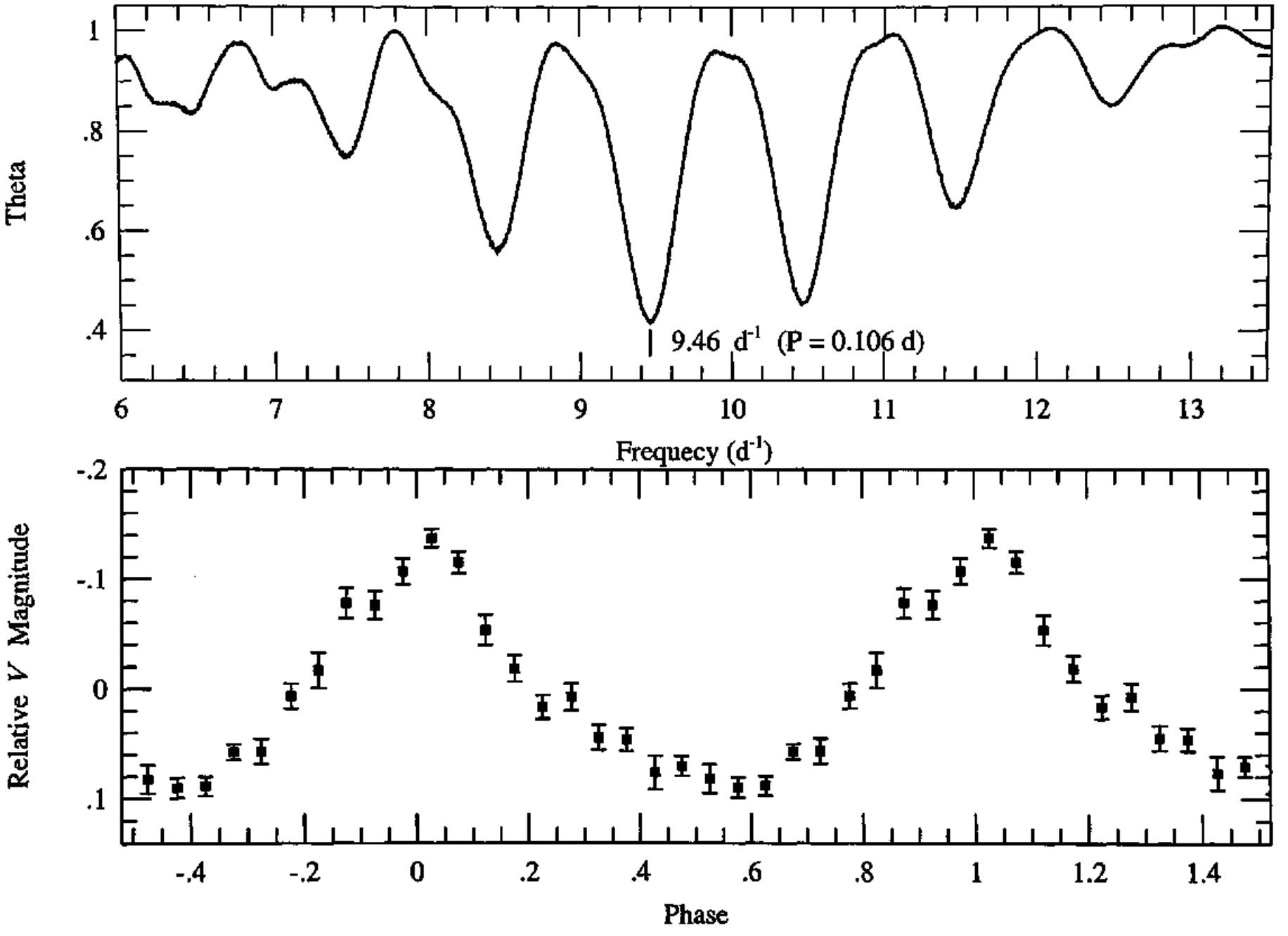
Theta
1
.8
.6
.4
9.46 d-1 (P = 0.106 d)
6
7
8
9
10
11
12
13
Frequecy (d-1)
Relative V Magnitude
-.2
-.1
0
.1
-.4
-.2
0
.2
.4
.6
.8
1
1.2
1.4
Phase

Fig. 16

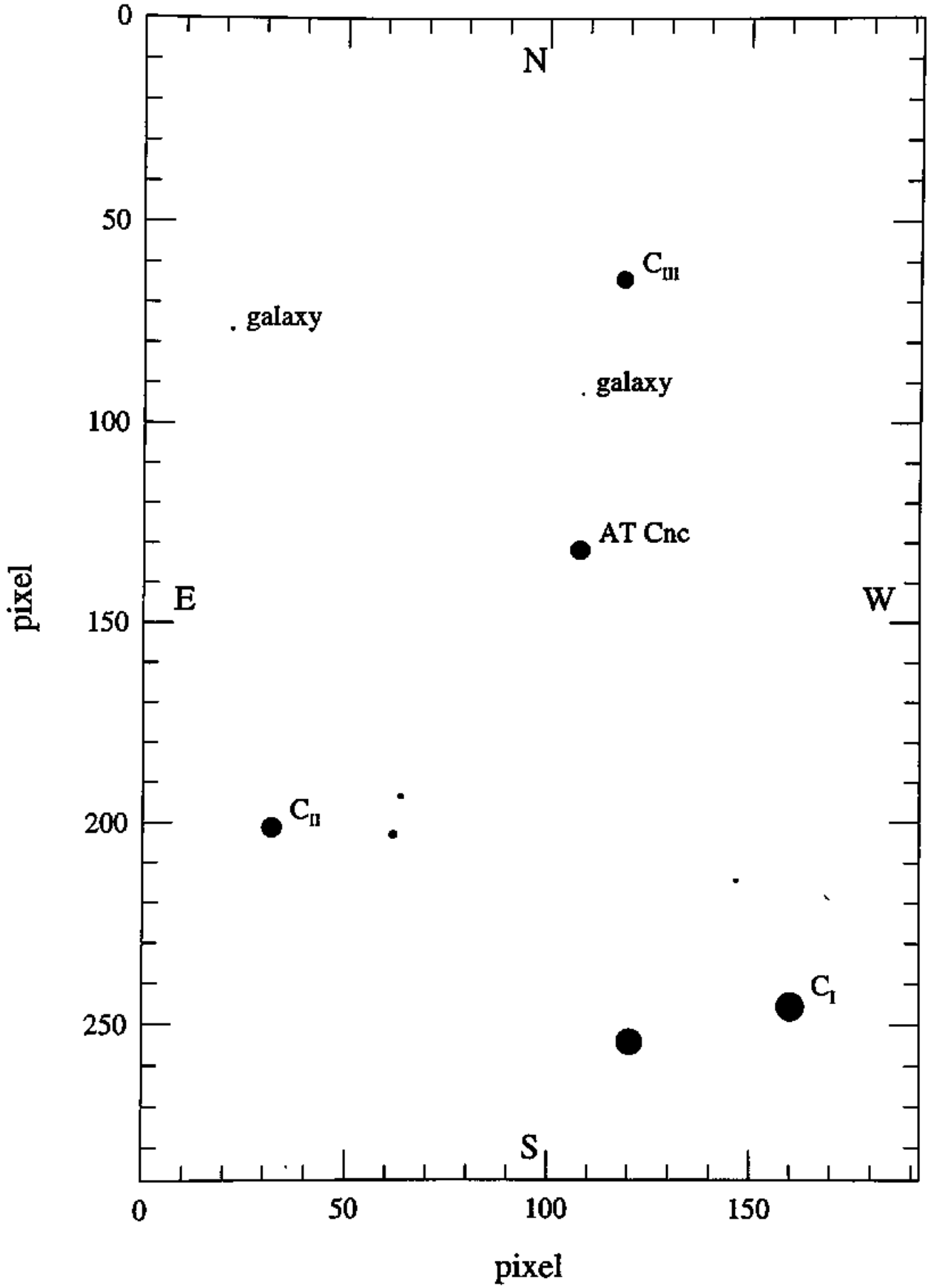
0
50
100
150
200
250
N
S
E
W
pixel
pixel
C_{III}
C_{II}
C_{I}
AT Cnc
. galaxy
. galaxy
0
50
100
150

Fig. 17

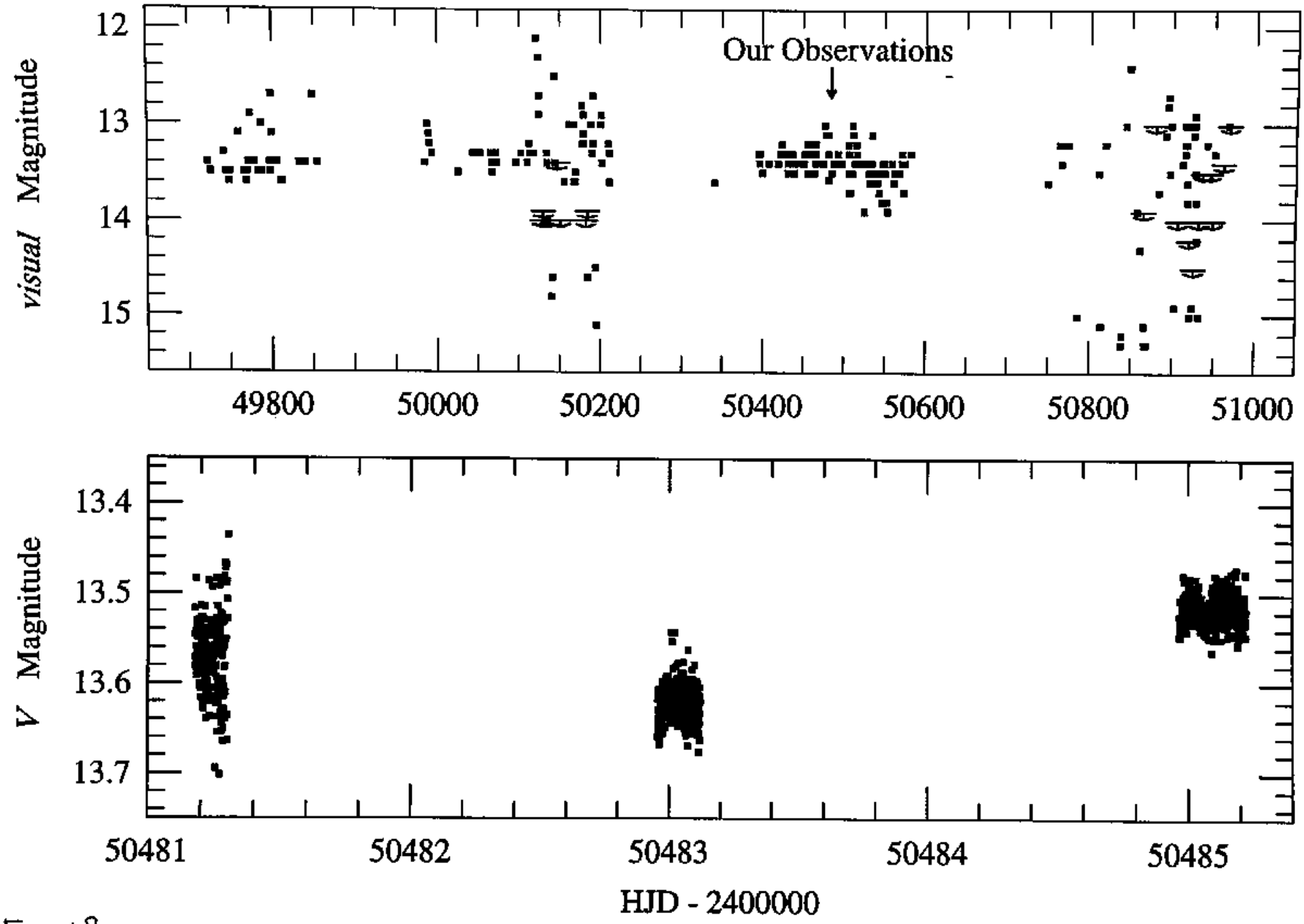
Our Observations
visual Magnitude
12
13
14
15
49800
50000
50200
50400
50600
50800
51000
V Magnitude
13.4
13.5
13.6
13.7
50481
50482
50483
50484
50485
HJD - 2400000

Fig. 18

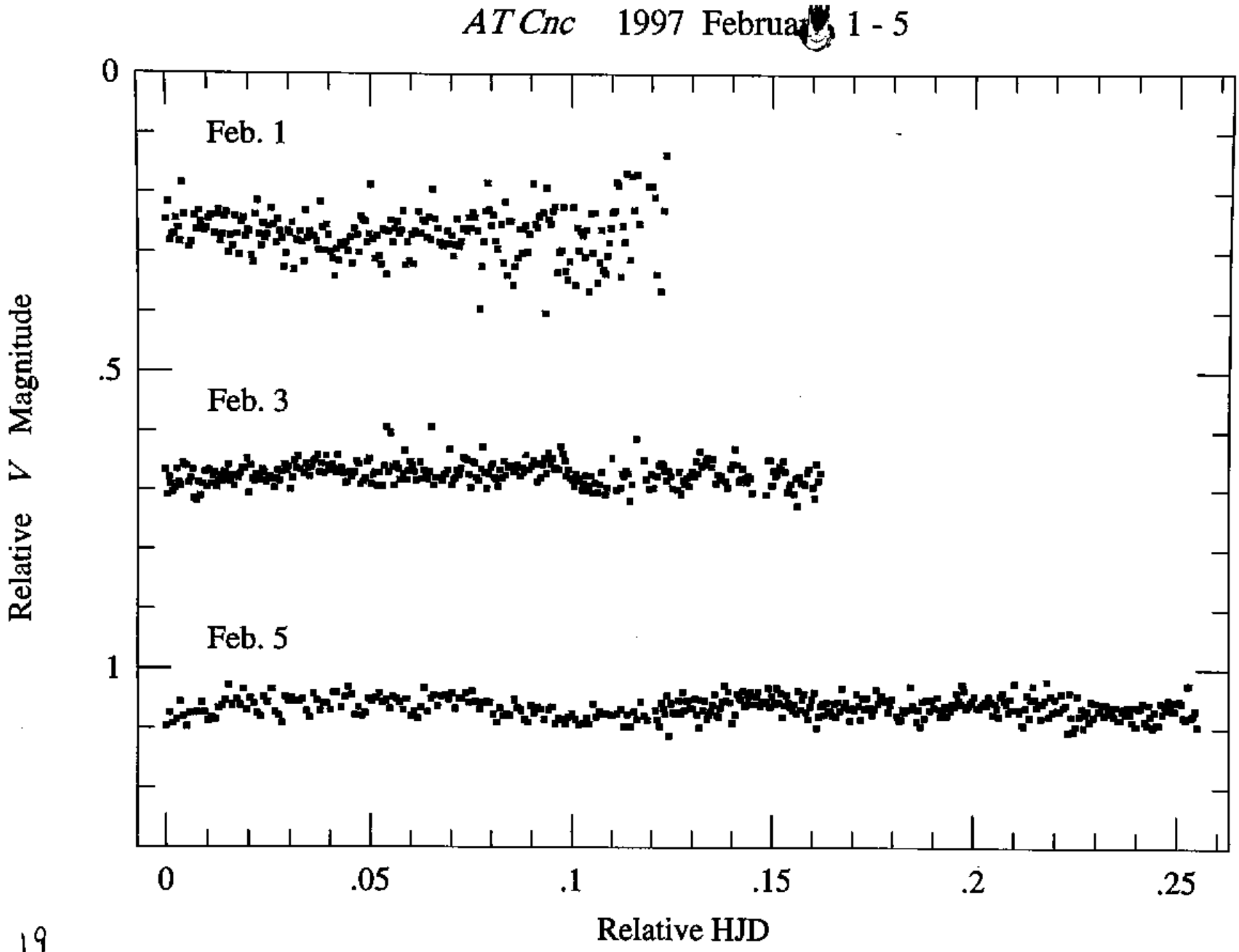
AT Cnc 1997 February 1 - 5
Feb. 1
Feb. 3
Feb. 5
Relative V Magnitude
0
.5
1
0
.05
.1
.15
.2
.25
Relative HJD

Fig. 19

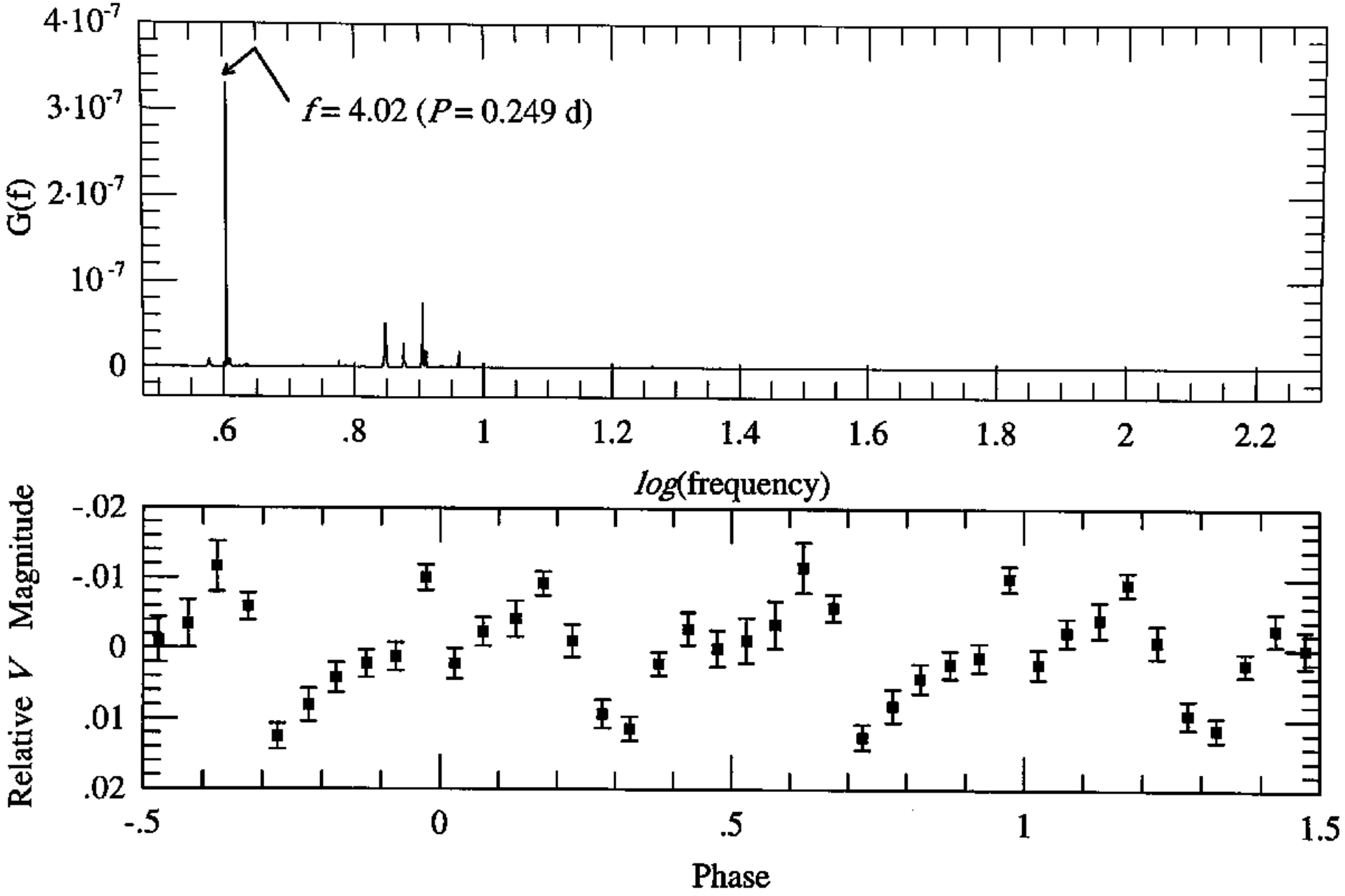
4·10-7
3·10-7
2·10-7
10-7
0
G(f)
f = 4.02 (P = 0.249 d)
.6
.8
1
1.2
1.4
1.6
1.8
2
2.2
log(frequency)
-.02
-.01
0
.01
.02
Relative V Magnitude
-.5
0
.5
1
1.5
Phase

Fig. 20

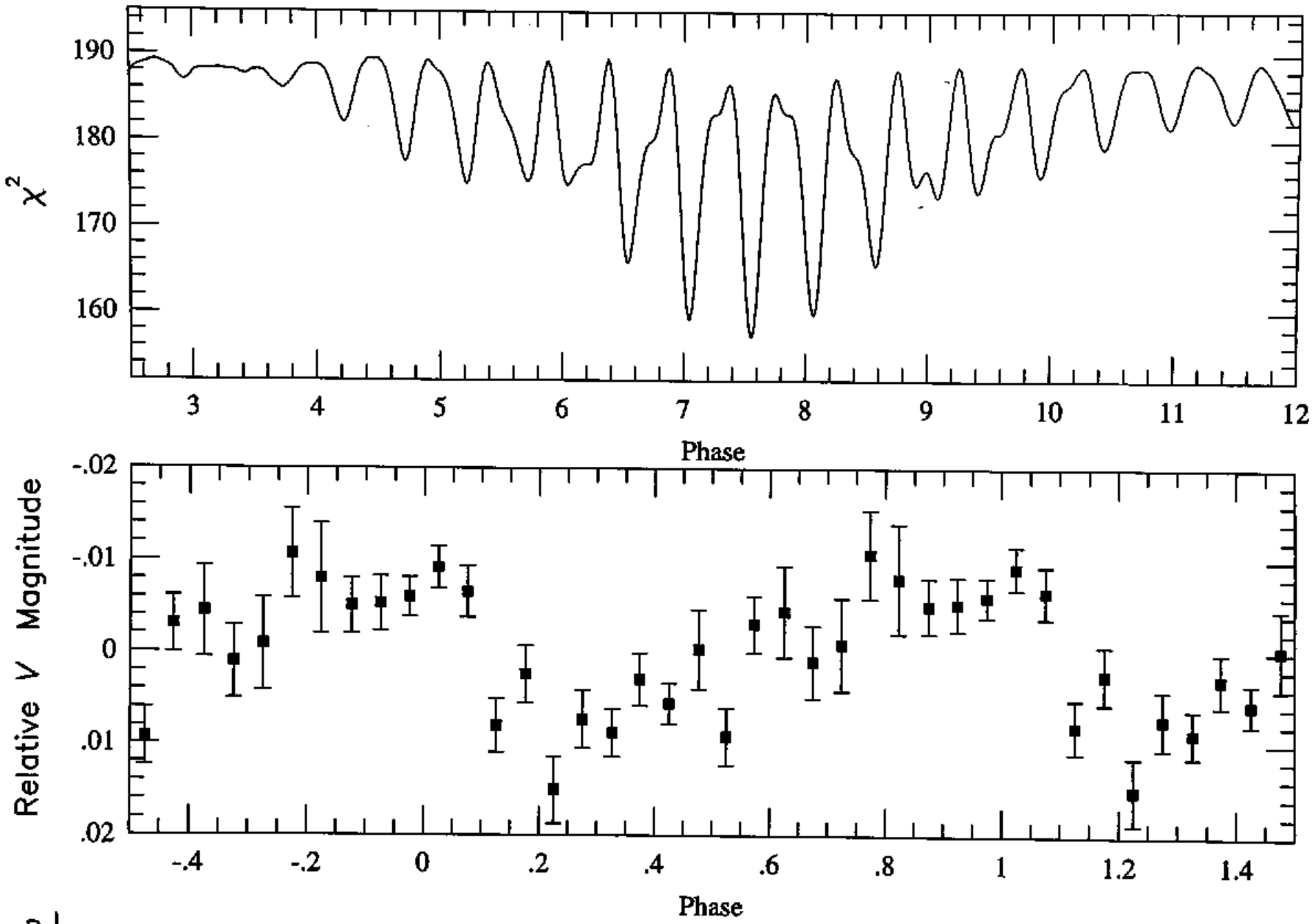
190
180
170
160
χ^2
3
4
5
6
7
8
9
10
11
12
Phase
-.02
-.01
0
.01
.02
Relative V Magnitude
-.4
-.2
0
.2
.4
.6
.8
1
1.2
1.4
Phase

Fig. 21

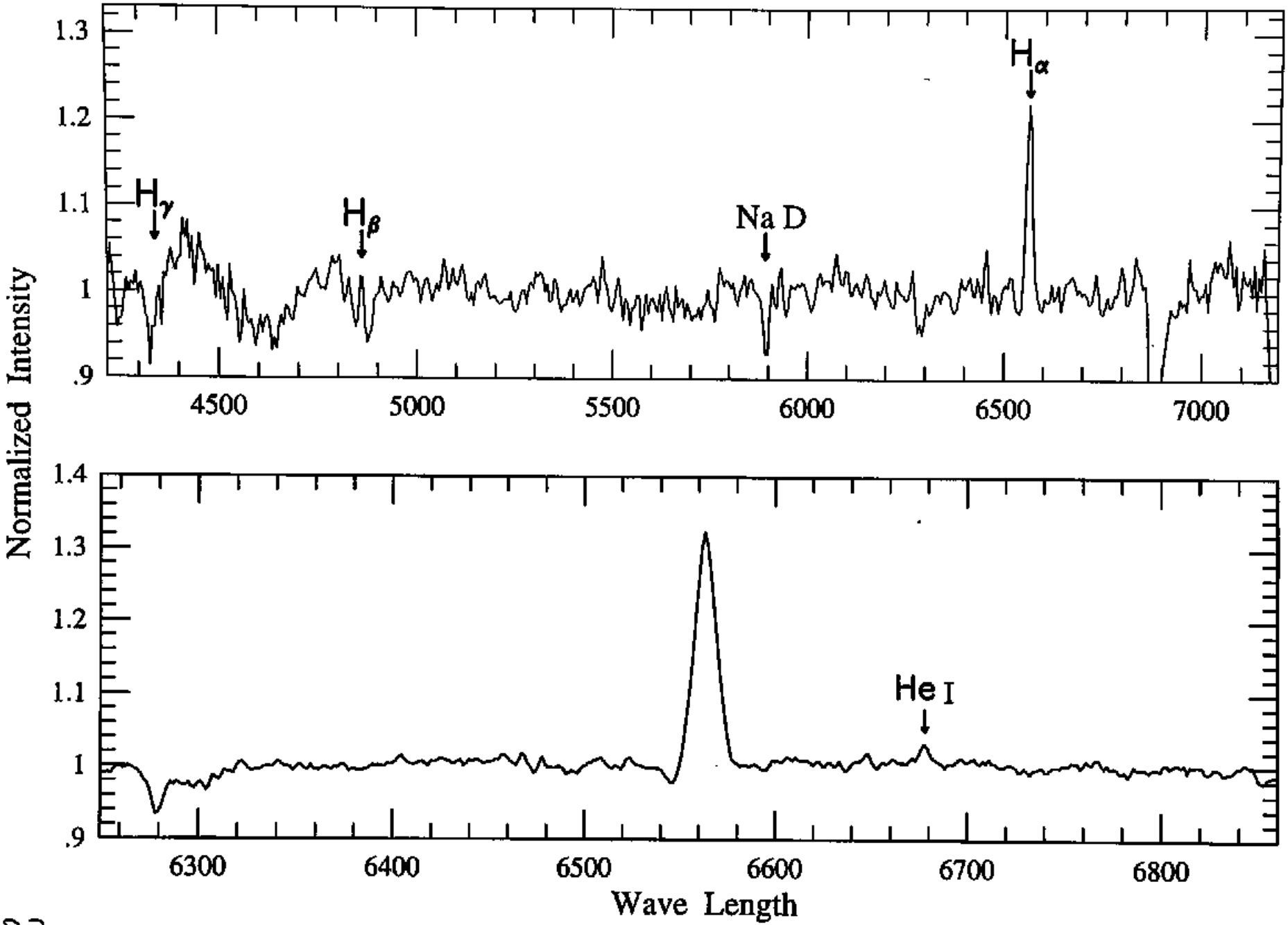
Normalized Intensity
1.3
1.2
1.1
1
.9
H_γ
H_β
Na D
H_α
4500
5000
5500
6000
6500
7000
1.4
1.3
1.2
1.1
1
.9
He I
6300
6400
6500
6600
6700
6800
Wave Length

Fig. 22

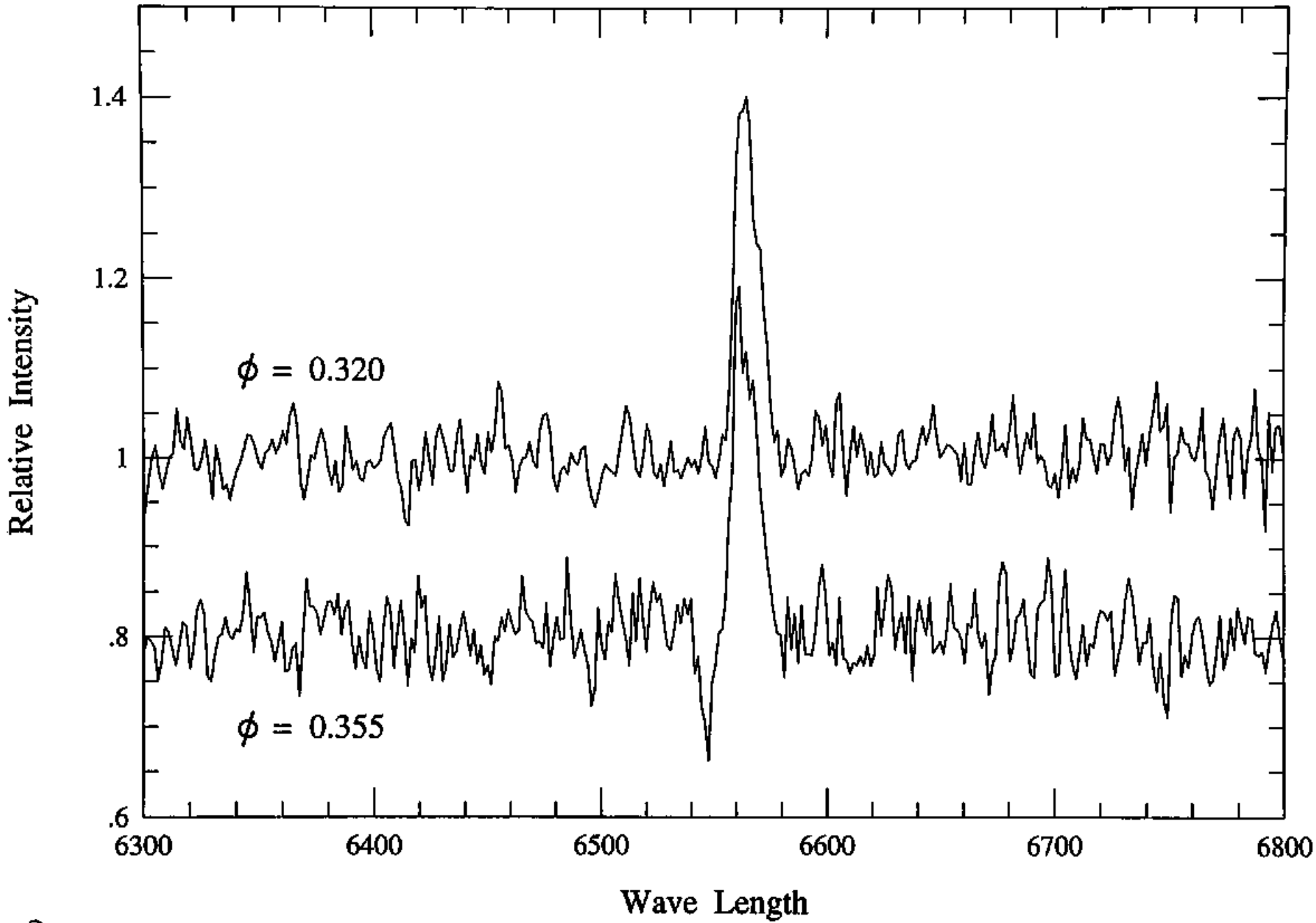
1.4
1.2
1
.8
.6
Relative Intensity
ϕ = 0.320
ϕ = 0.355
6300
6400
6500
6600
6700
6800
Wave Length

Fig. 23

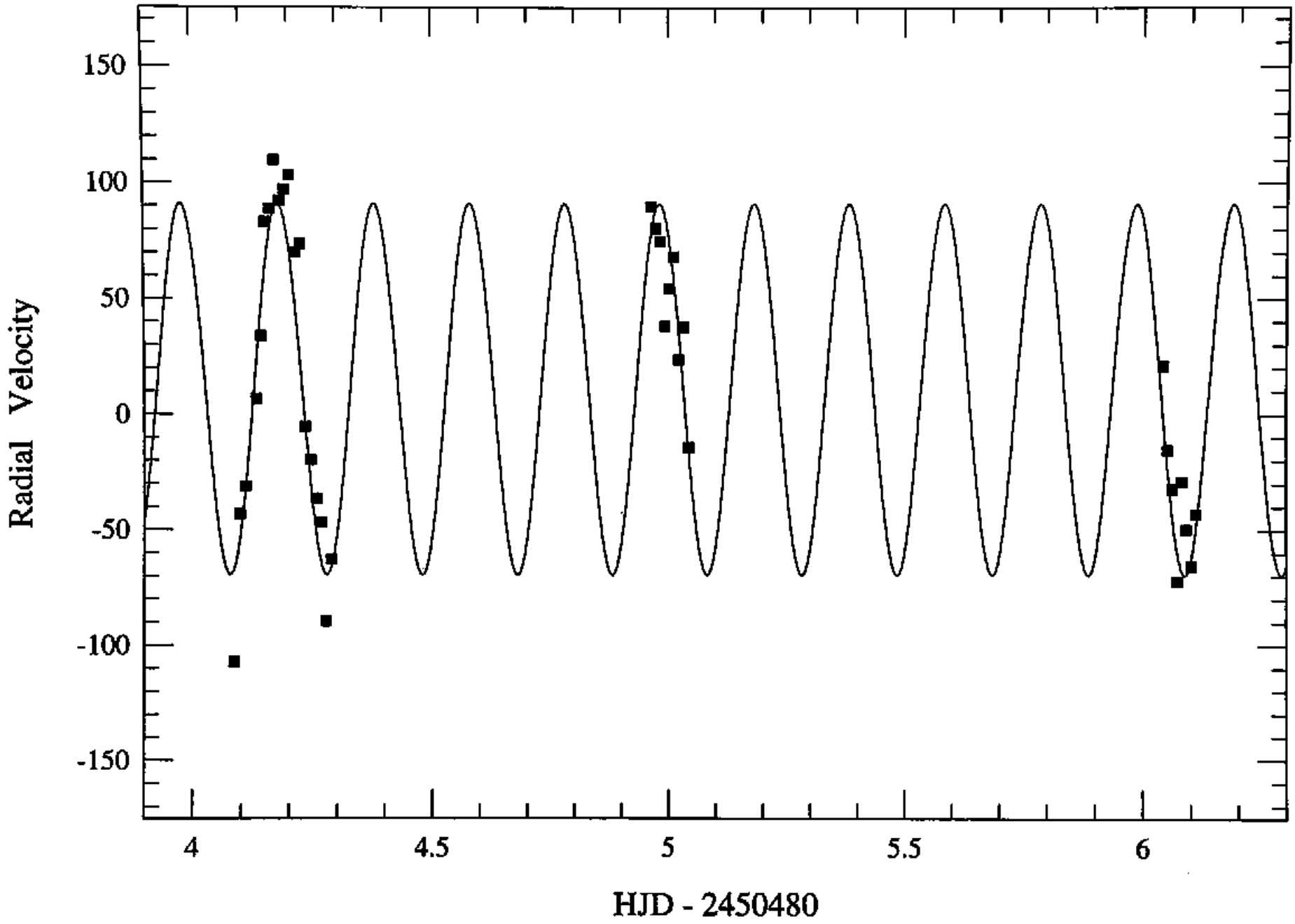

Fig. 24

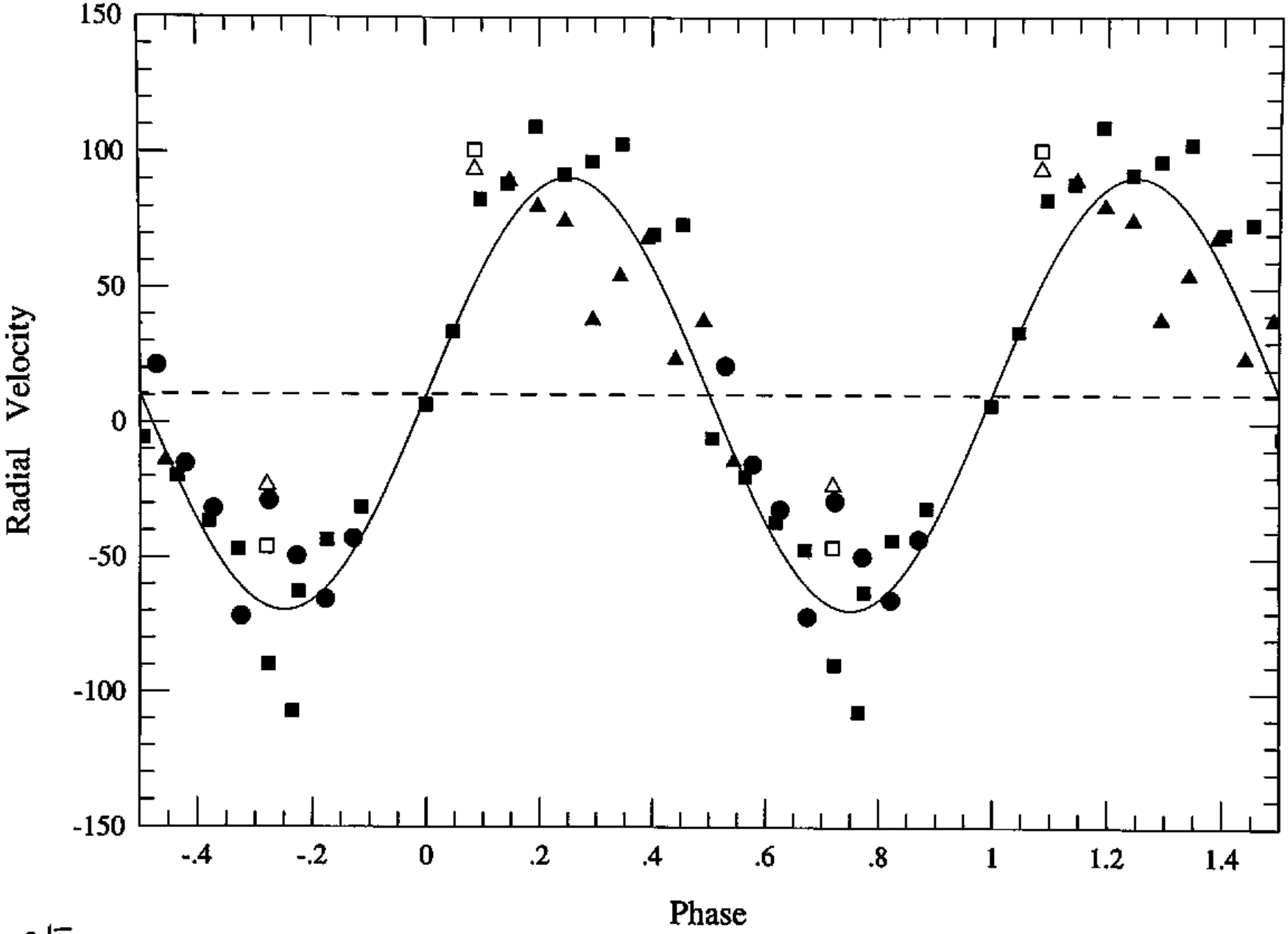

Fig. 25

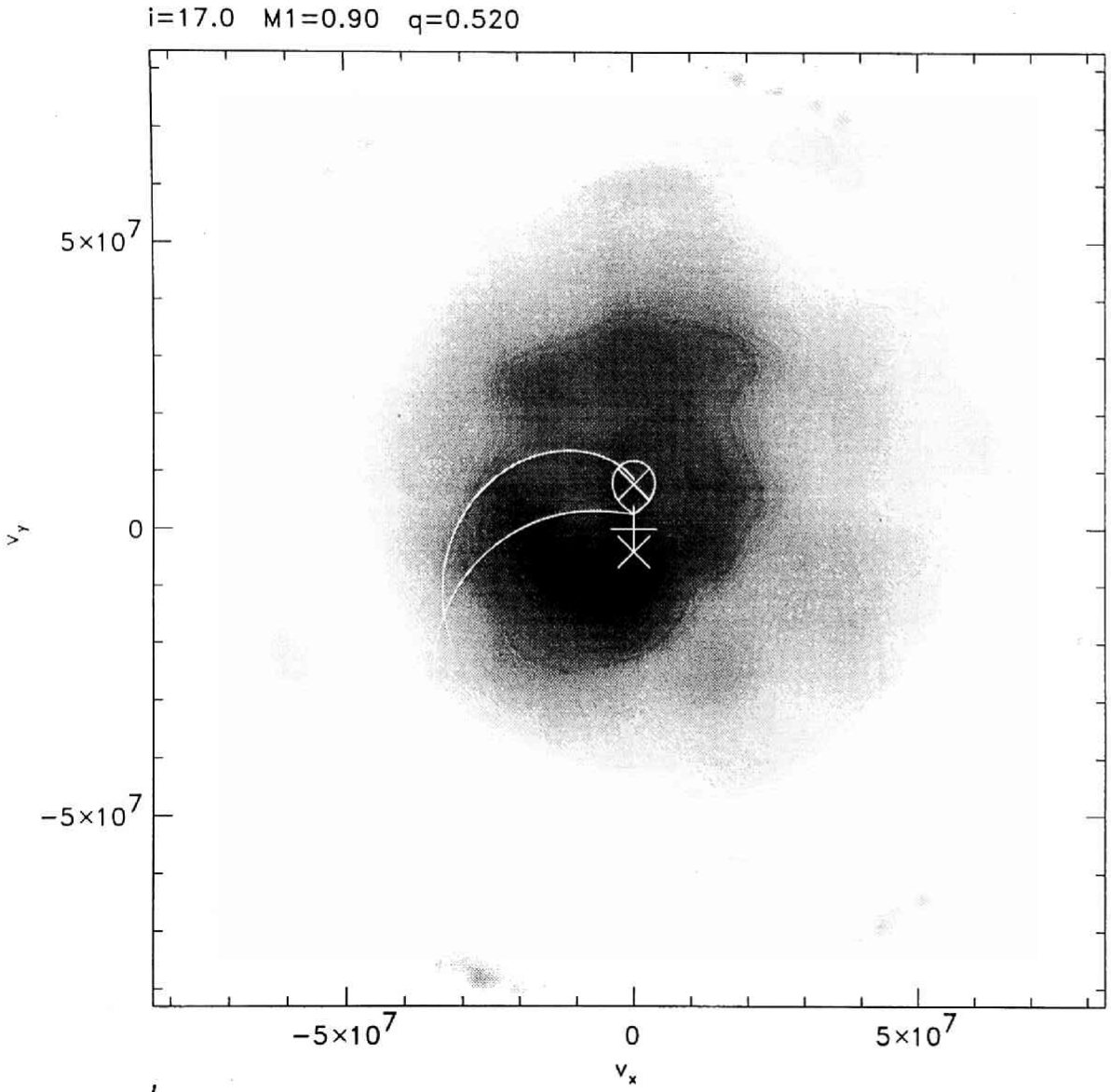

Fig. 26

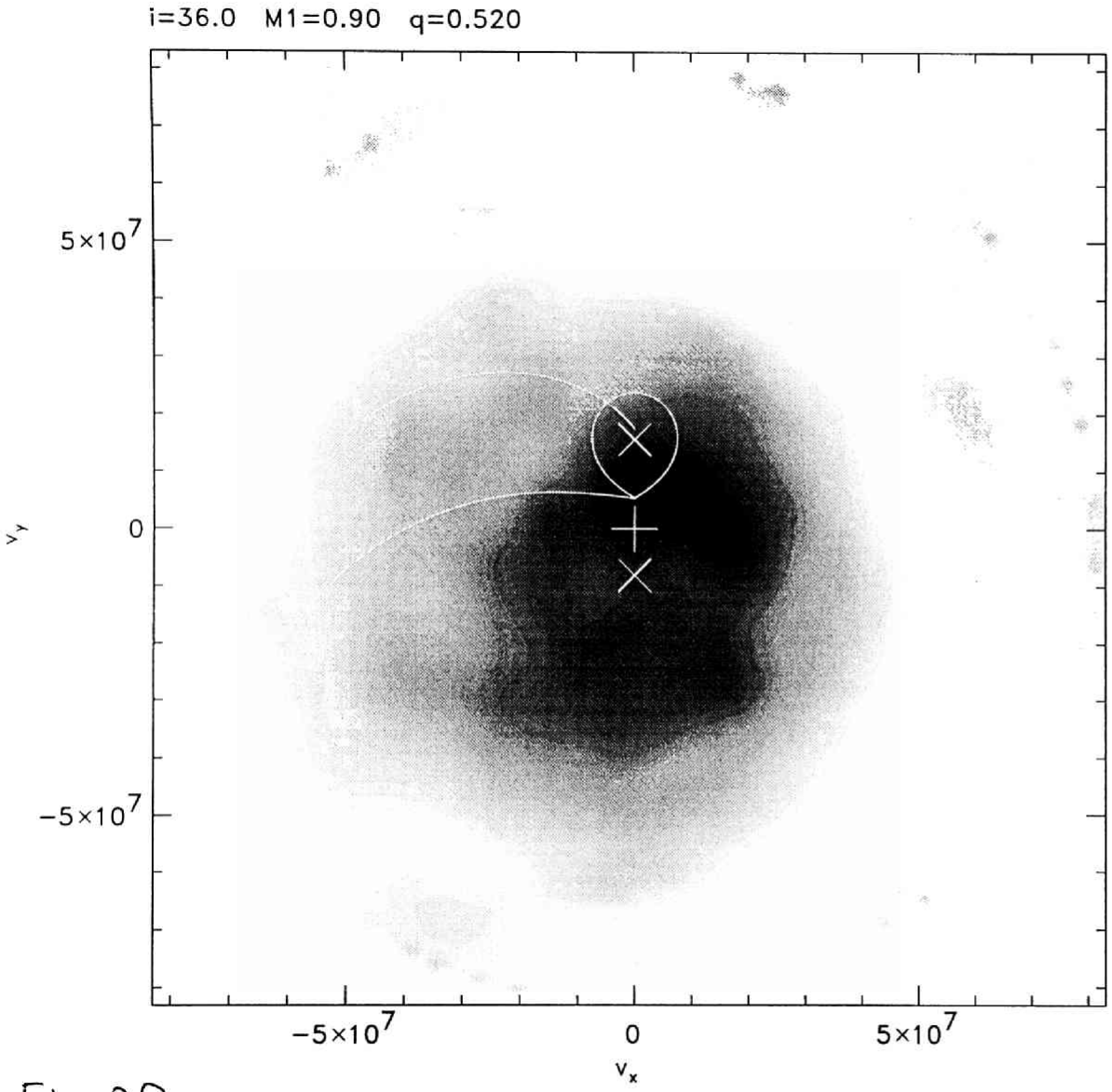

Fig. 27